

# **Mineralogical and isotope geochemical investigations of high Mg-calcites:**

**Laboratory and field studies**

**Dissertation  
zur Erlangung des Doktorgrades  
der Mathematisch-Naturwissenschaftlichen Fakultät  
der Christian-Albrechts-Universität  
zu Kiel**



vorgelegt von  
Vasileios Mavromatis  
Kiel 2009



Ich versichere an Eides statt, dass die vorliegende Abhandlung ausschließlich unter Verwendung der angegebenen Hilfsmittel entstanden ist und, abgesehen von der Beratung durch meine akademischen Lehrer, nach Inhalt und Form meine eigene Arbeit darstellt.

Kiel, den .....

.....

Vasileios Mavromatis

Referent: .....  
Korreferent: .....  
Tag der mündlichen Prüfung: .....  
Zum Druck genehmigt: Kiel, .....

Der Dekan

## Acknowledgments

Hereby I would like to thank all these people which with one or other way contributed on this work.

This work was made possible after my involvement in the Collaborative Research Center (SFB) 574. For the invitation, I want to thank PD Dr. Mark Schmidt. Without his supervision, his support and his patience this work would not be completed.

A big role on this work had PD Dr. Reiner Botz to whom I am deeply thankful for his help and guidance. Without our discussions, his hints and suggestions this thesis would never had its final shape.

I would like to thank Prof. Dr. Klaus Wallmann for co-reviewing this thesis.

For her assistance in the lab, the dozens of little notes I found on my desk and especially for her patience with my bad German, I thank “mein” Inge Dold.

For all the ‘tips and tricks’ and the ‘how to’ at the first steps of my PhD and his encouragement and constructive discussions about the present work, even at the time he was ‘down under’, I specially thank Dr. Christoph Beier.

XRD analyses (several hundreds of them) would not be possible without the assistance of Petra Fiedler. I have also to thank her for the daily advice to smile.

A special ‘thank you’ goes to Dr. Christian Hensen, for providing pore water data, for the fruitful discussions on early diagenesis and his support especially at the last, very demanding stages of this work.

For their tips on programming and the constant supply of scientific material unavailable in CAU-Kiel, I wish to thank my old friends Olga Zacharopoulou and Stelios Flampouris.

Special thanks go to my office mates Laia Comas-Bru and Udo Laurer for the excellent working environment. For their assistance with scientific and technical issues (lab work, handling software, translations) I wish to thank

Katharina Niederndorfer, Elisabetta Ballarini, Hristomir Hristov, Sven Fahrner and Simon van der Wulp. Specially, I want to thank all of them for the after-work activities (cooking, coffeeing and alcohol consumption).

For their assistance in handling specific software/instruments I wish to thank: N.-S. Dr. Rahmoun (FTIR), N. Dr. Andersen and L. Haxhijaj (stable isotopes), R. Surberg, K. Kißling and C.-D. Dr. Garbe-Schönberg (ICP-OES and AES), U. Schuldt (SEM-EDX), J. Lippke (BET) and V. Bass (lab analytics).

## Table of contents

Acknowledgments	v
Summary	xi
Zusammenfassung	xiii
Chapter I	
<b>Introduction</b>	
1.1 Occurrence of sedimentary carbonates	1
1.2 Mg-calcites	2
1.3 Precipitation of Mg-calcites	3
1.4 Dissolution of Mg-calcites	4
References	6
Chapter II	
<b>Authigenic carbonate formation in mud volcanoes “Mounds 11 and 12”, Costa Rica forearc</b>	
Abstract	11
2.1 Introduction	12
2.1.1 Authigenic carbonates	12
2.1.2 Study area and geological background	13
2.2 Sampling and analytical methods	15
2.2.1 Core sampling	15
2.2.2 X-ray diffraction (XRD measurements)	17
2.2.3 Carbonate content, organic carbon	17
2.2.4 Pore water analyses	17
2.2.5 Microscopy	19
2.2.6 Stable isotope analyses	19
2.3 Results	20

## Table of contents

---

2.3.1 Fluid geochemistry	20
2.3.2 Petrography, mineralogy and carbonate content of concretions	22
2.3.3 Stable isotopic composition of concretions	23
2.4 Discussion	24
2.4.1 Pore fluid geochemistry	24
2.4.2 Occurrence and stable oxygen- and carbon isotope composition of authigenic carbonate concretions in sediments	27
2.4.2.1 Stable oxygen isotope values of concretions	29
2.4.2.2 Stable carbon isotope values of concretions	31
2.5 Conclusions	34
References	35

## Chapter III

### **Laboratory determination of oxygen isotope fractionation of high Mg-calcite between 25 and 80°C**

Abstract	43
3.1 Introduction	44
3.2 Methods	45
3.2.1 $\text{Ca}_x\text{Mg}_{1-x}\text{CO}_3$ syntheses	47
3.2.2 Partial dissolution technique	46
3.2.3 X-ray diffraction (XRD measurements)	47
3.2.4 Infrared spectroscopy	47
3.2.5 SEM and EDX measurements	48
3.2.6 Ca and Mg analyses (ICP-AES)	48
3.2.7 Stable oxygen isotope analyses	48
3.3 Results and discussion	49
3.3.1 Mineralogy of precipitants	49
3.3.2 Vibration band characteristics of CaMg-carbonate	52
3.3.3 Chemical composition of synthesized CaMg-carbonates	54
3.3.4 Stable oxygen isotope fractionation of HMC-H <sub>2</sub> O	55
3.4 Conclusions	60
References	60

## Chapter IV

**Dissolution kinetics of a marine authigenic high-Mg calcite sample:  
an experimental approach**

Abstract	69
4.1 Introduction	70
4.2 Theoretical background	71
4.2.1 Mechanism of carbonate dissolution	71
4.2.2 Dissolution kinetics and constants	72
4.2.3 Equilibrium constants and IAP of dissolution for CaMg- carbonates	73
4.3 Methods	73
4.3.1 Sample preparation and characterization	73
4.3.2 X-ray diffraction (XRD measurements)	75
4.3.3 Experimental set-up	75
4.3.4 Ca and Mg analyses (ICP-AES)	76
4.3.5 Dissolution rates	76
4.3.6 Reactive surface calculation	76
4.4 Results and discussion	77
4.4.1 pH changes in aqueous solution by CaMg-carbonate disso- lution	77
4.4.2 Ca, Mg-release from CaMg-carbonates and solubility calcu- lations	80
4.4.3 Dissolution rate, rate constant, and reaction order determi- nation for CaMg-carbonate dissolution	83
4.4.4 Reactive surface determination of (Mg)-calcites	89
4.5 Geochemical applications and conclusions	90
References	91
Appendix	A-I



## Summary

Within the framework of this thesis investigations on formation and dissolution processes of Mg-calcites have been carried out. Based on the results of mineralogical and isotope geochemical investigations it was possible to reconstruct the formation processes of authigenic high Mg-calcite concretions sampled from mud mounds of the Costa Rica forearc. Furthermore, based on laboratory work, the oxygen isotope fractionation of high Mg-calcite in aqueous media was examined. Finally, dissolution experiments on CaMg-carbonates were performed and theoretic kinetic parameters could be defined for the dissolution processes.

*Chapter I* presents a short introduction describing the natural occurrence of Mg-calcites and their formation processes. Furthermore, different experimental techniques, which are applied to investigate precipitation- and dissolution processes of carbonates, are introduced.

Formation processes of authigenic carbonates in Mounds 11 and 12 (Costa Rica forearc) are discussed in *Chapter II*. The pore water geochemical profiles from sediment cores collected in the study area show the active diagenetic processes leading to carbonate mineral precipitation. Investigation of the stable carbon and oxygen isotope composition of the collected authigenic concretions indicates a complex formation scenario, possibly controlled by sediment erosion, varying fluxes of methane-rich fluid, and thus migration zones of carbonate formation. Based on the stable isotope composition of the authigenic concretions and the respected geochemical pore fluid composition a common deep fluid source is postulated for the two mud mounds.

The *third chapter* investigates the effect of  $Mg^{2+}$  incorporation on the oxygen isotope fractionation of high Mg-calcite in the temperature range between 25 and 80°C. Synthetic high Mg-calcites with various  $MgCO_3$  content are

prepared in the laboratory from oversaturated solutions with respect to calcite. A new technique for the separation of crystalline from amorphous carbonate was developed. The results, including a new expression for the Mg-calcite-water oxygen isotope fractionation, imply that the incorporation of  $Mg^{2+}$  in the calcite crystal lattice has a much bigger effect on the Mg-calcite - water oxygen isotope fractionation, than it was previously defined by laboratory precipitation experiments at 25°C. The new isotope fractionation factor (this study) rather fits to recently published thermodynamic calculations, and will help to improve our knowledge about the environmental conditions during natural Mg-calcite formation.

The investigation of CaMg-carbonate dissolution in aqueous media is presented in the *fourth* chapter. The run of the concentration vs. time curves could be fitted by a simple kinetic equation. Kinetic constants controlling the equation were determined and are comparable to previously published data. Furthermore, experiments performed in distilled water showed that dissolution rates of authigenic (13%)Mg-calcite are comparable to dissolution rates of calcite, when the geometric surface is used in the kinetic equation. In the case of dissolution experiments in NaCl solutions (0.6M), with ionic strength similar to seawater, the solvent obviously strongly determines the reaction order and dissolution rate of Mg-calcite. It is believed that the presented results could be used to improve the existing diagenetic models describing diagenetic dissolution/precipitation processes of CaMg-carbonates in e.g. cold seep areas.

## Zusammenfassung

Im Rahmen dieser Doktorarbeit wurden die Bildungs- und Lösungsprozesse von Mg-Kalzit erforscht. Auf der Grundlage von mineralogischen, sowie isotopengeochemischen Untersuchungen war es möglich, die Bildungsprozesse von authigenen Karbonatkonkretionen, die zum großen Teil aus hoch-Mg-Kalzit bestehen, und sich an Schlammvulkanen im Costa Rica Forearc-Bereich gebildet haben, zu rekonstruieren. Des Weiteren wurde die Sauerstoffisotopenfraktionierung zwischen synthetisch hergestelltem Mg-Kalzit und Wasser in einem Temperaturbereich zwischen 20 und 80°C bestimmt. Darüber hinaus wurde das Lösungsverhalten unterschiedlicher Karbonate in destilliertem Wasser und 0.6M Kochsalzlösung untersucht, und kinetische Konstanten zur theoretischen Beschreibung der Lösungsgeschwindigkeiten bestimmt.

In Kapitel I wird eine kurze Einleitung zum natürlichen Vorkommen von Karbonaten, insbesondere von Magnesiumkalziten, in der Natur gegeben. Darüber hinaus wird eine Einführung in die Möglichkeiten zur Untersuchung von Fällungs- und Lösungsprozessen von Karbonaten im Labor gegeben.

Die Bildungsprozesse authigener Karbonate in den Schlammvulkanen Mound 11 und 12 des Costa Rica Forearcs werden in Kapitel II diskutiert. Geochemische Porenwasserprofile, die Sedimentkernen des Untersuchungsgebiets entnommen wurden, weisen auf aktive Karbonatdiageneseprozesse hin. Untersuchungen zur geochemischen Zusammensetzung von stabilen Kohlenstoff- und Sauerstoffisotopen an den beprobten authigenen Karbonatkonkretionen aus Oberflächensedimenten ergeben ein komplexes Bild möglicher Sedimenterosion, unterschiedlich starker Fluidausströmungen, und damit tiefenvariierender Karbonatbildungszonen. Basierend auf der geochemischen Zusammensetzung der authigenen Karbonate und der Porenwässer der beiden Schlammvulkane, wird eine gemeinsame tiefliegende Fluidquelle postuliert.

Im dritten Kapitel dieser Arbeit wird der Einfluss des Einbaus von  $Mg^{2+}$ -Ionen auf die Sauerstoff-Isotopenfraktionierung von Mg-Kalzit im Temperaturbereich zwischen 25 und 80°C untersucht. Synthetische Mg-Kalzite mit verschiedenen  $MgCO_3$ -Anteilen wurden dafür im Labor aus übersättigten Kalzit-Lösungen gewonnen. Im Laufe dieser Arbeit wurde auch ein neues Verfahren zur Trennung von kristallinem und amorphem Karbonat entwickelt. Die Ergebnisse, eingeschlossen die „Mg-Kalzit - Wasser“ Isotopenfraktionierung, lassen darauf schließen, dass die Erhöhung der O-Isotopenfraktionierung mit erhöhtem Anteil von  $Mg^{2+}$  im Kalzit-Kristallgitter, wesentlich größer ist, als bis vor kurzem anhand von Laborexperimenten angenommen wurde. Die Ergebnisse dieser Arbeit stimmen eher mit thermodynamischen Modellrechnungen überein, und können die Interpretationen zu Bildungsbedingungen natürlicher Mg-Kalzite entscheidend verbessern.

Im vierten Kapitel werden die Untersuchungen zum Lösungsverhalten von Ca,Mg-Karbonaten in destilliertem Wasser sowie in 0.6M Kochsalzlösung dargestellt. Die Konzentrations/Zeit-Verläufe während fortschreitender Lösung können mit einer einfachen kinetischen Gleichung beschrieben werden. Die entsprechenden kinetischen Konstanten dieser Gleichung wurden bestimmt und sind vergleichbar mit aus der Literatur bekannten Werten. Die Untersuchungen und Auswertungen zum Lösungsverhalten von authigenem (13%)-Mg-Kalzit ergaben, dass die berechneten Lösungsraten des Mg-Kalzits in destilliertem Wasser mit den Lösungsraten von Kalzit vergleichbar sind, wenn sie anhand der geometrischen Oberflächen berechnet werden. Aus Experimenten, die in NaCl-Lösungen (0,6M) ausgeführt wurden, deren Ionenkonzentrationen derjenigen von Meerwasser ähneln, ergibt sich eine starke Beeinflussung der Reaktionsordnung und damit der Lösungsrate durch das Medium. Die hier gewonnen Ergebnisse können dazu beitragen, die existierenden diagenetischen Modelle zur Beschreibung von Lösungs- und Ausfällungsprozessen in cold seeps zu verbessern.

## Introduction

### 1.1 Occurrence of sedimentary carbonates

Sediments and sedimentary rocks contain a variety of carbonate minerals. Calcite and dolomite are by far the most important carbonate minerals in ancient sedimentary rocks (Morse and Mackenzie, 1990). The distribution of carbonate sediments is determined by kinetic, biogeochemical processes, as well as by early diagenetic processes. According to their occurrence, carbonate minerals can be divided in those found in shoal to shallow environments and in these found in deep-water environments. The factors controlling the sources, the mineralogy and the diagenesis of these carbonates differ substantially.

Diagenesis of carbonates in the deep sea almost exclusively involves the dissolution of calcium carbonate, where only 20-30% of the flux to the seafloor is preserved (Archer, 1996). In open ocean basins, where rates of detrital sedimentation are moderate to low, sediments above 3000m water depth are generally high in calcium carbonate, whereas sediments below 6000m generally have very low calcium carbonate content. Between these depths, there is a poor correlation between the weight percent of calcium carbonate and depth (Archer, 1996). In sediments found at intermediate depths (e.g. mid ocean ridge crests, which have an average depth of 2500m) aragonite derives from pelagic pteropods and heteropods. Almost all deep-sea carbonate-rich sediments are composed of low Mg-calcites (LMC,  $< 5 \text{ mol } \% \text{ MgCO}_3$ ), which is derived from pelagic skeletal organisms (i.e. coccolithophores and foraminifera). High Mg-calcite (HMC) cements are rarely found in deep-sea environments.

Shallow-water carbonate-rich sediments are meet commonly to subtropic and tropic climatic zones but are found even at higher latitudes (Morse and Mackenzie, 1990). The limiting factors of their occurrence are water temperature and terrigenous input. They are usually dominated by aragonite, followed

by calcites rich in magnesium (> 5 mol %). The HMCs are derived from the skeletons of organisms, such as benthic foraminifera and sea urchins, and by direct precipitation of marine sediments. Dolomite appears only in special environments, but it is not a major component of the sediments.

## 1.2. Mg-calcites

Mg-calcites, perhaps because they are important mineral constituents in biological materials, have intrigued scientists for decades. Their biological association has also been a principal reason for disagreement concerning the solubility and solid solution behavior of these phases. Contrary to other mineral systems in which inorganic phases form the basis for interpretation of mineral behavior and stability, Mg-calcites of biogenic origin have been a principal material used to interpret the behavior at low temperatures (Mackenzie et al., 1983).

Incorporation of  $Mg^{2+}$  in calcite crystal lattice however occurs in inorganic precipitates. Under specific environments (i.e. pore waters) inorganic calcites can contain up to 25%  $MgCO_3$  in their crystal lattice. The fact that Mg-calcites are actually forming a solid solution between calcite and dolomite lead to an extensive investigation of their thermodynamic stabilities.

A substantial number of studies involving the solubility and precipitation as well as other chemical behaviors of Mg-calcites in seawater or other aqueous solutions have been carried out (i.e. Plummer and Mackenzie, 1974; Thorstenson and Plummer, 1977; Walter and Morse, 1984a; Walter and Morse, 1985; Busenberg and Plummer, 1989; Pokrovsky, 1996; Morse et al., 1997). The last decade global warming intensively attracted the attention of the scientific community and Mg-calcites used for reconstruction of paleoclimatic conditions. All of these studies show that precipitation and dissolution of Mg-calcites are still a topic under investigation as controversial results often occur. For example, precipitation of Mg-calcites is still remaining enigmatic with questions like the control mechanism of  $Mg^{2+}$  incorporation in calcite to be unresolved. Similar dissolution experiments of biogenic and inorganic Mg-calcites provided results with inconsistent solubilities (Mackenzie et al., 1983). The next two para-

graphs give a short introduction on the background of experimental studies on Mg-calcites. Using references from the international literature an approach to basic questions concerning the precipitation and the dissolution of Mg-calcites are shortly reviewed.

### 1.3 Precipitation of Mg-calcites

Precipitation experiments on Mg-calcites in the literature are mainly oriented on the control of the mineral polymorph precipitating from solutions of (or similar to) seawater composition. Although the last decades many authors investigated the role of several ions on the precipitation mechanism of Mg-calcites, reports on precipitation kinetics and rates are of limited number, mainly because several studies showed that the calcium carbonate polymorph most commonly obtained in the presence of magnesium was aragonite (Berner, 1975; Berner et al., 1978; Rushdi et al., 1992; Raz et al., 2000).

Historically, on the precipitation of HMC at either low temperatures or pressures, some experiments have been carried out during the last decades. Baron (1960) prepared Mg-rich calcites at temperatures as low as 25 °C under a few atmospheres of CO<sub>2</sub> pressure. Erenburg (1961) described artificial mixed carbonates in the CaCO<sub>3</sub> – MgCO<sub>3</sub> series prepared at 50 °C. His preparations run from 17.1 to 55.9 mol % MgCO<sub>3</sub> with no evidence of order in the structure. Glover and Sippel (1967) were the first reporting synthesis of calcite with Mg content ranging from 0 to 34 mol %. The initial precipitate on their experiments after 1 to several hours was usually HMC, which slowly disappeared as aragonite formed. The reproducibility of these experiments was very poor. Later, they synthesized CaMg-carbonates using seawater and the obtained products had MgCO<sub>3</sub> content close to that of dolomite.

The thermodynamic stability of precipitated Mg-calcites was also a topic of extensive research. Calcite with a magnesium content of 10 mol % has the same solubility as aragonite, and thus can precipitate from seawater. This magnesium content is thus considered to be highly compatible with thermodynamically stable magnesian calcite (Chave et al. 1962; Berner 1975). Higher Mg-

bearing calcites are metastable, and can be synthesized readily at high temperatures and pressures (Goldsmith et al. 1955).

The importance of transformation of a metastable mineral precipitated in supersaturated solution were stated by Nancollas (1982) and Nancollas et al. (1983). Through a series of dissolution/re-precipitation reactions, an unstable HMC can be replaced by stable LMC or dolomite. Later on Morse et al. (1997) define precisely the relation between Mg/Ca ratio and temperature with the precipitated mineral polymorph at temperature range between 0 and 35 °C.

Recently, Raz et al. (2000) studied the calcium carbonate precipitates formed from solutions with Mg:Ca ratios equal to or greater than four. The same authors showed that when Mg-calcite produced via an amorphous precursor phase, and in the absence of any other additive, they contain 21 mol % MgCO<sub>3</sub>. The barrier to growth rate that is created during incorporation of Mg<sup>2+</sup> ions in calcite crystal lattice (House et al., 1988; Zhang and Dawe, 2000), was shown to be overcome by the initial formation of an amorphous calcium carbonate (ACC) precursor. ACC, which has been shown to stabilize by presence of Mg<sup>2+</sup> in biominerals (Aizenberg et al., 1996; Aizenberg et al., 2002; Addadi et al., 2003), may possibly also provide a mechanism for the incorporation of Mg<sup>2+</sup> in the calcite lattice (Raz et al., 2000; Loste et al., 2003).

## 1.4 Dissolution of Mg-calcites

High Mg-calcites (10-20% MgCO<sub>3</sub>) together with aragonite form the major carbonate phases in shallow water carbonate sediments, participating in subsequent diagenetic reactions to produce the commonly observed stable low-Mg calcite mineralogy of sedimentary carbonate rocks. Quantification of the rate and identification of the mechanism by which this transformation is accomplished has thus been a key goal of studies conducted over the past 40 years (Morse and Advirson, 2002).

Experimental work conducted prior to ca. 1970, (i.e. Land 1966, 1967) do not contain absolute reaction rates but are rather concerned with relationships between solid phase stoichiometry, bulk solution composition, and the relative

rate of magnesium vs. calcium release to solution. However, Land (1967) observed incongruent dissolution of Mg-calcites at 25 °C at long term experiments.

In general the problems concerning dissolution kinetics of Mg-calcites are related with the relationship between activity of solution components and saturation state with respect to a calcite of a given magnesium content, the differences in reactivity of phases with different origin (synthetic or inorganic vs. biogenic) and the quantification of reactive surface in biogenic samples (Morse and Advirson, 2002).

In the case of Mg-calcites, the relation of reaction rates to the distance from equilibrium ( $1-\Omega$ ), a common method defining kinetic rates and constants for carbonate minerals (Mackenzie et al., 1983), becomes problematic. This problem arises from the question of whether Mg-calcites ever attain a true metastable equilibrium state, and how to represent this relationship in thermodynamic calculations (Bertram et al., 1991). First Thorstenson and Plummer (1977) approached this problem by introducing the concept of stoichiometric saturation. They proposed that the equilibrium constant is given by the product of activities:

$$\text{IAP} = \text{Ca}_{1-x}^{2+} \text{Mg}_x^{2+} \text{CO}_3^{2-}$$

where  $x$  is the mole fraction of magnesium in crystal lattice. Mg-calcite is thus assumed to react as a one-component phase having a fixed composition.

Stoichiometric saturation was suggested as a resolution to the problem of thermodynamic equilibrium of Mg-calcites, however this concept was controversial at the time of its introduction (see responses by Garrels and Wollast, 1978; Lafon, 1978; Thorstenson and Plummer, 1978). Plummer and Mackenzie (1974), in earlier free drift experiments dissolving biogenic magnesian calcite at fixed  $\text{PCO}_2$ , derived equilibrium constants for the dissolution rate from reciprocal root time ( $t^{-0.5}$ ) plots of free drift data (see below). Their approach assumed that only the  $\text{CaCO}_3$  component attains a true saturation state. However, subsequent solubility determinations have demonstrated the utility of the concept of stoichiometric saturation, and Walter and Morse (1984a) have shown that Mg-calcite reaction orders computed from rate vs.  $(1-\Omega)$  relations are not far away to those of pure calcite.

Bertram et al. (1991), applied the stoichiometric saturation, explored the effect of temperature on dissolution of synthetic Mg-calcites (2 to 19 mol %  $\text{MgCO}_3$ ), finding solubility to decrease with temperature in a manner similar to pure calcite. Using pH-stat techniques, Walter and Morse (1985) measured dissolution rates of carefully treated biogenic Mg-calcites (11–18 mol %  $\text{MgCO}_3$ ). They observed reaction orders are somewhat higher ( $n = 3.2\text{--}3.5$ ) compared to low-Mg calcite

Biogenic calcites exhibit greater structural and chemical heterogeneity and accommodate components such as water and hydroxyl (Mackenzie et al., 1983; Gaffey, 1988), sodium, and bicarbonate compared to inorganic counterparts. Microstructural differences in biogenic Mg-calcites have a stronger influence on their dissolution kinetics than their relative thermodynamic stabilities. Biogenic Mg-calcites have also structural differences (i.e. larger unit cell volumes) compared to synthetic phases (Bischoff et al., 1983). Bischoff et al. (1987) concluded that biogenic phases, when compared to synthetic Mg-calcites of similar Mg content, are more soluble.

Comparing dissolution rates of pure calcite and biogenic Mg-calcites, Walter and Morse (1984b, 1985) observed that the primary differences were controlled by relationships between total surface area, grain size and microstructure. They observed that dissolution rates are not increasing proportionally to increase of total surface area. By assuming a unit ratio of reactive to total surface area in synthetic calcite they showed that the complex microstructures characteristic of biogenic Mg calcites result in reactive surface areas that constitute as little as 1% or less of the total area. Thus, in these cases, total surface area measurements are virtually useless as a measure of reactive area.

## References

Addadi L., Raz S. and Weiner S. (2003) Taking Advantage of Disorder: Amorphous Calcium Carbonate and Its Roles in Biomineralization. *Adv Mater* **15**, 959-970.

---

Aizenberg J., Addadi L., Weiner S. and Lambert G. (1996) Stabilization of amorphous calcium carbonate by specialized macromolecules in biological and synthetic precipitates. *Adv Mater* **8**, 222-226.

Aizenberg J., Addadi L., Weiner S. and Lambert G. (1996) Stabilization of amorphous calcium carbonate by specialized macromolecules in biological and synthetic precipitates. *Adv Mater* **8**, 222-226.

Archer D. (1996) An atlas of the distribution of calcium carbonate in sediments of the deep sea. *Glob Biogeochem Cycles* **10**, 159-174.

Baron G. (1960) The synthesis of dolomite. Application to the phenomenon of dolomitization. *Rev Inst F Petrole* **15**, 3-68

Berner R.A. (1975) The role of magnesium in the crystal growth of calcite and aragonite from sea water. *Geochim Cosmochim Acta* **39**, 489-504.

Berner R. A. (1978) Equilibrium, kinetics, and the precipitation of magnesian calcite from seawater; discussion. *Am J Sci* **278**, 1475-1477.

Bertram M. A., Mackenzie F. T., Bishop F. C. and Bischoff W. D. (1991) Influence of temperature on the stability of magnesian calcite. *Am Mineral* **76**, 1889-1896.

Bischoff W. D., Bishop F. C. and Mackenzie F. T. (1983) Biogenically produced magnesian calcite; inhomogeneities in chemical and physical properties; comparison with synthetic phases. *Am Mineral* **68**, 1183-1188.

Bischoff W. D., Mackenzie F. T. and Bishop F. C. (1987). Stabilities of synthetic magnesian calcites in aqueous solution; comparison with biogenic materials. *Geochim Cosmochim Acta* **51**, 1413-1423.

Busenberg E. and Plummer L. N. (1989) Thermodynamics of magnesian calcite solid-solutions at 25 degrees C and 1 atm total pressure. *Geochim Cosmochim Acta* **53**, 1189-1208.

Chave K. E., Deffeyes K. S., Weyl P. K., Garrels R. M. and Thompson, M. E. (1962) Observations on the Solubility of Skeletal Carbonates in Aqueous Solutions. *Science* **137**, 33 – 34.

Erenburg B. G. (1961) Artificial mixed carbonates in the  $\text{CaCO}_3$  -  $\text{MgCO}_3$  series. *Zhurnal Struktr Khim* **2**, 178-182.

Gaffey S. J. (1988) Water in skeletal carbonates. *J Sediment Res* **58**, 397-414.

Glover, E. D. and Sippel, R. F., 1967. Synthesis of magnesium calcites. *Geochim Cosmochim Acta* **31**, 603-613.

Garrels R. M. and Wollast R. (1978). Discussion of equilibrium criteria for two-component solids reacting with fixed composition in an aqueous phase-example: the magnesian calcites. *Am J Sci* **278**, 1469– 1474.

Goldsmith J. R., Graf D. L. and Joensuu O. I. (1955) The occurrence of magnesian calcites in nature. *Geochim Cosmochim Acta* **7**, 212-230

House W. A., Howson M. R. and Pethybridge A. D. (1988) Crystallization kinetics of calcite in the presence of magnesium ions. *Faraday Trans.* **84**, 2723-2734.

Lafon G.M., (1978) Equilibrium criteria for two-component solids reacting with fixed composition in an aqueous phase; example, the magnesian calcites; discussion. *Am J Sci* **278**, 1455– 1468.

Land L. S. (1966) Diagenesis of metastable carbonates. Thesis Lehigh Univ. Bethlehem, PA.

Land P.S. (1967) Diagenesis of skeletal carbonates. *J Sediment Petrol* **37**, 914-930.

Loste E., Wilson R. M., Seshadri R. and Meldrum F. C. (2003) The role of magnesium in stabilising amorphous calcium carbonate and controlling calcite morphologies. *J Cryst Growth* **254**, 206-218.

Mackenzie F. T., Bischoff W. D., Bishop F. C., Loijens M., Schoonmaker J. and Wollast R. (1983) Magnesian calcites; low-temperature occurrence, solubility and solid-solution behavior. *Rev Mineral Geochem* **11**, 97-144.

Morse J. W. and Arvidson R. S. (2002) The dissolution kinetics of major sedimentary carbonate minerals. *Earth Sci Rev* **58**, 51-84.

Morse J.W. and Mackenzie F.T. (1990) *Geochemistry of Sedimentary Carbonates*. Elsevier.

Morse J. W., Wang Q. and Tsio M. Y. (1997) Influences of temperature and Mg:Ca ratio on CaCO<sub>3</sub> precipitates from seawater. *Geology* **25**, 85-87.

Nancollas G. H. (1982) Phase transformation during precipitation of calcium salts. In *Biological Mineralization and Demineralization* (ed. G. H. Nancollas), pp. 79-99. Springer-Verlag.

Nancollas G. H., Sawada K. and Schuttringer E. (1983) Mineralization reactions involving calcium carbonates and phosphates. In: *Biomineralization and Biological Metal Accumulation* (ed. P. Westbroek and E. W. De Jong), 155-169.

Plummer L. N. and Mackenzie F. T. (1974) Predicting mineral solubility from rate data; application to the dissolution of magnesian calcites. *Am J Sci* **274**, 61-83.

Pokrovsky O. S. (1998) Precipitation of calcium and magnesium carbonates from homogeneous supersaturated solutions. *J Cryst Growth* **186**, 233-239.

Raz S., Weiner S. and Addadi L. (2000) Formation of high-magnesian calcites via an amorphous precursor phase: Possible biological implications. *Adv Mater.* **12**, 38-42.

Rushdi A. I., Pytkowicz R. M., Suess E. and Chen C. T. (1992) The effects of magnesium-to-calcium ratios in artificial seawater, at different ionic products, upon the induction time, and the mineralogy of calcium carbonate; a laboratory study. *Geol Rundsch Z Allg Geol* **81**, 571-578.

Thorstenson D. C. and Plummer L. N. (1977) Equilibrium criteria for two-component solids reacting with fixed composition in an aqueous phase; example, the magnesian calcites. *Am J Sci* **277**, 1203-1223.

Thorstenson D. C. and Plummer L. N. (1978) Equilibrium criteria for two-component solids reacting with fixed composition in an aqueous phase; example, the magnesian calcites; reply. *Am J Sci* **278**, 1478– 1488.

Walter L. M. and Morse J. W. (1984a) Magnesian calcite stabilities; a reevaluation. *Geochim Cosmochim Acta* **48**, 1059-1069.

Walter L. M. and Morse J. W. (1984b). Reactive surface area of skeletal carbonates during dissolution; effect of grain size. *J Sediment Petrol* **54**, 1081-1090.

Walter L. M. and Morse J. W. (1985) The dissolution kinetics of shallow marine carbonates in seawater; a laboratory study. *Geochim Cosmochim Acta* **49**, 1503-1513.

Zhang Y. and Dawe R. A. (2000) Influence of  $Mg^{2+}$  on the kinetics of calcite precipitation and calcite crystal morphology. *Chem Geol* **163**, 129-138.

## Chapter II

# **Authigenic carbonate formation in mud volcanoes “Mounds 11 and 12”, Costa Rica forearc**

### Abstract

Authigenic concretions retrieved from sediment cores collected in mud volcanos “Mounds 11 and 12” were examined for their isotopic and mineralogical composition. The  $\delta^{13}\text{C}$  and  $\delta^{18}\text{O}$  values of all concretionary carbonate samples are correlated. The range of  $\delta^{18}\text{O}$  values from 34.0 to 37.7 ‰ (V-SMOW) represents variable mixing situations between seawater and migrating fluids enriched in  $^{18}\text{O}$ , which probably derived from the deep subsurface. The  $\delta^{13}\text{C}$  values of the concretions show a wide range of  $\delta^{13}\text{C}$  values between -14.2 and -52.2 ‰ (V-PDB). The isotopically lighter concretions probably reflect significant contributions of oxidized methane as  $\text{CO}_2$  source, whereas the isotopically heavier concretions indicating the presence of heavier DIC presence in the fluids in which they were formed.

Both the occurrence of  $^{12}\text{C}$ -rich concretions ( $\delta^{13}\text{C}$  to -14.2 ‰; V-PDB) in aerobic sediments close to the bottom sea water and the obvious independence of  $^{12}\text{C}$  rich carbonate cementations from the present pore water geochemical conditions indicates authigenic carbonate formation at former times when migrating fluids of deep origin reached the surface sediment and created stimulating biogeochemical conditions to methane oxidizing biota.

Single concretions appear to be rather homogeneous in their isotope composition indicating similar temperature/water conditions and the same  $\text{CO}_2$  sources during concretion growth. Thus, it is believed that authigenic carbonates from mound 11 and 12 were most likely affected by deep source fluids during the different stages of their formation.

## 2.1 Introduction

### 2.1.1 Authigenic carbonates

Cold seep authigenic carbonates are archives of the past environmental and chemical conditions during the time of their formation. They are abundant in active and passive continental margins (Aloisi et al., 2000; Han et al., 2004; Paull et al., 2007; Stakes et al., 1999) and they can provide important information on local and regional tectonics and hydrodynamic conditions near the seafloor (Klaucke et al., 2008).

The chemical and isotopic composition of authigenic precipitates provide information about the changes in the composition of the hosting fluids in which they were formed. Stable carbon and oxygen isotope values of authigenic precipitates are commonly used to unravel the major processes and mechanisms of formation (Naehr et al., 2007; Peckmann et al., 2001).

Commonly, early diagenetic biogeochemical processes that play a basic role on formation of authigenic carbonates are the sulfate reduction of sedimentary organic matter (Claypool and Kaplan, 1974), the anaerobic oxidation of methane (AOM; Boetius et al., 2000) and the methane formation by CO<sub>2</sub> reduction (Whiticar and Faber, 1986). The transformation of organic matter to inorganic carbon provides dissolved inorganic carbon (DIC) with a characteristic <sup>13</sup>C imprint (Irwin et al., 1977). The DIC δ<sup>13</sup>C values of pore fluids affected by sulphate reduction, are negative to -25‰ (Meyers, 1994) and even lower δ<sup>13</sup>C values to -90‰ when they are affected by AOM (Schoell, 1980). However, positive δ<sup>13</sup>C carbonate values are characteristic for the methane generation by CO<sub>2</sub> reduction because of <sup>12</sup>C enrichment in the produced methane (Botz et al., 1996). At greater sediment depths thermocatalytic decarboxylation of organic matter can provide DIC enriched in <sup>12</sup>C.

The oxygen isotopic composition of carbonate minerals gives important information about the temperature of mineral formation and/or the oxygen isotope value of the fluid (e.g. Kim et al., 2007b; Kim and O'Neil, 1997; Tarutani et al., 1969). Hence, the δ<sup>18</sup>O values of authigenic carbonate are related to vari-

able sources of the pore water in which the carbonates precipitated. Isotopic composition of marine pore waters are influenced by shallow and/or deeper processes, e.g. early re-crystallisation of opal and carbonates, gas hydrate formation and decomposition (Ussler and Paull, 1995), hydration of volcanic ashes as well as clay mineral formation and dehydration (Dählmann and De Lange, 2003).

The Costa Rican forearc is characterized by numerous cold vent sites where authigenic carbonates are abundant (Hensen et al., 2004; Mörz et al., 2005a; Mörz et al., 2005b; Sahling et al., 2008; Schmidt et al., 2005). This forearc has been subject to numerous research activities over the last decade. Studies with respect to forearc structure and tectonics, gas hydrate occurrences, fluid migration processes, methane releases from the sea bottom and biological activities have been published (Han et al., 2004; Hensen and Wallmann, 2005; Hensen et al., 2004; Klauke et al., 2008; Linke et al., 2005; Mau et al., 2007; Mau et al., 2006; Moerz et al., 2005; Ranero et al., 2008; Sahling et al., 2008; Schmidt et al., 2005).

Although previous work tried to characterize authigenic carbonate concretions at the seafloor (Han et al., 2004), their complex origins and relations to modern vent fluids remained unknown. The present work deals with the formation of authigenic carbonates collected from mounds 11 and 12 (Fig. 2.1). Stable carbon and oxygen isotopic compositions of carbonate concretions are discussed in the light of interstitial water sources and diagenetic processes occurring in the sediments.

### **2.1.2 Study area and geological background**

Mounds 11 and 12 are located south-east of the Nicoya Peninsula, where the oceanic Cocos plate subducts at a rate of about  $8.8 \text{ cm}\cdot\text{yr}^{-1}$  beneath the Caribbean Plate (Kimura et al., 1997; Ranero and Von Huene, 2000). Off-shore Costa Rica the oceanic plate is characterized by four morphotectonic segments (Von Huene et al., 2000). From southeast to northwest these are: the oceanic crust of the Cocos Ridge followed by a “rough” segment containing numerous seamounts (Mounds 11 and 12 are located in this segment), the “smooth” oceanic crust generated at the Cocos-Nazca spreading centre and

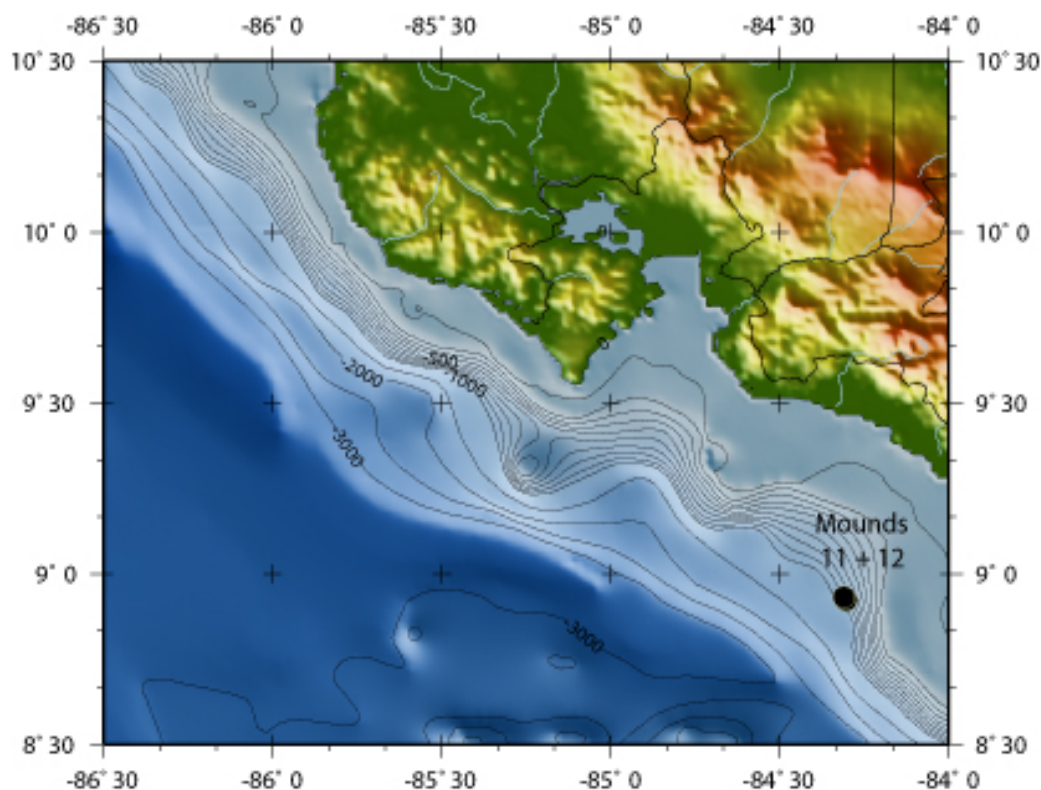


Figure 2.1: Bathymetric map of Costa Rica. Mud volcanoes “mounds 11 and 12” are indicated.

the “rough” oceanic crust generated at the East Pacific Rise (Sahling et al., 2008; Von Huene et al., 2000). These crustal domains bend differently into the Middle America Trench, and therefore the trench axis is only about 1 km deep at the crest of Cocos Ridge, increases to 3.5-km depth within the seamount province, and exceeds a depth of 5-km off Nicaragua (Von Huene et al., 2000).

Both mounds, 11 and 12, together with two additional mounds (mound Grillo and mound #103; Klaucke et al., 2008) are located ~32 km landward in a line parallel to the trench, at ~1000 m of water depth (Moerz et al., 2005; Sahling et al., 2008). The slope around the mounds is depressed and the two mounds are located at the downslope end of this depression. The slope steepens towards the trench (SW) and is cut by prominent canyons (Fig. 2.2).

Mound 11 is located in the southernmost part of the study area and has two distinct summits, reaching up to 25 m above the surrounding seafloor (Klaucke et al., 2008). The two summits of mound 11 are about 300 m apart and each of them composed of several individual edifices, each up to 250m in diameter (Klaucke et al., 2008). Gravity cores and video observation of mound 11 (Mörz et al., 2005a; Schmidt et al., 2005) show that it is covered by at least 2

m of fine-grained sediment and bacterial mats at both summits (Hensen et al., 2004; Mau et al., 2006; Schmidt et al., 2005).

Mound 12 is located slightly more than 1 km north of mound 11 and displays a completely different structure (Klaucke et al., 2008). Mound 12 consists of only one cone-shaped summit, with a diameter of 800 m and the side-scan sonar images presented by Klaucke et al. (2008) revealed a widening of this mound with increasing depth. Video observations (Linke et al., 2005; Mau et al., 2006), show the presence of bacterial mats, mytilid mussels and carbonate precipitates exposed to seawater (for details see Linke et al. (2005) and Mau et al. (2006)).

## 2.2 Sampling and analytical methods

### 2.2.1 Core sampling

Sampling at mounds 11 and 12 took place during several cruises with R/V Sonne (SO) and R/V Meteor (M), respectively M54 in 2002 (Soeding et al.,

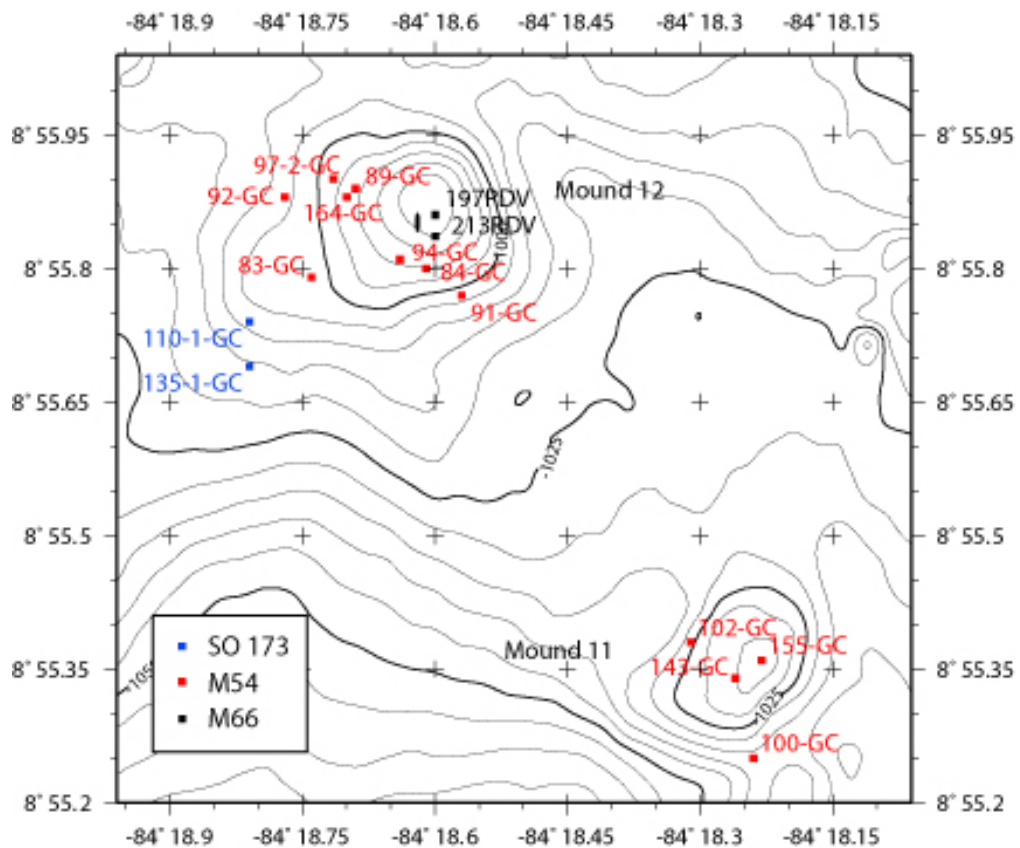


Figure 2.2: Bathymetric map of Mounds 11 and 12. Core locations are indicated.

2003), SO 173 in 2003 (Flüh et al., 2004) and M66 in 2005 (Brueckmann et al., 2008). Gravity cores (6m) were used for sampling. The location of the 15 cores used for the present work, core-length and water depth can be found in Table 2.1. Locations of the mounds and cores are shown in Fig. 2.2.

The sediment cores were cut in pieces of 1m and split on board into archive and working halves. The working parts were processed immediately for further pore water geochemical analyses (see Section 2.2.4).

Surface core sediments consist of silty to sandy clay (Mörz et al., 2005a; Schmidt et al., 2005). Vertical channels usually filled with very soft sediment appear in some cores (e.g. M54-84, 97/2). Some of the channels are filled with carbonate grains (millimeter-sized). Large, up to 10 cm size carbonate concretions (see description in Table 2.2), and carbonate grains (millimeter-sized) are abundant throughout the whole sediment depth. Cores M54-143 (119-126 cmbsf, soupy sediment), SO173-135/1(349-358 cmbsf, degassing bubbles), and M66-197 (318-348 cmbsf degassing bubbles) contained gas hydrate layers. Although millimeter-sized carbonate grains occur in several depths, the separation of the authigenic grains from the detrital carbonate grains after core sampling is difficult, magnifying the probability of carbonate chemistry misinterpretation. Thus, for the present work, authigenic carbonate concretions with diameters larger than 1cm were collected from the cores (Table 2.2).

Table 2.1: Location and depth of the gravity cores used for the present study.

<b>Cruise</b>	<b>Core No.</b>	<b>Core length (m)</b>	<b>Latitude N</b>	<b>Longitude W</b>	<b>Water depth (m)</b>	<b>Mound</b>
SO 173	110-1	6	8°55,68	84°18,62	1008	12
	135-1	6,5	8°55,69	84°18,81	1015	12
M54	84	2,8	8°55,80	84°18,61	980	12
	89	2,3	8°55,89	84°18,69	997	12
	91	2,8	8°55,77	84°18,57	1010	12
	92	2,8	8°55,88	84°18,77	1012	12
	94	4,7	8°55,81	84°18,64	994	12
	97-2	3,8	8°55,90	84°18,70	1001	12
	100	2,8	8°55,25	84°18,24	1044	11
	102	2,3	8°55,38	84°18,31	1039	11
	143	1,52	8°55,34	84°18,26	1019	11
	155	1,75	8°55,36	84°18,23		11
M66	164	2,9	8°55,69	84°18,82	1022	12
	197	3,5	8°55,36	84°18,80	1013	12
	213	2,5	8°55,85	84°18,60	980	12

### **2.2.2 X-ray diffraction (XRD measurements)**

Mineral composition of bulk concretions were determined by X-ray diffraction measurements (PW 1710/Philips, Co-K $\alpha$ , 0.02° s<sup>-1</sup>), between 2 and 80 degrees. XRD detection limit is about 2 % of the total mass of the crystalline materials. The d-104 peak has been used to determine the molar percentage of MgCO<sub>3</sub> in the crystal lattice of calcite (Goldsmith et al., 1961). The standard error is about  $\pm 1\%$  of the MgCO<sub>3</sub> content in the crystal lattice according to lab standards.

### **2.2.3 Carbonate content, organic carbon**

Total carbon (TC) was analyzed by combustion of bulk samples at 900°C (702-LI Ströhlein Instruments). Total inorganic carbon content (TIC) was measured with a Carbon Coulometer by sample treatment with phosphoric acid (20%). The precision of this method based on lab standards is  $\pm 2\%$ . Total organic carbon (TOC) was calculated by subtraction using the TC and TIC values measured.

### **2.2.4 Pore water analyses**

Sediment samples for pore water analyses were collected from all cores at intervals of 25-30 cm. Pore waters were squeezed using a pressure filtration system (nitrogen up to 5 bars, 0.2  $\mu\text{m}$  cellulose acetate membrane filters). Pore water samples were immediately analyzed for total alkalinity using the method of Ivanenkov and Lyakhin (1978). Total H<sub>2</sub>S was determined using standard photometric procedures (Grasshoff et al., 1999). Sulfate concentration of pore water was measured using ion chromatography (SYKAM with LCA A14 column, UV-detection) and chloride concentrations were determined by the Mohr-titration method (Grasshoff et al., 1999). Dissolved major elements in pore waters have been analyzed with ICP-AES.

Bulk sediment samples were taken for CH<sub>4</sub> analysis by 3 ml syringes and injected into 24 ml septum vials containing 9 ml of concentrated NaOH solution. After closing and subsequent shaking, methane is enriched in the headspace of

Table 2.2a: Mineralogy and stable isotope composition of carbonate concretions and from mound 12. The total organic carbon (TOC) and total carbonate content (CaCO<sub>3</sub>) are also given.

Cruise/core	Depth (cm)	Mineralogy	Description*	$\delta^{13}\text{C}$ ‰ (V-PDB)	$\delta^{18}\text{O}$ ‰ (V-SMOW)	CaCO <sub>3</sub> %	TOC %
SO173/110-1	2-5	Aragonite	4,8 cm (1)	-41,62	34,14	38	1,66
SO173/110-1	50-60	Aragonite	10.4 cm (1)	-49,41	34,03	38	
SO173/110-1	60-63	Aragonite	3.4 cm (1)	-46,72	34,30	23	1,62
SO173/135-1	70	HMC (17%)	~1 cm (2)	-47,46	35,09	50	0,94
SO173/135-1	220	HMC (17%)	~1 cm (2)	-48,91	35,38	47	1,57
SO173/135-1	260	HMC (16%)	2 cm (2)	-47,33	34,84	50	0,79
M54/84	13-16	HMC (17%)	7 cm (3)	-28,14	36,31	75	1,57
M54/84	135-138	HMC (14%)	4.3 cm (1)	-31,49	36,08	64	0,34
M54/84	162	HMC (17%)	4.5 cm (2)	-36,36	35,86	48	0,76
M54/84	266-271	HMC (17%)	5 cm (3)	-26,29	36,94	50	0,53
M54/89	3-10	HMC (17%)	6.4 cm (1)	-48,24	35,33	72	0,94
M54/89	36	HMC (18%)	1.6 cm (2)	-49,70	35,47	49	1,25
M54/89	217	HMC (19%)	3.4 cm (3)	-42,83	35,82	59	0,6
M54/91	303	HMC (18%)	1.5 cm (2)	-44,60	35,65	47	0,68
M54/92	74-76	Aragonite, HMC (20%)	4.3 cm (3)				
				-43,36	35,24	69	1,15
M54/92	125	Aragonite, HMC (16%)	~1 cm (2)				
				-46,89	35,00	48	0,86
M54/92	138	HMC (17%)	~1 cm (2)	-49,03	35,37	56	0,6
M54/92	150	HMC (17%)	4.7 cm (1)	-48,91	35,37	72	0,34
M54/92	170	HMC (19%)	3.5 cm (3)	-47,96	35,23	61	0,92
M54/92	230	HMC (18%)	8.4 cm (1)	-52,16	35,15	69	
M54/94	53	HMC (18%)	1.8 cm (1)	-33,05	36,45	68	0,63
M54/94	144	HMC (16%)	3 cm (3)	-29,81	36,40	63	1,17
M54/94	208	HMC (16%)	1.5 cm (2)	-26,70	37,05	54	0,64
M54/94	322	Aragonite, HMC (14%)	2 cm (2)				
				-24,56	37,10	49	1,28
M54/97-2	111	Aragonite, HMC (18%)	2.2 cm (2)				
				-48,76	35,90	72	0,14
M54/97-2	160	Aragonite, HMC (17%)	4.2 cm (3)				
				-40,23	35,27	70	0,94
M54/97-2	165	HMC (18%)	7 cm (1)	-38,44	35,37	66	
M54/97-2	170	HMC (18%)	5.8 cm (1)	-51,37	35,47	49	1,72
M54/97-2	175	HMC (15%)	4.5 (3)	-46,91	35,58	63	0,96
M54/97-2	353	Aragonite	1.9 cm (2)	-46,78	34,70	63	0,33
M54/164	155	HMC (16%)	3 cm (1)	-51,65	35,15	57	0,13
M66/197	62	HMC (17%)	4.5 cm (3)	-36,22	36,49	67	0,65
M66/197	96	HMC (18%)	3.8 cm (1)	-30,26	36,11	41	1,76
M66/197	112	HMC (17%)	4,2 cm (3)	-39,46	36,27	58	0,52
M66/197	261	HMC (17%)	2,6 cm (1)	-35,56	36,17	63	0,64
M66/213	top	Aragonite	5.8 cm (3)	-41,70	35,05	75	0,75

\* (1) tubular, (2) roundish (3) irregular spheres

the vial. Onboard determination of methane was performed using a Shimadzu GC14A gas chromatograph (4m 1/8' SS column, Porapack Q-50/80 mesh-, FID-detector). All analytical procedures applied on board of research vessels and at GEOMAR laboratories are documented in detail at [http://www.geomar.de/zd/labs/labore\\_umwelt/Meth\\_englisch.html](http://www.geomar.de/zd/labs/labore_umwelt/Meth_englisch.html). Detailed results for pore water geo-chemical parameters and organic carbon and carbonate content of sediments can be found in the Appendix.

Table 2.2b: Mineralogy and stable isotope composition of carbonate concretions and from mound 11. The total organic carbon (TOC) and total carbonate content (TC) are also given.

## Authigenic carbonate mineral formation in Costa Rica forearc

Cruise/co re	Depth (cm)	Mineralogy	Descrip- tion*	$\delta^{13}\text{C}$ ‰ (V-PDB)	$\delta^{18}\text{O}$ ‰ (V- SMOW)	$\text{CaCO}_3$ %	TOC %
M54/100	135	HMC (17%)	2 cm (2)	-26,58	36,70	53	0,76
M54/102	104	HMC (17%)	2.2 cm (3)	-26,80	37,68	62	0,76
M54/102	143	Aragonite, HMC (14%)	1.6 (2)	-28,32	36,48	44	1,6
M54/102	170	HMC (16%)	5 cm (3)	-24,44	37,39	70	0,34
M54/143	87	Dolomite	4 cm (3)	-14,20	37,65	77	0,51
M54/143	125	HMC (16%)	4.2 cm (2)	-25,52	36,31	29	2,2
M54/155	45	Aragonite	~1 cm (2)	-25,31	35,89	65	0,47
M54/155	90	HMC (17%)	~1 cm (2)	-17,99	36,98	65	0,56
M54/155	100	HMC (16%)	~1 cm (2)	-15,36	36,41	77	0,45

\* (1) tubular, (2) roundish (3) irregular spheres

### 2.2.5 Microscopy

Six thin-sections of selected rock samples were prepared and observed with a petrographic microscope. Microstructures of authigenic carbonates (6 samples) were observed using an electron microscope (Cam Scan CS 44, 15-20kV). The samples were prepared by dispersion onto a carbon film fixed on a steel mounting and gold-palladium coating was applied on the subsamples. Energy Dispersive X-ray (EDX) spectroscopy has been used to examine the chemical composition of selected spots on the carbonate concretions.

### 2.2.6 Stable isotope analyses

Carbonate samples were reacted with water-free (100%) phosphoric acid at 73°C in an online Carbo-Kiel carbonate preparation line. Carbon and oxygen isotope ratios of liberated  $\text{CO}_2$  were measured with a Finnigan MAT 251 IR-MS spectrometer. All data were calibrated against V-PDB standard. The standard deviation, based on replicate analyses of the standard (NBS-19) was about  $\pm 0.01\text{‰}$  for carbon and  $\pm 0.02\text{‰}$  for oxygen.

Stable oxygen isotope ratios of pore water samples were determined using the standard  $\text{CO}_2$  equilibration technique (Craig, 1961). Precision was 0.6 ‰ using lab standards. The  $\delta^{18}\text{O}$  values of liquid samples are reported relative to Standard Mean Ocean Water (V-SMOW). The  $\delta^{13}\text{C}$  values of methane were measured with a Finnigan MAT 251 isotope ratio mass spectrometer after gas chromatographic separation and combustion of  $\text{CH}_4$  (CuO-oven) to  $\text{CO}_2$  (Faber et al., 1998). Reproducibility of carbon isotope analysis is  $\pm 0.5\text{‰}$  for methane. The data are reported relative to the V-PDB standard.

## 2.3 Results

### 2.3.1 Fluid geochemistry

According to their geochemical profiles, the cores obtained from different sites can be split in two groups. In group A cores (e.g. M54-84, 91, 92, 100 and 102) the chemical composition of fluids is almost constant with depth and the geochemical values are similar to bottom sea water (as a representative of this group the core M54-100 is shown in Fig. 2.3). In group B sediment cores (e.g. M54-89, 94, 97/2, 143, 155, 164, SO173-110/1, 135/1, M66-197, 213) pore water concentrations at a depth range between 40 and 350 cm deviate significantly from bottom seawater values (two representative cores of this group, M54-155 and M66-197, are shown in Fig. 2.3).

Pore waters of group B cores are depleted in SO<sub>4</sub> at variable depths below the sediment surface (Fig. 2.3). Parallel, an increase in alkalinity is observed (Fig. 2.3). Alkali earth (Ca, Mg, Sr) concentrations are generally depleted below the depth of maximum alkalinity (Fig. 2.3). With exception of group A cores and M54-164 boron concentrations increase with depth (M54-155 and M66-197, Fig. 2.3). In cores M54-97/2, 134, 155, M66-197 and 213 Cl concentrations are reduced compared to seawater concentrations with increasing core depth.

Results of  $\delta^{18}\text{O}$ , and  $\delta^{13}\text{C-CH}_4$  from selected pore water samples from mounds 11 and 12 are summarized in Table 2.2. However it has here to be mentioned that several of the presented pore water data in Table 2.2 were not extracted from the same cores were the examined carbonate concretion sampled, but are used to present an overview image of the pore water chemistry in the area. For mound 11, the  $\delta^{18}\text{O}$  values of measured pore waters range between 1.97 to 4.72 ‰ (V-SMOW), whereas in mound 12 the measured values are significantly lower ranging from -0.80 to 1.06 ‰ (V-SMOW). The pore water methane  $\delta^{13}\text{C}$  values are -42.2 ‰ (V-PDB) at mound 11, whereas at mound 12  $\delta^{13}\text{C-CH}_4$  range between -100.8 and -50.3 ‰ (V-PDB).

## Authigenic carbonate mineral formation in Costa Rica forearc

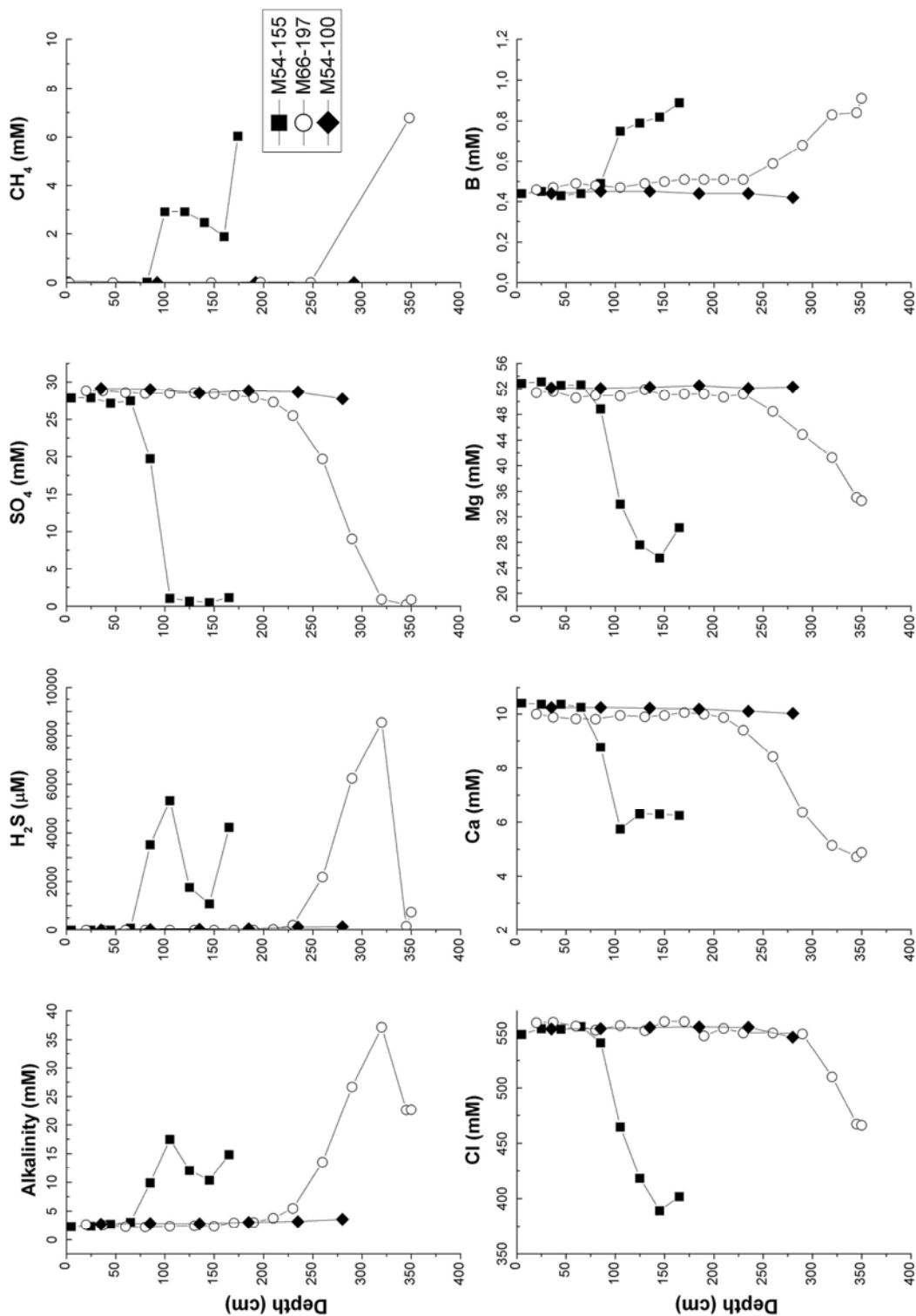


Figure 2.3: Pore water profiles of alkalinity, H<sub>2</sub>S, Cl, SO<sub>4</sub>, B, Ca, Mg, Sr at selected gravity cores of Mounds 11 and 12.

### 2.3.2 Petrography, mineralogy and carbonate content of concretions

The  $\text{CaCO}_3$  and TOC contents of concretions range between 23 % - 77 % (Table 2.2) and 0.1 - 2.2 % (Table 2.2), respectively.

The XRD results show that the examined concretions are similar to the host sediment and consist mainly of high Mg-calcite (HMC, 14-20 mol %  $\text{MgCO}_3$ ) occasionally with some aragonite (Table 2.2). Only one concretion contained dolomite. The minerals of the insoluble residue consist of quartz, clay minerals and feldspar which were not quantified.

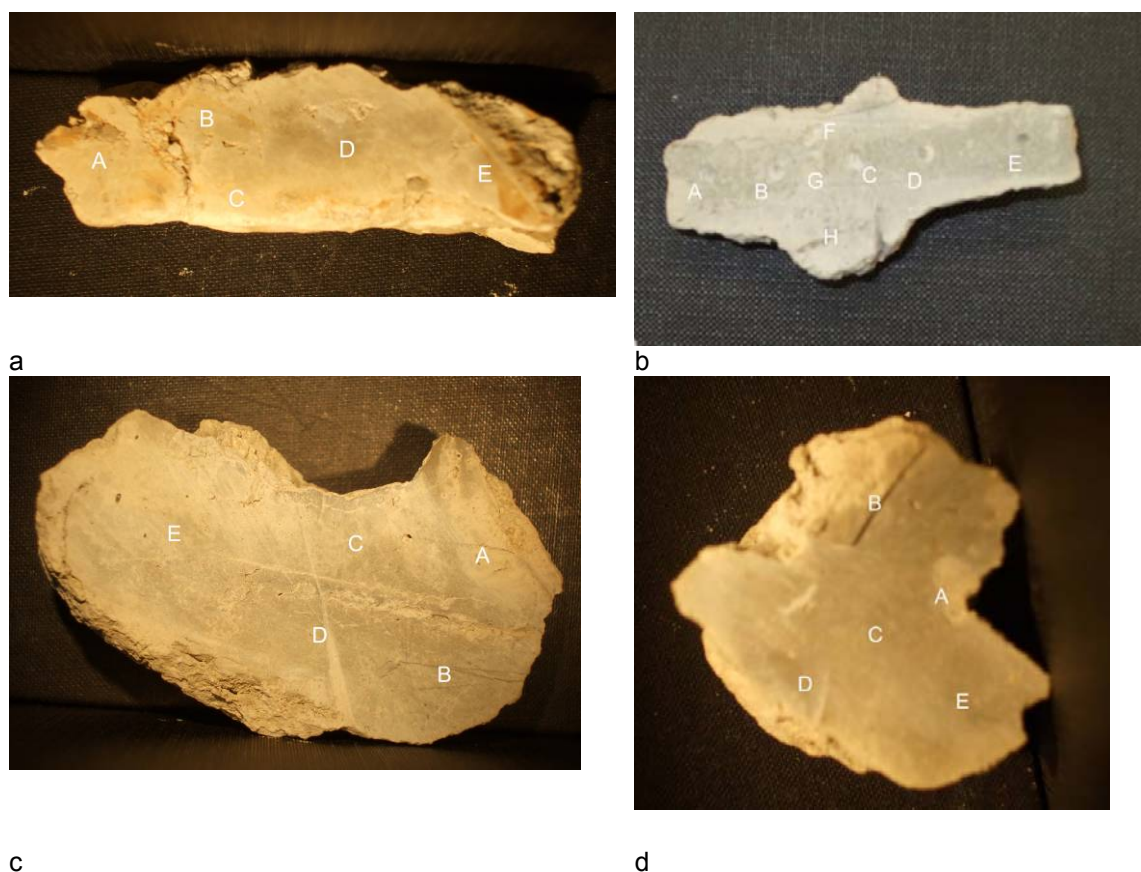


Plate 2.1: High resolution sampling for isotopic analyses of selected carbonate concretions (retrieval depth and sample length are indicated). a: M54-89 (3-10cm; 6.4 cm) b:M54-92 (230cm; 8.4 cm vertical placed in the sediment) c: M54-97/2 (165cm; 7 cm vertical placed in the sediment) d:M66-197 (62cm; 4.5 cm).

The examined concretions (Plate 2.1) are carbonate-cemented and lithified sediment. Their shapes differ from almost round nodules of about one cm in diameter to elongated spherical structures up to 10 cm in length (Plate 2.1, a-d). SEM observations showed carbonate crystals of  $\mu\text{m}$ -size grown on

detrital sediment grains (Plate 2.2, c-f). Si-phases consist of biogenic silica (identified by SEM) and quartz (Plate 2.2 f). Bedding was not observed. Thin sections (Plate 2.2 a-b) reveal occasionally fossils of foraminifera immersed in a fine grained sediment matrix.

Table 2.3:  $\delta^{18}\text{O}$ ,  $\delta^{13}\text{C}\text{-CH}_4$ ,  $\delta\text{D}$ , CI and B values of pore water from selected cores, at mounds 11 and 12.

	Core	Sample depth (cm)	CI (mM)	B (mM)	$\delta^{18}\text{O}\text{-H}_2\text{O}$ (V-SMOW)	$\delta^{13}\text{CH}_4\text{-H}_2\text{O}$ (V-PDB)
Mound 11	M54-143	125	490,42		-	
	M54-155	165	401,92	0.75	2,01	-42.211
	M54-137/1	7	267,28	1.51	3,05	
	M54-138	22,5	212,01	1.79	4,72	
	M54-109	205	402,56	0.81	1,97	
	M54-136/2	205	263,60	1.40	2,90	
	M54-143	152	260,55	1.03	4,04	
Mound 12	SO-173/127	22	225,11	1.89	3,78	
	M54-163/3	22	557,83	0.43	0,35	-100.768
	M54-97/2	370	360,62	0.56	1,06	
	M54-164	260	561,18	0.35	0,30	
	M66-197	348	466.26			-56.659
	M66-213	247	247.71			-50.277
	SO173-115	575	510,76	0.44	-0,61	-77.702
	SO173-118	32	558,71	0.36	-0,80	
SO173-135/1	540	517,31	0.4	-0,53		

### 2.3.3 Stable isotopic composition of concretions

The results of stable oxygen and carbon isotope measurements of the concretions can be found in Table 2. The carbonate samples from mound 11 have  $\delta^{13}\text{C}$  values ranging from -28.3 ‰ to -14.2 ‰ V-PDB. The  $\delta^{18}\text{O}$  values range between 35.89 ‰ and 37.68 ‰ V-SMOW. Mound 12 samples display a wider range of carbon isotope values between -52.2 ‰ and -24.6 ‰ (V-PDB) and their oxygen isotope values range between 34.03 ‰ and 37.10 ‰ (V-SMOW) respectively.

Sub-samples along profiles of selected concretions (Table 2.4 and Plate 2.1), show small variations in the  $\delta^{18}\text{O}$  values (max. 0.12). The  $\delta^{13}\text{C}$  values of these carbonate profiles, however, show larger variations between 3‰ and 11‰.

## 2.4 Discussion

### 2.4.1 Pore fluid geochemistry

Pore water chemical compositions of group A cores do not show differences from current seawater composition. Furthermore, the organic content and porosity of the group A core sediments sampled in both mounds 11 and 12 (Appendix) do not show significant differences compared to the sediments in cores of group B. Thus it is indicated that the differences in the pore water geochemical profiles are controlled by factors other than the geological settings of the area.

In group B cores, the depth of minimum sulphate concentration within the sediments, occurs between 75 and 415 cmbsf (Appendix). Parallel, a strong increase in alkalinity (more than 35 mM), produced at least partly through bicarbonate production during sulfate reduction, is observed in the upper meters of the sedimentary column. Alkalinity increase is usually accompanied by a drastic decrease in  $\text{Ca}^{2+}$  concentration (less than 3 mM) indicating calcium carbonate precipitation. At the base of the sulphate reduction zone the beginning of anaerobic oxidation of methane (AOM) can be assumed (Boetius et al. 2000). Depletion of  $\text{Cl}^-$ , a geochemical conservative element, occurs over depth denoting freshening of pore fluids. The observed gradients of all dissolved compounds (Fig. 2.3) and their correlation versus  $\text{Cl}^-$  concentrations over depth (Fig. 2.4), are explained by freshening through deep-source migrating fluids mixing with bottom seawater (Hensen et al., 2004; Schmidt et al., 2005). The increase of B-concentration with depth shows that the likely deep-sourced possible fluid is enriched in this element (Dählmann and De Lange, 2003; Hensen et al., 2007).

Gas hydrates, a possible freshwater source, have been reported to occur in the area (Hesse et al., 1985; Schmidt et al., 2005). At the conditions occurring in the study area at ~1000 m water depth (~5 °C, ~100 bars) gas hydrates are stable at seafloor (Schmidt et al., 2005) and hence today they probably not act as a major “fresh water” source. However, destabilization of gas hydrates during sampling, could possibly result in somewhat reduced concentrations of dissolved species. The dilution effect would be recorded in all the geochemical

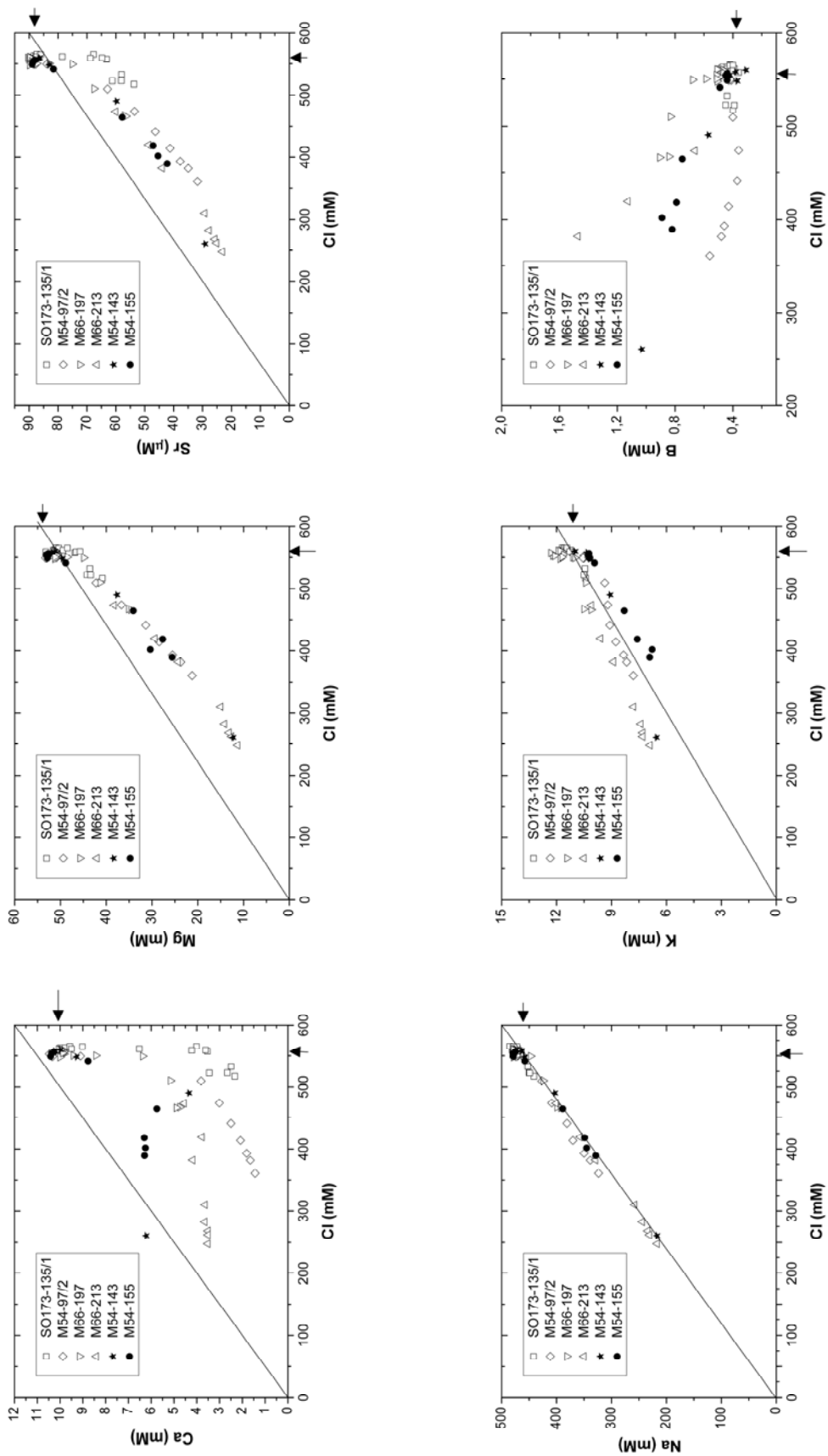


Figure 2.4: Diagrams showing Cl vs. Ca, Mg, Sr, Na, K and B from selected cores of mound 11 (closed symbols) and of mound 12 (open symbols). Trend lines indicate linear mixing between seawater and freshwater. Seawater values are indicated.

parameters of pore waters however, but not selectively to a few (Appendix). Furthermore, an in situ gas hydrate destabilization due to increased temperature should not be considered impossible under special occasions. Schmidt et al., (2005) presented data of higher, almost double, heat flow fluxes on the summit of Mound 11 compared to the background regional heat flux, which however were interpreted by the same authors to most probably indicate the result of “heat memory” of the mud (Vogt and Sundvor, 1996), reflecting past mud eruption events.

According to Hensen et al. (2004) other possible fluid sources that could explain the observed dilution, is the negative correlation of  $\delta D$  and  $\delta^{18}O$  values presented in their work, which is typical for clay mineral dehydration, most likely smectite to illite transformation (Dählmann and De Lange, 2003; Sheppard and Gilg, 1996). The same authors have also suggested that water produced from smectite to illite transformation in the area is significantly affecting the  $^{18}O$  composition of mound 11 pore fluids (Hensen et al., 2004). Furthermore, pore water samples collected from both mounds show a negative correlation of  $Cl^-$  concentrations with the  $\delta^{18}O$  values (Fig. 5). It has also to be note here that pore water samples enriched in  $B^-$  are correlating well with the respective “heavier”  $^{18}O$  values, a feature typical for fluids produced during smectite to illite transformation (You et al., 1995).

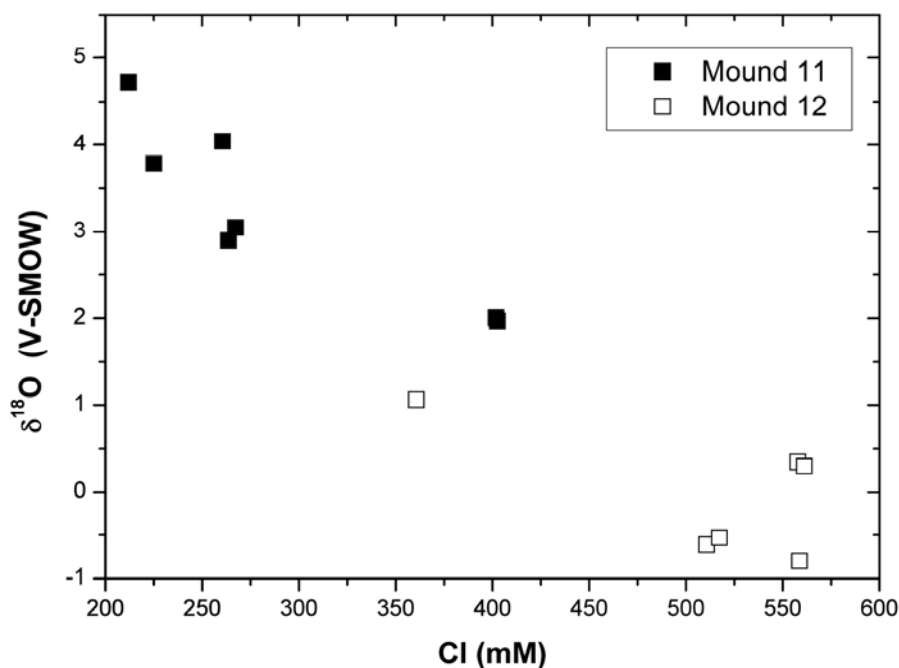


Figure 2.5:  $\delta^{18}O$ -H<sub>2</sub>O vs. Cl values from various sediment cores of mounds 11 and 12 area.

The pore water freshening controls the linear relation of components like Na and K vs. Cl (Fig. 2.4). However, Mg and Sr are consistently below the expected dilution line. Hydration of volcanic ashes, which are abundant in the area (Schacht et al., 2008), resulting in clay mineral formation, could very likely reduce alkali earth element concentrations in pore waters. The incorporation of Mg in calcite (Morse et al., 1997) and Sr in aragonite crystal lattice (Tang et al., 2008) could explain partially the removal of these elements from the pore fluids, however the role of this mechanism in the reduction of dissolved Mg and Sr in pore waters should be considered rather limited.

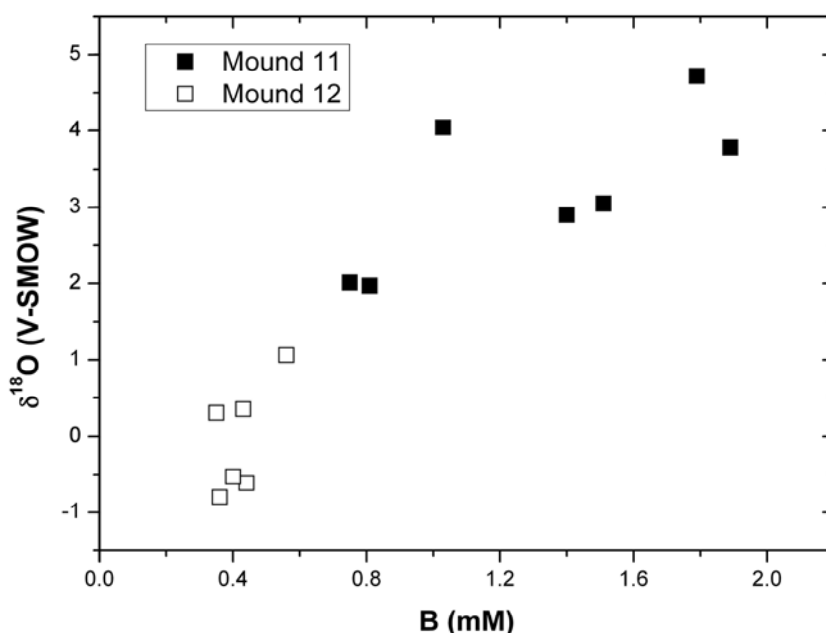


Figure 2.6:  $\delta^{18}\text{O}\text{-H}_2\text{O}$  vs B concentrations from various cores of mounds 11 and 12

#### 2.4.2 Occurrence, mineralogy and stable oxygen- and carbon isotope composition of authigenic carbonate concretions

Authigenic carbonate concretions in sediment cores from mounds 11 and 12 occur between 3 and 353 cmbsf (Table 2.2). The major carbonate mineral phase in the study area is high Mg-calcite (14-20 mol %  $\text{MgCO}_3$ ), and only 12 samples contain mixtures of HMC with aragonite (Table 2.2). Although the

mechanism controlling the HMC formation in the area has not been understood, the  $Mg^{2+}$  contents in HMC concretions sampled at various depths within the

Table 2.4:  $\delta^{13}C$  and  $\delta^{18}O$  values of profiles across individual concretions.

Sample	Depth (cm)	$\delta^{13}C$ (V-PDB)	$\delta^{18}O$ (V-SMOW)
M54/89a	3-10	-48,24	35,33
M54/89b		-46,59	35,19
M54/89c		-49,93	35,34
M54/89d		-46,86	35,06
M54/89e		-46,74	35,28
M54/92a	230	-52,16	35,16
M54/92b		-51,87	35,54
M54/92c		-51,93	35,26
M54/92d		-52,18	35,27
M54/92e		-51,77	35,03
M54/92f		-52,62	35,16
M54/92g		-52,19	35,02
M54/92h		-50,86	35,16
M54/97-2a	165	-38,44	35,37
M54/97-2b		-44,35	35,58
M54/97-2c		-39,31	35,42
M54/97-2d		-36,55	35,58
M54/97-2e		-47,56	35,64
M66/197a	62	-36,22	36,49
M66/197b		-37,3	35,97
M66/197c		-37,31	35,94
M66/197d		-36,66	35,87
M66/197e		-36,05	35,77

same sediment core do not show significant differences (max 6%, Table 2.2) suggesting similar pore water composition and formation conditions of HMC. The  $MgCO_3$  content in the samples is comparable with that of methane derived HMCs from deep eastern Mediterranean Sea (12%) (Aloisi et al., 2000), Oregon/Washington subduction zone (12%) (Ritger et al., 1987), Costa Rica margin (14%) (Han et al., 2004) and the Guayamas Basin (8-20%) (Paull et al., 2007). However, it still remains unclear why sometimes HMC-aragonite mixtures or pure aragonite precipitated from the sediment pore-waters (Burton, 1993)

A plot of  $\delta^{13}C$  vs.  $\delta^{18}O$  values of bulk carbonates result in a regression line (Fig. 2.7). The more  $^{13}C$  rich concretions ( $\delta^{13}C$  values  $> -30$  ‰) at mound 11 have also the most positive  $\delta^{18}O$  values up to 37.68 ‰ (V-SMOW), whereas mound 12 concretions have “lighter” carbon composition and less positive  $\delta^{18}O$  values. Moreover, in Fig. 2.7 a group of samples retrieved from the SE of the summit of mound 12 (cores M54-84, 94, M66-197 and 213) show intermediate

values for both stable carbon and oxygen isotopes, which may indicate mixing of end-member fluids with characteristic isotopic compositions.

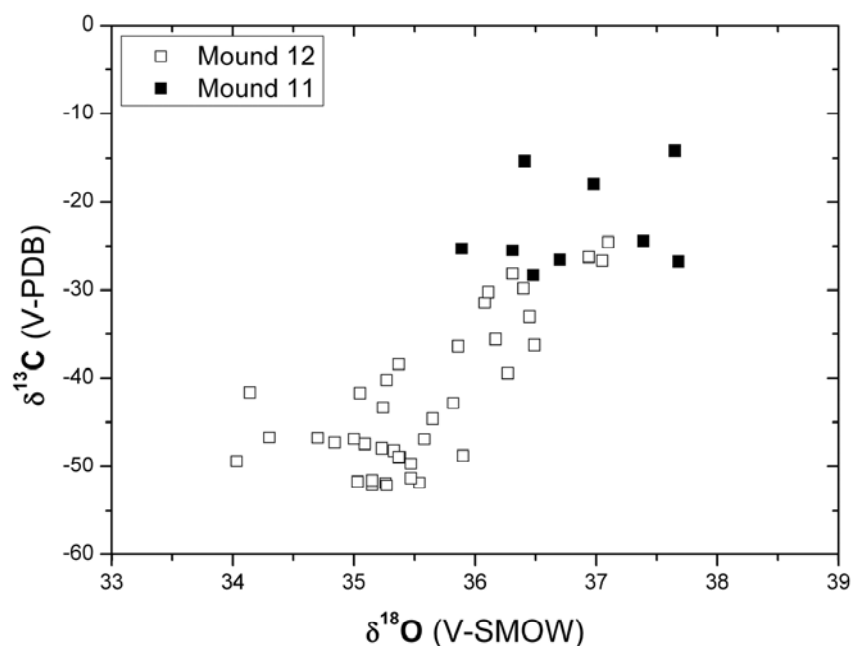


Figure 2.7:  $\delta^{13}\text{C}$  vs  $\delta^{18}\text{O}$  values of carbonate concretions collected at mounds 11 and 12.

#### 2.4.2.1 Stable oxygen isotope values of concretions

The stable oxygen isotope values of the concretions have a maximum range of 4 ‰ where the  $\delta^{18}\text{O}$  isotope profile measurements (Table 2.4) of selected concretions do not show significant  $\delta^{18}\text{O}$  variations. This indicates concretionary carbonate precipitation at similar pore water oxygen isotope values and constant sediment temperature.

Combining the measured  $\delta^{18}\text{O}$  value of pore waters (Table 2.3) from specific cores in Mound 11 and 12 and the  $\delta^{18}\text{O}$  value of mono-mineralic carbonate concretions (Table 2.2), and applying well established carbonate-water oxygen isotope fractionation equations for the individual mineral (Mg-calcite: (Tarutani et al., 1969) aragonite: (Kim et al., 2007a)) the carbonate formation temperatures can be estimated. All calculated isotope temperatures of carbonate formation range between  $<0$  and  $18\text{ }^{\circ}\text{C}$  (Table 2.5). Carbonates from mound 12 cores have calculated isotope formation temperatures between  $<0$  and  $8\text{ }^{\circ}\text{C}$  whereas the temperatures of carbonate formation in mound 11 sediments were calculated between  $2$  and  $18\text{ }^{\circ}\text{C}$ . However, the numerous minimum isotope

Table 2.5: Formation temperatures for carbonate concretions of Mounds 11 and 12 and  $\delta^{18}\text{O}$  pore water values at formation temperature of  $5^\circ\text{C}$ . The actual formation temperature in selected cores was based on the measured  $\delta^{18}\text{O}$  value of pore water presented in Table 3. The minimum and maximum  $\delta^{18}\text{O}$  values used, for the calculations are 1.1 and 4.7 ‰ and -0.8 and 2 ‰ (V-SMOW) for mounds 11 and 12 respectively. For the calculations the proposed equation of Tarutani et al., (1969) for Mg-calcite and Kim et al., (2007a) for aragonite were used.

Cruise/core	Depth (cm)	Mineralogy	Actual Temperature ( $^\circ\text{C}$ )	Min. Temperature ( $^\circ\text{C}$ )	Max. Temperature ( $^\circ\text{C}$ )	$\delta^{18}\text{O}$ ‰ (V-SMOW)
SO173/110-1	2-5	Aragonite		0	8	0.4
SO173/110-1	50-60	Aragonite		0	8	0.3
SO173/110-1	60-63	Aragonite		-1	7	0.6
SO173/135-1	70	HMC (17%)	1	0	7	0.4
SO173/135-1	220	HMC (17%)	0	-1	6	0.7
SO173/135-1	260	HMC (16%)	2	1	8	0.2
M54/84	13-16	HMC (17%)		-4	3	1.6
M54/84	135-138	HMC (14%)		-4	3	1.6
M54/84	162	HMC (17%)		-2	5	1.2
M54/84	266-271	HMC (17%)		-6	1	2.2
M54/89	3-10	HMC (17%)		0	7	0.7
M54/89	36	HMC (18%)		-1	6	0.7
M54/89	217	HMC (19%)		-2	4	1.0
M54/91	303	HMC (18%)		-1	6	0.9
M54/92	138	HMC (17%)		-1	6	0.7
M54/92	150	HMC (17%)		-1	6	0.7
M54/92	170	HMC (19%)		-0	7	0.4
M54/92	230	HMC (18%)		0	7	0.4
M54/94	53	HMC (18%)		-4	3	1.7
M54/94	144	HMC (16%)		-4	2	1.8
M54/94	208	HMC (16%)		-7	0	2.4
M54/97-2	165	HMC (18%)	7	-0	7	0.6
M54/97-2	170	HMC (18%)	6	-1	6	0.8
M54/97-2	175	HMC (15%)	5	-1	5	0.9
M54/97-2	353	Aragonite	5	-2	5	1.0
M54/100	135	HMC (17%)		5	16	2.0
M54/102	104	HMC (17%)		2	12	2.9
M54/102	170	HMC (16%)		2	13	2.7
M54/143	125	HMC (16%)	15	6	18	1.6
M54/155	45	Aragonite	5	4	17	2.1
M54/155	90	HMC (17%)	4	4	15	2.3
M54/155	100	HMC (16%)	6	6	17	1.8
M54/164	155	HMC (16%)		0	7	0.6
M66/197	62	HMC (17%)		-3	4	1.4
M66/197	96	HMC (18%)		-4	2	1.8
M66/197	112	HMC (17%)		-4	3	1.6
M66/197	261	HMC (17%)		-3	3	1.5
M66/213	top	Aragonite		-4	4	1.3

temperatures ( $<0^\circ\text{C}$  in Table 2.5) represent unlikely temperatures of carbonate formation in young marine sediments. On the other hand generally low maximum isotope formation temperatures agree very well with both measured bottom water and sediment temperatures ( $4.5\text{-}5.0^\circ\text{C}$ ; Linke et al., 2005; Schmidt et

al., 2005; Table 2.5: this study). This indicates concretionary carbonate formation during early stage of diagenesis at low temperature between 0 and 18 °C at changing pore water isotope compositions (see discussion below).

#### 2.4.2.2 Stable carbon isotope values of concretions

The stable carbon isotope compositions of authigenic carbonate materials (crusts, nodules, carbonatic cementations of sediment) in surface sediments of mounds 11 and 12 are negative between -14.2 ‰ and -52.2 ‰ (V-PDB). Normal marine carbonates which formed from ocean water near isotopic equilibrium (not regarding possible minor “vital” effects) with atmospheric CO<sub>2</sub> have  $\delta^{13}\text{C}$  values near 0 ‰. In contrast to those primary shell materials formed from atmospheric CO<sub>2</sub> source (equilibrated with the major ion HCO<sub>3</sub><sup>-</sup> in sea water), the observed negative carbon isotope values of lithified carbonatic materials from mounds 11 and 12 indicate significant contributions of organically-derived carbon during authigenic carbonate precipitation. CO<sub>2</sub> forms from anaerobic oxidation of organic matter during early diagenesis in organic-rich sediments (e.g. mounds 11 and 12 have organic carbon contents between 0.9 and 1.7 %; Table 2.2; Schmidt et al., 2005). For instance bacterial SO<sub>4</sub> reduction produces carbon isotope values of CO<sub>2</sub> as negative as -20 ‰ (Meyers, 1994). Even more negative carbon isotope values of -60 to -100 ‰ are typical for CO<sub>2</sub> formed by anaerobic CH<sub>4</sub> oxidation (Schoell, 1980). The relative enrichment of the light <sup>12</sup>C isotope in the produced CO<sub>2</sub> is the result of a kinetic carbon isotope fractionation effect associated with the bacterial processes. Although the carbon isotope values of the carbonate cementations of mound 11 and 12 sediments does not reach such negative values near -100 ‰ the negative values between approximately -25 and -50 ‰ indicate a mixed carbon source where CO<sub>2</sub> probably also derived from anaerobic bacterial oxidation of hydrocarbons (see below). Fig. 2.7 and Table 2.2 show that the  $\delta^{13}\text{C}$  values of the authigenic carbonates from mound 12 (which is most likely the older and less active mound; Klauke et al., 2008) cover a relatively large range of values (between -24.6 and -52.2 ‰). Furthermore the  $\delta^{13}\text{C}_{\text{carbonate}}$  values of mound 12 samples are on average more negative compared with the young and active mound 11 (Klauke et al., 2008). It should be noted that not only the  $\delta^{13}\text{C}$ -values of authigenic car-

bonates from mounds 11 and 12 differ but also pore water acid-titrated alkalinities (Appendix)

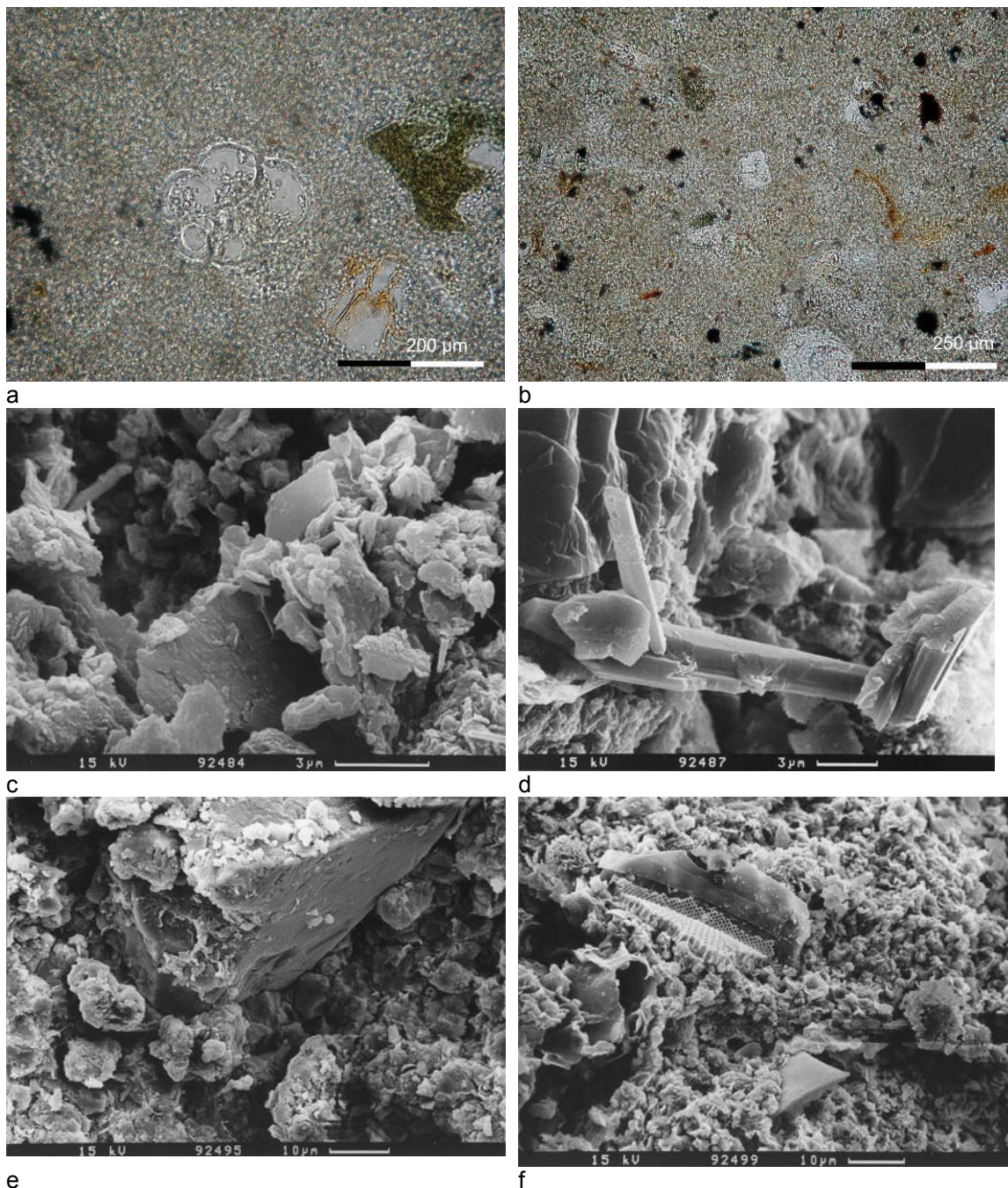


Plate 2.2: Thin sections (a, b) and scanning electron micrographs (c,d,e,f) of carbonate concretions. a: Re-crystallized shell surrounded by fine-grained cement. b: Grains of authigenic dolomite c: Carbonate grains d: Aragonite needle e: Grain of detrital sediment covered by authigenic carbonate overgrowths f: Fragment of siliceous fossil embedded in authigenic carbonate.

and the amount of authigenic carbonate are significantly lower in sediments from mound 11. That is the reason why only 9 carbonate samples could be taken from mound 11 surface sediments. These authigenic carbonates from mound 11 sediments have  $\delta^{13}\text{C}_{\text{carbonate}}$  values between -15.4 and -28.3 ‰ (Ta-

ble 2.2). Similar to those  $\delta^{13}\text{C}_{\text{carbonate}}$  values also the  $\delta^{13}\text{C}_{\Sigma\text{CO}_2}$  values of mound 11 are relatively “heavy” between -23.9 and -11.6 ‰ (Füri et al., 2010). However, the  $\delta^{13}\text{C}_{\Sigma\text{CO}_2}$  values of mound 12 are “lighter” and range between -68.2 and -60.3 ‰ (Füri et al., 2010) which is in the order of magnitude regarded as being typical for anaerobic bacterial oxidation of  $\text{CH}_4$  (Schoell, 1980). Hence, the negative range of  $\delta^{13}\text{C}_{\text{carbonate}}$  values of mound 12 (Table 2.2; Fig. 2.7) most likely is related to this  $^{12}\text{C}$ -rich carbon source.

Fig. 2.7 shows the  $\delta^{13}\text{C} - \delta^{18}\text{O}$  cross plot for all authigenic carbonate samples taken from mounds 11 and 12. Although much more pronounced in case of the stable carbon isotopes, Fig. 2.7 shows that an enrichment of  $^{13}\text{C}$  is accompanied by an enrichment of  $^{18}\text{O}$  in the carbonates. The correlation of the stable isotope data indicate a relationship between the carbon source and the carbonate formation temperature and/or pore water oxygen isotope composition. Temperature-related isotope fractionation cannot account for the observed covariance of carbon and oxygen isotopes as the carbon isotopes ( $^{13}\text{C}$ - $^{12}\text{C}$  mass difference of one unit) would be much less affected than the oxygen isotopes ( $^{18}\text{O}$ - $^{16}\text{O}$  mass difference of two units) in case of temperature changes. Clearly, oxidation processes of organic materials including hydrocarbons account for the negative  $\delta^{13}\text{C}$  values of the carbonates. On the other hand, if the regression line in Fig. 2.7 is extended towards  $\delta^{13}\text{C} = 0$  ‰ (an assumed admixed carbonate end-member with a stable carbon isotope value near normal-marine  $\text{HCO}_3^-$ ; c.f. Fig. 2.7 where contributions of shell material are sometimes recognizable) a  $\delta^{18}\text{O}$  value of 39.5 ‰ would be indicated for such a carbonate end-member. This extremely positive value indicates that fossils grown at ocean surface water conditions are not a likely carbonate end-member. However, sedimentary carbonate shells might have changed their primary isotopic composition in course of re-crystallization and cementation during early diagenesis especially in mud mounds where changes of geochemical conditions may occur rapidly (Hensen et al., 2005). Nevertheless, considering the oxygen isotopic fractionation between calcite and water at low sediment temperature (measured bottom water temperature near  $5^\circ\text{C}$ ; Linke et al., 2005; see also discussion of stable oxygen isotopes above) it is likely that those sediment pore fluids in the mounds had an isotopic composition near 5 ‰. This pore water oxygen isotope

composition is close to the measured most positive  $\delta^{18}\text{O}_{\text{H}_2\text{O}}$  value of 4.7 ‰ (Table 2.3) for the deeply originated fluid end-member.

Another extreme carbonate end-member is possibly defined by the formation of carbonate from more or less unaltered normal marine pore water ( $\delta^{18}\text{O} = 0$  ‰). If authigenic carbonate would have precipitated from such pore waters at low sediment temperature of 5°C an oxygen isotopic composition of the carbonate near 33 ‰ (V-SMOW) should be expected. Based on the correlation of  $\delta^{18}\text{O}$  and  $\delta^{13}\text{C}$  values of the carbonates a hypothetical carbon end-member value approximately between -60 and -70 ‰ would be indicated. This is very close to the actual  $\delta^{13}\text{C}-\Sigma\text{CO}_2$  values of -60 to -68 ‰ found at mound 12 (Füri et al., 2010). Although authigenic carbonate formation remains speculative this range of carbon isotope values is likely for the utilization of carbon reservoir which results from anaerobe  $\text{CH}_4$  oxidation processes.

## 2.5 Conclusions

Authigenic carbonate formation is a widespread process in mounds 11 and 12. The stable carbon and oxygen isotopic composition of carbonate concretions retrieved from sediment cores in the study area show a spatial distribution. Concretions from mound 12 have light stable carbon and oxygen values whereas authigenic carbonate samples from mound 11 have significantly heavier  $^{13}\text{C}$  and  $^{18}\text{O}$  compositions.

The oxygen isotope composition of pore waters from mound 11 shows that is strongly affected by deep fluids enriched in  $^{18}\text{O}$ . These fluids were generated most probably through smectite to illite transformation and it is believed that they were present at the time of carbonate formation on mound 11. Concretions on mound 12 on the other hand, are more likely generated in fluids with similar to seawater  $\delta^{18}\text{O}$  composition.

The co-variation of carbon with oxygen stable isotopes, show that on mound 11, except from the sedimentary organic matter, oxidation products of an isotopic lighter carbon source were present during authigenic carbonate formation, which most likely related to migration of hydrocarbons from greater depths. However, the extremely light carbon signature, of carbonates sampled

from mound 12, identify the carbon isotope signature as biogenic methane, possibly oxidized during AOM.

The intermediate stable carbon and oxygen values of carbonate concretions on the SE flank of mound 12 and the presence of pore-water profiles with typical deep source fluid signatures, it is likely to indicate the geological transition from the older mound 12 to the younger mound 11 and/or, in different extents the influence of deep source emanating fluids in both mounds.

## References

Aloisi G., Pierre C., Rouchy J. M. Foucher J. P. and Woodside J. (2000) Methane-related authigenic carbonates of eastern Mediterranean Sea mud volcanoes and their possible relation to gas hydrate destabilisation. *Earth Planet Sci Lett* **184**, 321-338.

Aloisi G., Wallmann K., Haese R. R. and Saliege J. F. (2004). Chemical, biological and hydrological controls on the  $^{14}\text{C}$  content of cold seep carbonate crusts: numerical modeling and implications for convection at cold seeps. *Chem Geol* **213**, 359-383.

Alperin M.J., Reeburg W.S. and Whiticar M.J. (1988) Carbon And Hydrogen Isotope Fractionation Resulting From Anaerobic Methane Oxidation. *Global Biogeochem Cy* **2**, 279-288.

Boetius A., Ravensschlag K., Schubert C. J., Rickert D., Widdel F., Gieseke A., Amann R., Jorgensen B. B., Witte U. and Pfannkuche O. (2000). A marine microbial consortium apparently mediating anaerobic oxidation of methane. *Nature* **407**, 623-626.

Bohrmann G., Greinert J., Suess E. and Torres M. (1998) Authigenic carbonates from the Cascadia subduction zone and their relation to gas hydrate stability. *Geology* **26**, 647-650.

Brueckman W., et al (2008) R/V Meteor Cruise Report M66/3a and 3b, 42 pp. GEO-MAR report.

Burton E. A. and Walter L. M. (1990) The role of pH in phosphate inhibition of calcite and aragonite precipitation rates in seawater. *Geochim Cosmochim Acta* **54**, 797-808.

Burton E. (1993) Controls of marine carbonate cement mineralogy: review and reassessment. *Chem Geol* **105**, 163-179.

Chen P.-C., Liu S. M., Jang C. J., Hwang R. C., Yang Y. L., Lee J. S. and Jang J. S. (2003) Interpretation of gas-liquid reactive crystallization data using a size-independent agglomeration model. *J Cryst Growth* **257**, 333-343.

Claypool G. E. and Kaplan I. R. (1974) The origin and distribution of methane in marine sediments. In: Kaplan, I. R. (Ed.), *Natural gases in marine sediments*.

Craig H. (1961) Standard for Reporting Concentrations of Deuterium and Oxygen-18 in Natural Waters. *Science* **133**, 1833-1834.

Dählmann A. and De Lange G. J. (2003) Fluid-sediment interactions at eastern Mediterranean mud volcanoes; a stable isotope study from ODP Leg 160. *Earth Planet Sci Lett* **212**, 377-391.

Dumke I., Faber E. and Poggenburg J. (1989) Determination of stable carbon and hydrogen isotopes of light hydrocarbons. *Anal Chem* **61**, 2149-2154.

Faber E., Botz R., Poggenburg J., Schmidt M., Stoffers P. and Hartmann M. (1998) Methane in Red Sea brines. *Org Geochem* **29**, 363-379.

Flüh E., Soeding E. and Suess E. (2004) RV Sonne Cruise Report SO173/1, 173/3 and 173/4, 492 pp. GEOMAR report 115.

Goldsmith J. R., Graf D. L. and Heard H. C. (1961) Lattice constants of the calcium-magnesium carbonates. *Am Mineral* **46**, 453-457.

Grasshof K., Ehrhardt M. and Kremling K. (1999) *Methods of seawater analysis*. Wiley-VCH, Weinheim Germany, 632 pp.

Han X., Suess E., Sahling H. and Wallmann K. (2004) Fluid venting activity on the Costa Rica margin; new results from authigenic carbonates. *Int J Earth Sci* **93**, 596-611.

Henry P., Lallemand S., Nakamura K.-I., Tsunogai U., Mazzotti S. and Kobayashi K. (2002) Surface expression of fluid venting at the toe of the Nankai wedge and implications for flow paths. *Mar Geol* **187**, 119-143.

Hensen C., Nuzzo M., Hornibrook E., Pinheiro L. M., Bock B., Magalhaes V. H. and Bruckmann W. (2007) Sources of mud volcano fluids in the Gulf of Cadiz--indications for hydrothermal imprint. *Geochim Cosmochim Acta* **71**, 1232-1248.

Hensen C. and Wallmann K. (2005) Methane formation at Costa Rica continental margin; constraints for gas hydrate inventories and cross-decollement fluid flow. *Earth Planet Sci Lett* **236**, 41-60.

Hensen C., Wallmann K., Schmidt M., Ranero C. R. and Suess E. (2004) Fluid expulsion related to mud extrusion off Costa Rica; a window to the subducting slab. *Geology* **32**, 201-204.

Hesse R., Lebel J. and Gieskes J. M. (1985) Interstitial water chemistry of gas-hydrate-bearing sections on the Middle America Trench slope, Deep Sea Drilling Project Leg 84 727-737.

Irwin H., Curtis C. and Coleman M. (1977) Isotopic evidence for source of diagenetic carbonates formed during burial of organic-rich sediments. *Nature* **269**, 209-213.

Ivanenkov V. N. and Lyakhin Y. I. (1978) Determination of total alkalinity in seawater. In: Bordovsky O.K. and V.N., I. Eds. *Methods of Hydrochemical investigations in the Ocean*. Nauka Publ., Moscow.

Kim S.-T., O'Neil J. R., Hillaire-Marcel C. and Mucci A. (2007) Oxygen isotope fractionation between synthetic aragonite and water: Influence of temperature and Mg<sup>2+</sup> concentration. *Geochim Cosmochim Acta* **71**, 4704-4715.

Kim S. T. and O'Neil J. R. (1997) Equilibrium and nonequilibrium oxygen isotope effects in synthetic carbonates. *Geochim Cosmochim Acta* **61**, 3461-3475.

Kimura G. et al. (1997). Proceedings of the Ocean Drilling Program; Initial reports; Costa Rica accretionary wedge; covering Leg 170 of the cruises of the drilling vessel

JOIDES Resolution, San Diego, California, to Balboa, Panama, sites 1039-1043, 16 October-17 December 1996.

Klaucke I., Masson D. G., Petersen C. J., Weinrebe W. and Ranero C. R. (2008) Multi-frequency geoacoustic imaging of fluid escape structures offshore Costa Rica: Implications for the quantification of seep processes. *Geochem Geophys Geosyst* **9**, 1-15.

Linke P., Wallmann K., Suess E., Hensen C. and Rehder G. (2005) In situ benthic fluxes from an intermittently active mud volcano at the Costa Rica convergent margin. *Earth Planet Sci Lett* **235**, 79-95.

Mau S., Rehder G., Arroyo I. G., Gossler J. and Suess E. (2007) Indications of a link between seismotectonics and CH<sub>4</sub> release from seeps off Costa Rica. *Geochem Geophys Geosyst* **8**, 1-13.

Mau S., Sahling H., Rehder G., Suess E., Linke P. and Soeding E. (2006) Estimates of methane output from mud extrusions at the erosive convergent margin off Costa Rica. *Mar Geol* **225**, 129-144.

Meyers P. A. (1994) Preservation of elemental and isotopic source identification of sedimentary organic matter. *Chem Geol* **114**, 289-302.

Morse J. W., Wang Q. and Tsio M. Y. (1997) Influences of temperature and Mg:Ca ratio on CaCO<sub>3</sub> precipitates from seawater. *Geology* **25**, 85-87.

Mörz T., Fekete N., Kopf A. J., Brueckmann W., Kreiter S., Huehnerbach V., Masson D. G., Hepp D. A., Schmidt M., Kutterolf S., Sahling H., Abegg F., Spiess V., Suess E. and Ranero C. R. (2005a) Styles and productivity of mud diapirism along the Middle American Margin, Part II, Mound Culebra and Mounds 11 and 12, *Mud volcanoes, geodynamics and seismicity*. (Martinelli G. and Panahi B., editors) 49-76pp. Springer, Dordrecht, Netherlands.

Mörz T., Kopf A. J., Brueckmann W., Fekete N., Huehnerbach V., Masson D. G., Hepp D. A., Suess E. and Weinrebe W. (2005b) Styles and productivity of mud diapirism along the Middle American Margin; Part I, Margin evolution, segmentation, dewatering and mud diapirism, in *Mud volcanoes, geodynamics and seismicity* (Martinelli G. and Panahi B., editors) 35-48pp. Springer, Dordrecht, Netherlands.

Naehr T. H., Eichhubl P., Orphan V. J., Hovland M., Paull C. K., Ussler III W., Lorenson T. D. and Greene H. G. (2007) Authigenic carbonate formation at hydrocarbon seeps in continental margin sediments: A comparative study. *Deep Sea Res Part II: Topical Studies in Oceanography* **54**, 1268-1291.

Paull C. K., Ussler III W., Peltzer E. T., Brewer P. G., Keaten R., Mitts P. J., Nealon J. W., Greinert J., Herguera J.-C. and Perez M. (2007) Authigenic carbon entombed in methane-soaked sediments from the northeastern transform margin of the Guaymas Basin, Gulf of California. *Deep Sea Res Part II: Topical Studies in Oceanography* **54**, 1240-1267.

Peckmann J., Reimer A., Luth U., Luth C., Hansen B. T., Heinicke C., Hoefs J. and Reitner J. (2001) Methane-derived carbonates and authigenic pyrite from the north-western Black Sea. *Mar Geol* **177**, 129-150.

Pokrovsky O.S. (1996) Experimental synthesis of calcium and magnesium carbonates: Factors controlling magnesian calcite formation in natural water. *Lithology and Mineral Resources* **31**, 474-482.

Ranero C. R., Grevemeyer I., Sahling H., Barckhausen U., Hensen C., Wallmann K., Weinrebe W., Vannucchi P., Huene R. V. and McIntosh K. (2008) Hydrogeological system of erosional convergent margins and its influence on tectonics and interplate seismogenesis. *Geochem Geophys Geosyst* **9**, 1-17.

Ranero C. R. and Von Huene R. (2000) Subduction erosion along the Middle America convergent margin. *Nature* **404**, 748-755.

Ritger S., Carson B. and Suess E. (1987) Methane-derived authigenic carbonates formed by subduction-induced pore-water expulsion along the Oregon/Washington margin. *Bull Geol Soc Am* **98**, 147-156.

Sahling H., Masson D. G., Ranero C. R., Huhnerbach V., Weinrebe W., Klauke I., Burk D., Bruckmann W. and Suess E. (2008) Fluid seepage at the continental margin offshore Costa Rica and southern Nicaragua. *Geochem Geophys Geosyst* **9**, 1-22.

Schacht U., Wallmann K., Kutterolf S. and Schmidt M. (2008) Volcanogenic sediment-seawater interactions and the geochemistry of pore waters. *Chem Geol* **249**, 321-338.

Schmidt M., Hensen C., Moerz T., Mueller C., Grevenmeyer I., Wallmann K., Mau S. and Kaul N. (2005) Methane hydrate accumulation in "Mound 11" mud volcano, Costa Rica forearc. *Mar Geol* **216**, 83-100.

Schoell M. (1980) The hydrogen and carbon isotopic composition of methane from natural gases of various origins. *Geochim Cosmochim Acta* **44**, 649-661.

Sheppard S. M. F. and Gilg H. A. (1996) Stable isotope geochemistry of clay minerals; The story of sloppy, sticky, lumpy and tough, Cairns-Smith (1971). *Clay Miner* **31**, 1-24.

Soeding E., Wallmann K., Suess E. and Flüh E. (2003) FS Meteor, cruise report M54/2-3: Caldera-Curacao: GEOMAR Report 111.

Stakes D. S., Orange D. L., Paduan J. B., Salamy K. A. and Maher N. (1999) Cold-seeps and authigenic carbonate formation in Monterey Bay, California. *Mar Geol* **159**, 93-109.

Tang J., Dietzel M., Boehm F., Koehler S. J. and Eisenhauer A. (2008)  $\text{Sr}^{2+}/\text{Ca}^{2+}$  and  $^{44}\text{Ca}/^{40}\text{Ca}$  fractionation during inorganic calcite formation: II. Ca isotopes. *Geochim Cosmochim Acta* **72**, 3733-3745.

Tarutani T., Clayton R. N. and Mayeda T. K. (1969) The effect of polymorphism and magnesium substitution on oxygen isotope fractionation between calcium carbonate and water. *Geochim Cosmochim Acta* **33**, 987-996.

Ussler W. and Paull C. K. (1995) Effects of ion exclusion and isotopic fractionation on pore water geochemistry during gas hydrate formation and decomposition. *Geo Mar Lett* **15**, 37-44.

Valentine D. L. and Reeburgh W. S. (2000) New perspectives on anaerobic methane oxidation. *Environ Microbiol* **2**, 477-484.

Von Huene R., Ranero C., Weinrebe W. and Hinz K. (2000) Quaternary convergent margin tectonics of Costa Rica, segmentation of the Cocos Plate and Central American volcanism. *Tectonics* **19**, 314-334.

Whiticar M. J. (1999) Carbon and hydrogen isotope systematics of bacterial formation and oxidation of methane. *Chem Geol* **161**, 291-314.

Whiticar M. J. and Faber E. (1986) Methane oxidation in sediment and water column environments--Isotope evidence. *Org Geochem* **10**, 759-768.

You C. F., Chan L. H., Spivack A. J. and Gieskes J. M. (1995a) Lithium, boron, and their isotopes in sediments and pore waters of Ocean Drilling Program Site 808, Nankai Trough; implications for fluid expulsion in accretionary prisms. *Geology* **23**, 37-40.

You C. F., Spivack A. J., Gieskes J. M., Rosenbauer R. and Bischoff J. L. (1995b) Experimental study of boron geochemistry; implications for fluid processes in subduction zones. *Geochim Cosmochim Acta* **59**, 2435-2442.



## Chapter III

# Laboratory determination of oxygen isotope fractionation of high Mg-calcite between 25 and 80°C

## Abstract

High magnesium calcite (HMC) was synthesized from oversaturated solutions with respect to calcite at 25, 40, 60 and 80°C. In order to remove any amorphous carbonate (AC) from synthesized CaMg-carbonates, a partial dissolution technique was applied. The purified HMC (~6-32 mol % MgCO<sub>3</sub>) allowed the effect of Mg<sup>2+</sup> on the HMC-water oxygen isotope fractionation to be estimated. The effect can be expressed by an extended term added to the calcite-water oxygen isotope fractionation equation of Kim S. T. and O'Neil J. R. (1997) "Equilibrium and nonequilibrium oxygen isotope effects in synthetic carbonates." *Geochim. Cosmochim. Acta* 61, 3461-3475:

$$1000\ln\alpha_{\text{HMC-H}_2\text{O}} = 18.03x - 32.42 + (0.6x^3 - 5.47x^2 + 16.78x - 17.21)C_{\text{Mg}}$$

where  $x$  is  $10^3/T$  in Kelvin and  $C_{\text{Mg}}$  is the percentage of Mg<sup>2+</sup> incorporated in the crystal lattice.

Inorganic formation of Mg-calcite with up to 25 mol % MgCO<sub>3</sub> is observed in a number of marine and lacustrine environments. The above relationship provides additional information on temperature related oxygen isotope fractionation to existing thermodynamic calculations and isotope fractionation data derived from natural samples.

### 3.1 Introduction

Calcite, originated either as shells of organisms or inorganic precipitates, plays an important role in aquatic environments. Over the past decades numerous studies have been published on both, dissolution and precipitation of calcite in aqueous solutions (e.g. Mackenzie et al., 1983; Morse, 1983; Morse and Arvidson, 2002; Morse et al., 2007). In particular, the incorporation of  $Mg^{2+}$  in the calcite crystal lattice was intensively studied (Glover and Sippel, 1967; Bischoff et al., 1987; Budd and Hiatt, 1993; Böttcher et al., 1997). Despite these scientific efforts made, various aspects such as oxygen isotope fractionation between Mg-calcite and water, incorporation of  $Mg^{2+}$  and the role of  $Mg^{2+}$  in stabilizing amorphous calcium carbonate are still under debate (Reddy and Wang, 1980; Mucci and Morse, 1983; Zhang and Dawe, 2000; Zhou and Zheng, 2005; Horita and Clayton, 2007; Zheng and Zhou, 2007).

The incorporation of  $Mg^{2+}$  ions in calcite was investigated in laboratory experiments by mixing oversaturated solutions (Falini et al., 1994; Wada et al., 1995; Pokrovsky, 1998). However, in the presence of  $Mg^{2+}$ , a prediction of the carbonate polymorph formed under high saturation experiments is difficult (Pokrovsky, 1998). Several studies showed that the calcium carbonate polymorph most commonly obtained in the presence of magnesium was aragonite (Berner, 1975; Berner et al., 1978; Rushdi et al., 1992; Raz et al., 2000). However a transformation from one  $CaCO_3$  mineral phase into another (i.e. transformation of HMC to aragonite) has been suggested (Glover and Sippel, 1967).

Incorporation of  $Mg^{2+}$  ions in calcite crystal lattice, creates a barrier to growth rate (House et al., 1988; Zhang and Dawe, 2000). Analyses of calcium carbonate precipitated during low saturation experiments suggested that this effect may be overcome by the initial formation of an amorphous calcium carbonate (ACC) precursor which may possibly also provide a mechanism for the incorporation of  $Mg^{2+}$  in the calcite lattice (Raz et al., 2000; Loste et al., 2003). According to Raz et al. (2000), the presence of  $Mg^{2+}$  causes an increase in the degree of supersaturation. This results in precipitation of metastable, particularly amorphous particles. In biological produced amorphous calcium carbonate

material,  $Mg^{2+}$  has been shown to act as inhibitor for the stabilization of ACC (Aizenberg et al., 1996; Aizenberg et al., 2002; Addadi et al., 2003).

It has been documented that the presence of  $Mg^{2+}$  also affects the oxygen isotope fractionation of calcite (Tarutani et al., 1969; Jimenez-Lopez et al., 2004). Tarutani et al. (1969), precipitated Mg-calcites of various  $MgCO_3$  contents (4-12 mol %) and reported that the  $^{18}O$  content is enriched by 0.06‰ in the  $10^3 \ln \alpha$  scale, for each mol % of  $MgCO_3$  incorporated in the crystal lattice. However Jimenez-Lopez et al. (2004), found a higher increase of 0.17‰  $^{18}O$  per mol % of  $MgCO_3$  incorporated in Mg-calcites at 25°C.

In the present study, we try to define the relationship between Mg content and oxygen isotope fractionation of HMC samples and water. Precipitation experiments from oversaturated solutions, with respect to calcite, were performed at 25, 40, 60 and 80°C.

## 3.2 Methods

### 3.2.1 $Ca_xMg_{1-x}CO_3$ syntheses

The Mg-calcite samples were precipitated by direct mixing of equal-volumes (150 ml)  $CaCl_2$ - $MgCl_2$  and  $Na_2CO_3$  analytical grade reagent solutions. Calculated concentrations and Mg:Ca ratios of final (mixed) solutions are presented in Table 3.1. Initial solutions were kept at the respective experimental temperature in closed vessels for several hours before use to avoid undefined precipitation temperatures.

Table 3.1: Mg:Ca ratios and concentrations of the initial solutions used during this work. The concentrations refer to the mixture of the two initial solutions.

Ratio	Concentrations (in moles/L)		
	$CaCl_2$	$MgCl_2$	$Na_2CO_3$
1:1	0.005	0.005	0.04
1:2	0.010	0.005	0.04
1:3	0.015	0.005	0.04
1:4	0.020	0.005	0.04
1:6	0.030	0.005	0.04
1:7	0.035	0.005	0.04
5:1	0.005	0.025	0.04

Precipitation experiments were performed in 500 ml sealed reaction vessels. Prior to mixing the solutions  $\sim 10$  mg of HMC (7 mol %  $\text{MgCO}_3$ ) seed crystals (echinoderm *Cidaris sp.*,  $3.3 \text{ m}^2 \text{ g}^{-1}$  total surface) were added according to Mucci and Morse (1983). The reaction vessels were then stored at temperatures 25, 40, 60 and  $80^\circ\text{C}$  for 35 days. Directly after the end of each experimental run, the precipitants ( $\sim 0.5$  g) were dried by washing with pure ethanol and suction filtration ( $0.2 \mu\text{m}$ ) at room temperature (Schmidt et al., 2005).

### 3.2.2 Partial dissolution technique

Synthesized CaMg-carbonate samples were reacted in stirred slurry of 100 ml distilled water which was slowly acidified using ( $\sim 0.002$  M) HCl until a final pH of 6 was reached. This dissolution process is believed to have removed most of the amorphous carbonate from the high Mg-calcite sample (Brecevic and Nielsen, 1989; Clarkson et al., 1992). Scanning electron micrographs of samples before and after leaching can be seen in Plate 3.1. It is important to be noted that selected samples were repeatedly leached by the partial dissolution technique. The intermediate products were characterized by XRD and stable isotope analysis.

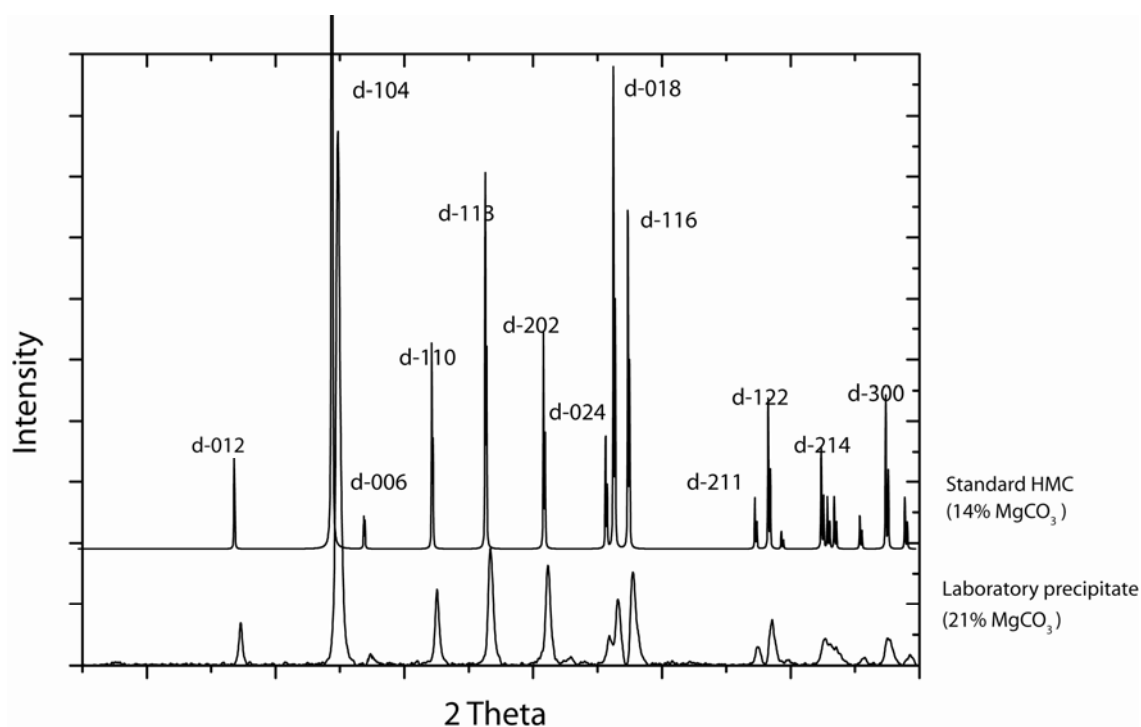


Figure 3.1: X-ray diffraction patterns of the standard HMC (14 mol %  $\text{MgCO}_3$ , JCPDS files card 43-697) and a laboratory precipitated HMC.

### 3.2.3 X-ray diffraction measurements (XRD)

The mineralogy of synthesized CaMg-carbonates and HMC seeds were determined by X-ray diffraction measurements (PW 1710/Philips, Co-K $\alpha$ , scan speed 0.02° s<sup>-1</sup>). The detection limit of the method is approximately 2% of the total mass of the sample. The presence of MgCO<sub>3</sub> in the crystal lattice has been determined using the d-104 peak (Goldsmith et al., 1961). The standard error in this calculation has been estimated according to laboratory standards as  $\pm 1\%$  of the MgCO<sub>3</sub> content.

### 3.2.4 Infrared Spectroscopy

The FTIR spectra of the precipitated samples were measured in the wave-number region 350-4000 cm<sup>-1</sup> using the KBr method with a Bruker IFS66v spectrometer. A total of 1.5 mg of ground sample was mixed with 200 mg KBr and then pressed under vacuum to a pellet. FTIR spectra were recorded under vacuum, with 512 scans and a resolution of 2 cm<sup>-1</sup>. Analysis of spectra (peak intensity and peak area determination) was performed with the OPUS 5.5 software.

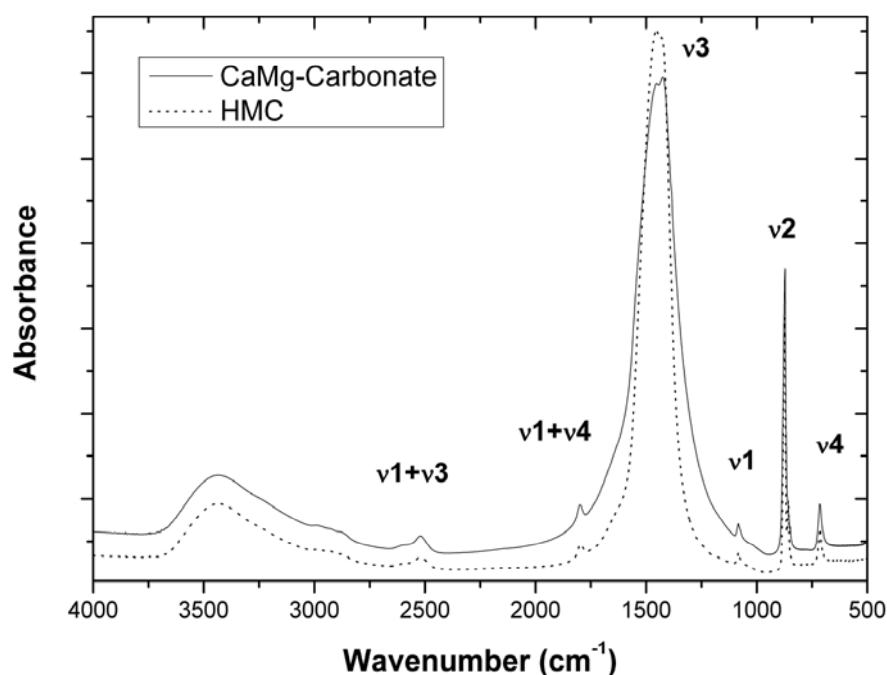


Figure 3.2: FTIR pattern of initially precipitated CaMg-carbonate and partially dissolved HMC (Sample 25-5a). The characteristic vibration bands are marked.

### 3.2.5 SEM and EDX measurements

MORphology and size of the particles of the synthesized material were studied by using a scanning electron microscope Cam Scan CS 44 operated at 15-20 kV. The samples were prepared by dispersion onto a carbon film fixed on a steel mounting. Gold-Palladium coating was applied to the powdered material. Surficial elemental concentrations have been measured using Energy Dispersive X-ray (EDX) spectroscopy, using the same carbon coated steel mountings used for SEM analyses. This method can provide very precise results for the elemental composition of a sample, but it is restricted to small  $\mu\text{m}$ -scaled spots of the analyzed particles. Furthermore, the penetration of the beam is limited to the surface of the material (0.1-1  $\mu\text{m}$ ). Hence the results are used in order to detect elemental (in-)homogeneities of the carbonate material but does not represent mean concentrations for the whole sample.

### 3.2.6 Ca and Mg analyses (ICP-AES)

After partial dissolution of the bulk sample  $\text{Ca}^{2+}$  and  $\text{Mg}^{2+}$  concentrations of crystalline materials were analyzed by Inductively Coupled Plasma Atomic Emission Spectrometry (JY 170 Ultrace). Each homogenized carbonate sample was dissolved in 5 ml 10% HCl solution. The standard error of the method was estimated as 0.3% for  $\text{Mg}^{2+}$  and 0.5% for  $\text{Ca}^{2+}$  according to deviations from laboratory standards. The Mg-content in carbonate is given in mol %  $\text{MgCO}_3$ .

### 3.2.7 Stable oxygen isotope analyses

The CaMg-carbonate samples were reacted with 100% phosphoric acid at 73°C in an online Carbo-Kiel carbonate preparation line. The oxygen isotope ratio of the liberated  $\text{CO}_2$  was measured with a Finnigan MAT 251 IR-MS spectrometer. The data were calibrated against V-PDB standard. The standard deviation, based on replicate measurements of the standard (NBS-19) was about  $\pm 0.06$  ‰. Replicates of the same samples processed at different laboratories

(IFM-GEOMAR and Leibniz Laboratory for Radiometric Dating and Stable Isotope Research, University of Kiel) produced deviations of  $\pm 0.05\%$  in  $\delta^{18}\text{O}$ .

The oxygen isotope ratios of the initial solutions were determined using the standard  $\text{CO}_2$  – water equilibration technique (Craig, 1961).

All  $\delta^{18}\text{O}$  values are reported relative to V-SMOW, calculated after Coplen et al. (1983) without further corrections.

### 3.3 Results and Discussion

#### 3.3.1 Mineralogy of synthesized CaMg-carbonates

X-ray diffraction analyses of synthesized HMCs show comparable diffraction patterns to Mg-calcite standard (Joint Committee on Powder Diffraction Standards, JCPDS files card 43-697, calcite, magnesian, 14 mol %  $\text{MgCO}_3$ ). The variations in the main d-104 peak indicate variable amounts (8-28 %  $\text{MgCO}_3$ ) of  $\text{Mg}^{2+}$  present in the crystal lattice (Fig. 3.1, Table 3.2). Although crystal seeds were used to control the mineralogy of the precipitant (Mucci and Morse, 1983) in a few cases the presence of other CaMg-carbonate minerals were detected by XRD. Specifically, the solutions which started with initial Mg:Ca ratios of 5:1 result in mineral mixtures that do not contain any Mg-calcite. The minerals obtained from solutions with high Mg:Ca (>5) ratios were variable mixtures of monohydrocalcite, dolomite, magnesite and nesquehonite. Similar conclusions have been presented by Loste et al. (2003) at initial Mg:Ca ratio 4:1. For the present work, only the pure HMC samples were selected. From experimental runs where pure, by means of XRD, HMC samples had been formed.

Precipitation of  $\text{CaCO}_3$  polymorphs from supersaturated solutions has previously been reported to form ACC (Ogino et al., 1987; Brecevic and Nielsen, 1989; Sawada et al., 1990; Loste et al., 2003; Schmidt et al., 2005). Amorphous material cannot be identified by XRD analyses, but its presence has been detected by infrared spectroscopy of natural biominerals (Beniash et al., 1997; Raz et al., 2000; Levi-Kalishman et al., 2002) and of inorganic precipitants

(Brecevic and Nielsen, 1989; Loste et al., 2003; Schmidt et al., 2005). Furthermore Schmidt et al. (2005) have reported that the presence of amorphous material influences the isotopic composition of the bulk CaMg-carbonate sample. In accordance with these earlier investigations, it can be expected that the presence of amorphous carbonate causes a relatively low oxygen isotope fractionation between (bulk) mineral phase and water compared to pure crystalline materials. Hence, we removed the amorphous carbonate by fractionated dissolution prior to isotope analysis of residual HMC, whereas partial surface dissolution of crystalline material cannot be excluded (Plate 3.1f). The partial dissolution did not cause difference in the main XRD Mg-calcite peaks within the standard error of the method, indicating negligible effects of the method on the HMC-crystallinity.

Table 3.2: Oxygen isotope values and Mg<sup>2+</sup> contents of initial solutions and precipitants of our experiments. The 103Inα values refer to the samples after dissolution of ACC has occurred. The Mg % - XRD were calculated from d-104 calcite peaks. For Mg % - ICP the ratio Mg/(Ca+Mg) has been calculated in the solid residual after partial dissolution.

Sample	Temp (°C)	Initial Mg:Ca ratio	δ <sup>18</sup> O (bulk carbonate) ‰ VSMOW	δ <sup>18</sup> O (HMC) ‰ VSMOW	δ <sup>18</sup> O (H <sub>2</sub> O) ‰ VSMOW	10 <sup>3</sup> Inα (HMC-H <sub>2</sub> O)	MgCO <sub>3</sub> % (XRD)	MgCO <sub>3</sub> % (ICP-AES)
25-1a	25	1:2	22,57	23,19	-8,50	31,5	15	24,8
25-2a	25	1:3	21,15	21,94	-8,50	30,3	11	17,3
25-3a	25	1:4	20,40	21,33	-8,52	29,6	9	12,9
25-4a	25	1:6	21,03	21,15	-8,56	29,5	12	10,0
25-5a	25	1:7	19,82	20,73	-8,53	29,1	7	6,1
25-1b	25	1:2	22,41	23,15	-8,50	31,4	14	23,8
25-2b	25	1:3	21,38	22,13	-8,50	30,4	12	17,1
25-3b	25	1:4	20,72	21,46	-8,50	29,8	8	12,7
25-4b	25	1:6	19,34	21,10	-8,50	29,4	8	8,6
40-1a	40	1:2	18,94	19,77	-8,52	28,2	20	30,3
40-2a	40	1:3	17,96	18,88	-8,55	27,3	13	22,5
40-3a	40	1:4	17,94	18,42	-8,56	26,8	11	18,0
40-4a	40	1:6	17,49	17,88	-8,53	26,3	9	11,4
40-5a	40	1:7	17,31	17,49	-8,55	25,9	8	7,5
60-1a	60	1:2	17,62	17,88	-8,56	24,3	28	32,
60-2a	60	1:3	16,67	16,86	-8,50	23,3	19	23,4
60-3a	60	1:4	16,49	16,54	-8,53	23,0	14	19,4
60-4a	60	1:6	15,32	15,69	-8,55	22,2	10	11,7
60-5a	60	1:7	15,11	15,44	-8,55	21,9	10	9,3
80-1a	80	1:2	13,39	13,45	-8,55	20,0	11	31,9
80-3a	80	1:4	12,75	12,82	-8,55	19,3	10	19,8
80-4a	80	1:6	12,66	12,69	-8,50	19,2	9	14,6
80-5a	80	1:7	12,20	12,22	-8,52	18,8	9	7,6

Observations in the scanning electron microscope revealed differences in the texture of the precipitants formed at low and at high temperatures. At 25°C samples consist of spheroidal carbonate particles, clusters of crystals and

dumbbells (Plate 3.1a). Their diameter varies between 1 and 10  $\mu\text{m}$ . Similar carbonate particles have previously been described by other authors who have performed CaMg-carbonate precipitation experiments by direct mixing of the initial solutions at 25°C, having similar or different Mg:Ca ratios (Kitamura, 2001; Meldrum and Hyde, 2001; Loste et al., 2003; Kralj et al., 2004; Ajikumar

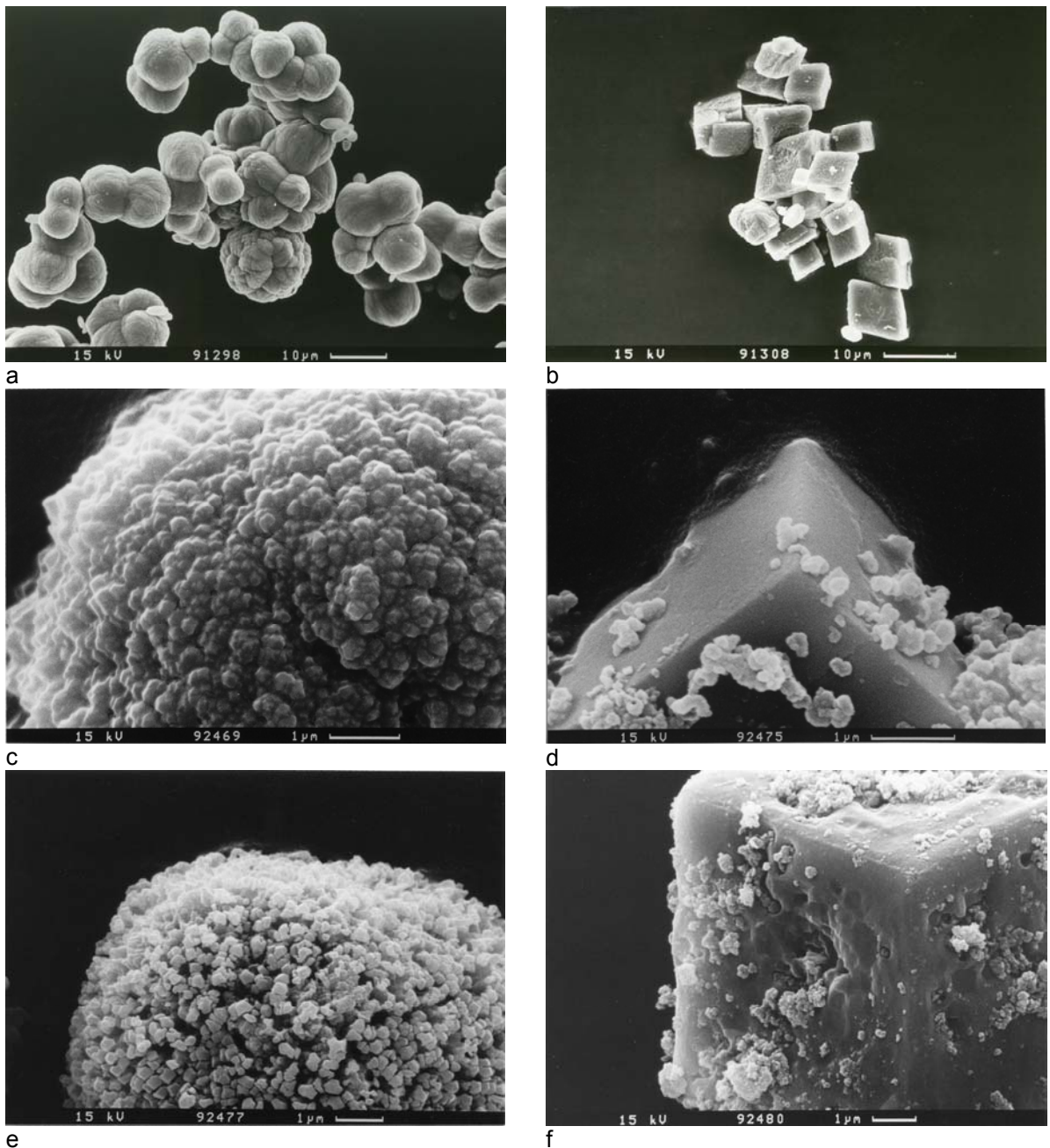


Plate 3.1: Scanning electron micrographs of high Mg-calcite crystals precipitated at 25°C (a,c,e) and 80°C (b,d,f). Micrographs c and d show the initial bulk material surface under magnification (scale given), whereas e and f represent the same samples after dissolution of amorphous carbonate has occurred.

et al., 2005; Chen et al., 2006). At precipitation temperatures of 80°C rhombohedra are abundant with variable size in the  $\mu\text{m}$ -scale (Plate 3.1b). In general, it was observed that particle sizes decrease and crystallinity increases with increasing temperature (25-80°C range). A detailed discussion on the morphology of the precipitated material is beyond the scope of the present work, and detailed description of the texture of the precipitants can be found elsewhere (Comas-Bru, 2007). Furthermore, it should be noted that differences in the morphology were not found to be related to the stable oxygen isotopic composition of precipitated CaMg-carbonates (Comas-Bru, 2007).

### 3.3.2 Vibration band characteristics of synthesized CaMg-carbonate

The three main infrared absorption bands of carbonate vibration modes ( $\nu_3$ : 1415-1480  $\text{cm}^{-1}$ ;  $\nu_2$ : 870-880  $\text{cm}^{-1}$ ;  $\nu_4$ : 711-716  $\text{cm}^{-1}$ ) can be measured in the synthesized CaMg-carbonate (Fig. 3.2). Their wave numbers correspond to the absorption bands known for (Mg)-calcite (e.g. Adler and Kerr, 1962). The  $\nu_1$  vibration mode, infrared inactive in a well ordered calcite crystal, was also observed as a weak absorption band at about 1084  $\text{cm}^{-1}$  together with the overtone band at 1801  $\text{cm}^{-1}$  ( $\nu_1 + \nu_4$ ). The occurrence of the  $\nu_1$  infrared absorption band is usually assigned to disordering of the calcite lattice by e.g.  $\text{Mg}^{2+}$  incorporation (White, 1974), and is observed in synthesized carbonates (Aizenberg et al., 1996; Brecevic et al., 1996; Donners et al., 2002) and carbonate biominerals (Aizenberg et al., 1996; Aizenberg et al., 2002; Addadi et al., 2003). The increase of the positional disorder of the  $\text{CO}_3^{2-}$  group due to the incorporation of  $\text{Mg}^{2+}$  in the crystal lattice of synthetic and biogenic samples of Mg-calcite was also proven by Raman spectroscopy (Bischoff et al., 1985). Furthermore, Gueta et al. (2007) presented that disordering effects in calcite (i.e. Ca-O distance variation) can affect the length of the  $\nu_2$  and  $\nu_4$  bands and thus the  $\nu_2/\nu_4$  ratio. The  $\nu_4$  vibration mode is more sensitive to changes in the Ca-O distance, resulting to variations in peak intensity ratios from 3 for the ideal calcite crystal (Beniash et al., 1997), to 10, for a highly disordered one (Gueta et al., 2007).

Infrared absorption spectroscopy (i.e.  $\nu_2/\nu_4$  ratio determination) has also been used for the detection of amorphous phases in CaMg-carbonate (Beniash

et al., 1997; Levi-Kalishman et al., 2000; Raz et al., 2000; Schmidt et al. 2005). Moreover, a broadening of all the characteristic carbonate infrared absorption bands has been previously reported to indicate the presence of amorphous carbonate (Aizenberg et al., 2002; Aizenberg et al., 2003). To determine differences in the amorphous content of the synthesized CaMg-carbonates before and after the partial dissolution the  $\nu_2/\nu_4$  peak intensity ratios and the half-width of the  $\nu_3$  band were determined (Table 3.3). The synthesized bulk CaMg-carbonate samples and the material collected after subsequent partial dissolution (mainly HMC), display noticeable differences in their FTIR spectra (Fig. 3.2). The  $\nu_2/\nu_4$  intensity ratio is always lower after sample digestion compared to the ratio of the initial precipitate (Table 3.3), indicating that crystallized material is preferably left by partial dissolution. The half-width of the  $\nu_3$  absorption band is reduced by a factor of 0.5 to 0.9 due to the partial dissolution (Table 3.3, Fig. 3.2). This factor of reduction is in the same range as the  $\nu_2/\nu_4$  ratio is reduced by the partial dissolution.

Table 3.3: Infrared spectra data for CaMg-carbonate samples before and after partial dissolution

Sample	$\nu_2/\nu_4$ (bulk carbonate)	$\nu_2/\nu_4$ (HMC)	halfwidth of $\nu_3$ band (bulk carbonate)	halfwidth of $\nu_3$ band (HMC)
25-1a	6	5	1,2	1
25-2a	9	7,3	1	0,9
25-3a	7,7	4,4	1,2	0,9
25-4a	7,7	4,4	1,2	1
25-5a	8,3	5	1,2	0,7
40-1a	9	7,4	1,1	0,8
40-2a	9,2	7,1	1,3	0,7
40-3a	6,8	5,8	1,2	0,9
40-4a	8,3	7,5	1,1	0,9
40-5a	6,5	5,5	1,1	1
60-1a	4,8	4,4	1	0,7
60-2a	5,6	5	1,3	0,7
60-3a	4,8	4	1,1	0,9
60-4a	7,8	5,7	1,1	0,9
60-5a	6,3	5,5	1,3	0,9
80-1a	8	6,6	0,7	0,6
80-3a	6,9	5,1	1	0,6
80-4a	5,9	3,7	1,1	0,8
80-5a	4,8	3,3	1,5	0,9

### 3.3.3 Mg-content of synthesized HMC

The Mg-content of HMC, determined by ICP-AES after removal of amorphous carbonate, range between 6 and 32 mol %  $\text{MgCO}_3$  (Table 3.2). The Mg-content of HMC is generally increasing with increasing Mg:Ca ratio of the mixed initial solution (Table 3.2). The degree of incorporation of Mg into the calcite lattice during precipitation from supersaturated solutions can be described as a function of the saturation degree  $\Omega_{\text{MgCO}_3}$  (Pokrovsky, 1998). Based on literature data and own precipitation experiments Pokrovsky (1998) favored Mg(5-30%)-calcite formation between  $\Omega_{\text{MgCO}_3} \sim 3$ -4. This is in perfect agreement with the data presented in this study (Fig. 3.3), where high Mg(6-32%)-calcite was formed at supersaturation conditions of  $\Omega_{\text{MgCO}_3} = 3 - 3.5$ . The saturation degree calculation is conducted with PHREEQC (Parkhurst and Appelo, 1999), based on a modified Minteq thermodynamic data set (using the solubility equilibrium constant  $K_{\text{MgCO}_3}$  of Königsberger et al., 1992, which was also used by Pokrovsky, 1998).

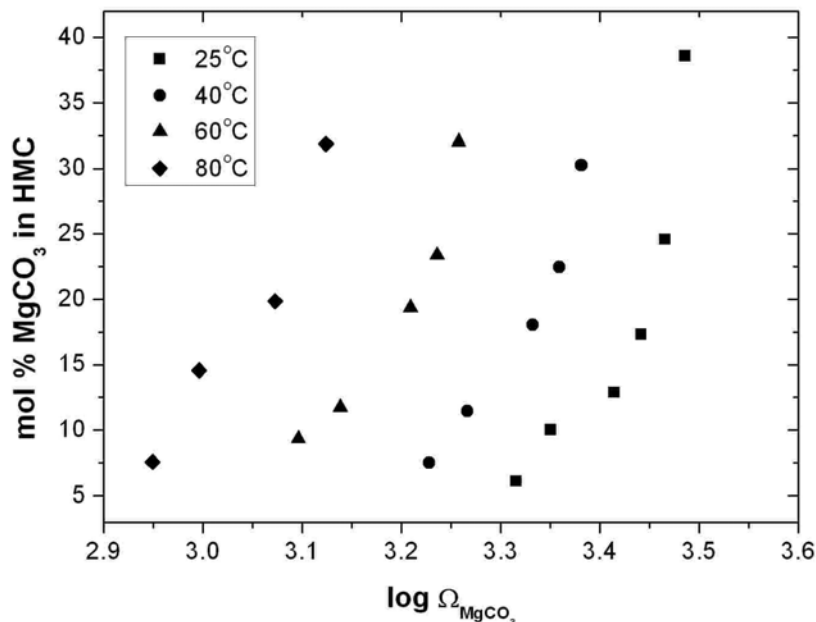


Figure 3.3: Influence of the saturation degree of  $\text{MgCO}_3$ , on the composition of precipitated solid phases in the temperature range 25 - 80°C.

The magnesium-content data of HMC analyzed by ICP-AES (Table 3.2) is used for the calculations presented in Fig. 3.3. This data differs somewhat

from the calculated  $\text{MgCO}_3$  content using XRD (Table 3.2). The discrepancy was also noted by Bischoff et al. (1983) who measured the  $\text{Mg}^{2+}$  content in biogenic Mg-calcites by using both XRD and wet chemical techniques (AAS). We noted that the difference between XRD and ICP-AES increases with increasing Mg:Ca ratios of the initial solution (Table 3.2). It is indicated that the Mg-content measured by XRD probably underestimates the Mg-content of synthesized HMC (Table 3.2). This observation can be result of zoning phenomenon, as crystal growth took place in batch reactors where the saturation degree  $\Omega$  of Mg-calcite in solution is constantly changing over time due to precipitation. Furthermore it is expected that the  $\text{MgCO}_3$  content of the Mg-calcite crystal to be reduced from the inner to the outer layers following the reduced  $\Omega$  values of solution (Pokrovsky, 1998). Thus if it is considered that X-ray diffraction has penetration depths of few microns, the underestimation of  $\text{MgCO}_3$  content in the crystals calculated from the XRD patterns compared to ICP-AES results can be explained. Moreover, EDX element analyses of selected samples revealed that within the same sample variations in Mg:Ca ratio of up to 10% occur. These differences may also depend on the formation process as it has been shown that  $\text{Mg}^{2+}$  is not uniformly incorporated into calcite crystal surfaces (Zhang and Dawe, 2000). Hence, for the following discussions and isotope fractionation calculations the Mg content of HMC determined by ICP-AES is applied.

### 3.3.4 Stable oxygen isotope fractionation of HMC-H<sub>2</sub>O

Oxygen isotope data presented in Table 3.2 refer to the precipitated CaMg-carbonate material before (bulk carbonate) and after (HMC) applying the partial dissolution process. The latter values have been used for the calculation of the temperature-dependent oxygen isotope fractionation between HMC of various Mg-contents and water (Table 3.2). The  $\delta^{18}\text{O}$  values of HMC precipitated at temperatures between 25 and 80°C range between 12.2 and 23.2 ‰ (Table 3.2). The  $\delta^{18}\text{O}$  values decrease with increasing temperature, which may reflect thermodynamically controlled mineral-water isotope fractionation in the carbonate precipitation experiments. However, rapid precipitation as a result of mixing supersaturated initial solutions (Table 3.1) could lead to deviation from

equilibrium fractionation. Thus, one cannot exclude that isotope equilibrium was not finally be reached in our precipitation experiments, although a temperature relationship exists (Kim and O'Neil, 1997; Mickler et al., 2004).

The  $\delta^{18}\text{O}$  values of HMC samples have been compared with that of the bulk precipitants (Table 3.2). All the bulk samples which probably contain amorphous carbonate of unknown quantities have  $\delta^{18}\text{O}$  values lower than the respected partially dissolved HMC samples. Differences in the  $\delta^{18}\text{O}$  value have a maximum of 0.9 ‰ for samples precipitated at 25°C, but less than 0.07 ‰ for precipitants formed at 80°C. These somewhat lower  $\delta^{18}\text{O}$  values of bulk precipitation products are probably best explained by a postulated lower oxygen isotope fractionation factor for loosely bound oxygen in the polycarbonate framework of amorphous carbonate. Selected bulk samples were treated 3 times by the partial dissolution technique to evaluate when the amorphous material is more or less quantitatively removed from the bulk precipitants. No significant differences were recorded by FTIR spectroscopy and  $\delta^{18}\text{O}$ -measurements between the several steps (Table 3.4), probably indicating nearly quantitative removal of amorphous carbonate in one partial dissolution treatment.

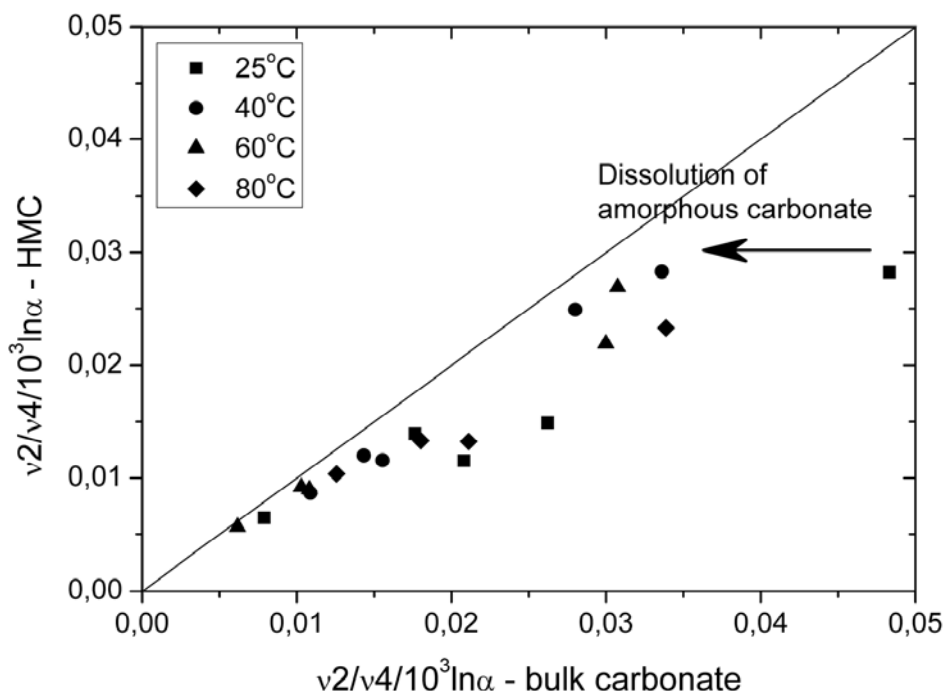


Figure 3.4: Normalized  $v_2/v_4/10^3 \ln \alpha$  versus  $\text{MgCO}_3$  content before and after dissolution. The arrow indicates the effect of dissolution of amorphous carbonate.

To estimate the effect of amorphous carbonate on the oxygen isotope fractionation of the precipitated CaMg-carbonates the  $\nu_2/\nu_4$  infrared intensity ratios and the  $1000\ln\alpha$  values were used. In general the differences before and after partial dissolution of  $\nu_2/\nu_4$  peak intensity ratios and the  $1000\ln\alpha$  values are negatively correlated (Table 3.2 and Table 3.3). For detailed evaluation the Mg-normalized  $\nu_2/\nu_4$  ratios over  $10^3\ln\alpha$  of the bulk CaMg-carbonates are plotted against the respected value of the samples after partial dissolution (Fig. 3.4). Assuming that the partial dissolution will remove amorphous carbonate and will not affect the crystalline (dis)order of HMC, the deviation of the Mg-normalized  $(\nu_2/\nu_4)/10^3\ln\alpha$  values from the bisecting line is a measure for the influence of amorphous content on  $\delta^{18}\text{O}$ -value of the precipitated material (Fig. 3.4). The largest deviations and thus highest influence of amorphous carbonate on the  $\delta^{18}\text{O}$ -value can be measured for the low (25°C) temperature precipitates. This is in accordance to Schmidt et al. (2005) and the observed mineralogy and morphology in this study.

The isotope fractionation between HMC and water does not only vary with temperature but also with the Mg-content in HMC (Table 3.2). E.g.  $1000\ln\alpha_{\text{HMC-H}_2\text{O}}$  at 25°C increases with increasing  $\text{MgCO}_3$ -content of calcite by about  $0.14 \pm 0.04$  per mol %  $\text{MgCO}_3$ . The increase at 40, 60 and 80°C per mol %  $\text{MgCO}_3$  substituted in the calcite lattice is  $0.10 \pm 0.03$ ,  $0.07 \pm 0.03$  and  $0.04 \pm 0.02$ , respectively. Considering all experimentally derived  $10^3\ln\alpha$  HMC-H<sub>2</sub>O values at temperatures between 25 and 80°C (Table 3.2) the following equation can be calculated:

$$1000\ln\alpha_{\text{HMC-H}_2\text{O}} = 18.03x - 32.42 + (0.6x^3 - 5.47x^2 + 16.78x - 17.21)C_{\text{Mg}}$$

where  $x$  is  $10^3/T$  and  $C_{\text{Mg}}$  is the molar percentage of  $\text{MgCO}_3$  incorporated into the crystal lattice. The first two terms of the equation are derived from the calcite-water fractionation equation after Kim and O'Neil (1997), and the third term mathematically describes the effect of the Mg-content of HMC on the oxygen isotope fractionation (this study).

For the calculation of the equation, the mean increase per  $\text{MgCO}_3$  mol % in the  $10^3\ln\alpha$  value was calculated for each temperature, expressed as differ-

ence from the calcite-water fractionation line of Kim and O'Neil (1997). A 3rd-order polynomial equation was fitted to the deviation data. The fit was then added to the calcite-water fractionation line of Kim and O'Neil (1997). Finally, this fit was added to the calcite-water fractionation line of Kim and O'Neil (1997).

The calculated oxygen isotope fractionation equation with Mg-content of 10 mol % is presented in Fig. 3.5 and is compared with the respected calcite-water fractionation equation of Kim and O'Neil (1997), and the statistical-mechanical HMC(10%)-water fractionation line calculated after Chacko and Deines (2008). Experimentally determined oxygen isotope fractionation data of 10 mol % HMC formed in water at 25°C (Tarutani et al., 1969; Jimenez-Lopez et al., 2004), is also plotted in Fig. 3.5.

The  $10^3 \ln \alpha_{\text{HMC-H}_2\text{O}}$  values of laboratory precipitates from this study fall above Kim and O'Neil's (1997) calcite-water oxygen isotope fractionation line. This is general in accordance to other published Mg-calcite - water fractionation values (Tarutani et al., 1969; Jimenez-Lopez et al., 2004; Chacko and Deines, 2008). For instance at 25°C, we calculate a positive shift of  $10^3 \ln \alpha$  of  $0.14 \pm 0.04$  per mol  $\text{MgCO}_3$ , which is comparable to the value given by Jimenez-Lopez et al. (2004), who determined an increase in the  $10^3 \ln \alpha$  value of  $0.17 \pm 0.02$  per mol  $\text{MgCO}_3$  at 25°C. However, Tarutani et al. (1969) reported an increase of  $10^3 \ln \alpha$  of about 0.06 per mol  $\text{MgCO}_3$ . Jimenez-Lopez et al., (2004) argued that the presence of organic acids in the Tarutani et al. (1969) experiments could have caused the lower oxygen isotope fractionation data of Tarutani et al. (1969). Moreover, lower fractionation data can also be caused by misestimating the  $\text{Mg}^{2+}$  content by using XRD for this calculation (Jimenez-Lopez et al., 2004).

Table 3.4: Stable oxygen isotope values and infrared spectral data at the several steps of dissolution.

Sample	bulk carbonate	1 <sup>st</sup> step		2 <sup>nd</sup> step		3 <sup>rd</sup> step		
		$\nu_2/\nu_4$	$\delta^{18}\text{O}$ (V-SMOW)	$\nu_2/\nu_4$	$\delta^{18}\text{O}$ (V-SMOW)	$\nu_2/\nu_4$	$\delta^{18}\text{O}$ (V-SMOW)	$\nu_2/\nu_4$
25-2a	21.15	9	21.94	7.3	21.96	7.3	21.97	7.2
40-4a	17.49	8.3	17.88	7.5	17.85	7.4	17.91	7.5

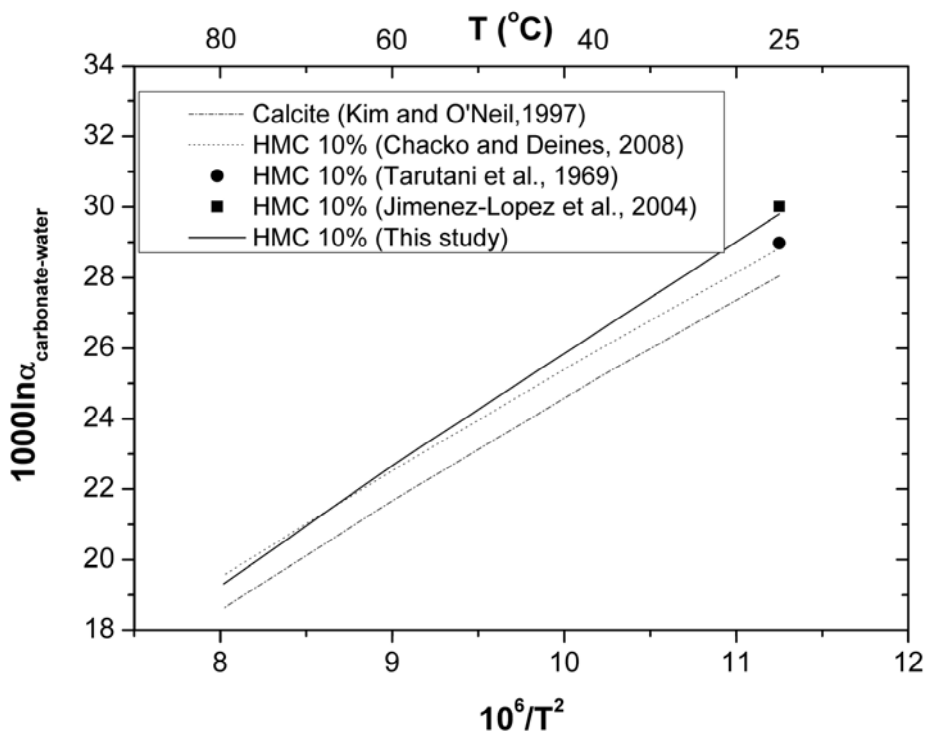


Figure 3.5: Oxygen isotope fractionation of laboratory precipitated HMC with 10 %  $\text{MgCO}_3$  content in comparison with calcite-water fractionation line from Kim and O'Neil (1997) and 10% HMC derived from Tarutani et al. (1969) and Chacko and Deines (2008).

Tarutani et al. (1969) extrapolated the defined  $10^3 \ln \alpha_{\text{HMC-CC}}$  difference at 25°C to a wide range of temperature. Our laboratory experiments indicate, however, that at 80°C the  $\text{Mg}^{2+}$  incorporation in the HMC lattice has a minor effect on the HMC - water oxygen isotope fractionation, whereas at low temperatures, (e.g. 25, 40°C) the HMC - water oxygen isotope fractionation significantly increases relative to that of pure (Mg-free) calcite. A similar relationship was described by statistical mechanical calculations (Chacko and Deines, 2008 in Fig. 3.5). The authors showed that the effect of magnesium on the oxygen isotope fractionation in the carbonate – water system is reduced with increasing temperatures. However, at temperatures lower than 40°C our experimentally derived data show higher oxygen isotope fractionation of about one unit on the  $10^3 \ln \alpha$  scale relative to the theoretical calculated values. At present an explanation for the differences at low temperatures between experimental determined oxygen isotope fractionation values and theoretical data cannot be given. However, Chacko and Deines (2008) suggest that the phosphoric acid fractionation factors used to determine the oxygen isotope fractionations of car-

bonates is not entirely optimized. Applying the approach of Boettcher (1996) by using end-member phosphoric acid fractionation values of calcite (Kim et al., 2007) and magnesite (Sharma et al., 2002), the acid fractionation factor of 10%-HMC at 73°C reaction temperature can be estimated. The difference in the phosphoric acid oxygen isotope fractionation between 10 mol % HMC and calcite at 73° C (reaction temperature) is about 0.2 ‰. The small difference, however, cannot explain the observed deviation between the statistical mechanical calculation of Chacko and Deines (2008) and our experimental derived HMC-water oxygen isotope fractionation.

### 3.4 Conclusions

The stable oxygen isotope fractionation of the HMC-water system was investigated experimentally by temperature controlled carbonate precipitation from supersaturated solutions with respect to CaMg-carbonates. The experiments were conducted at temperatures between 25 and 80°C in closed reaction vessels with mixtures of  $\text{CaCl}_2$ - $\text{MgCl}_2$  and  $\text{Na}_2\text{CO}_3$  solutions. At these conditions mainly (micro)crystalline HMC with  $\text{MgCO}_3$ -contents between 6 and 32 mol % was formed. The degree of  $\text{Mg}^{2+}$ -incorporation into calcite crystal lattice could be correlated to the saturation degree of magnesite in the initially mixed solution. The data show that the Mg-content of HMC increases exponentially with increasing degree of supersaturation of magnesite ( $\log \Omega_{\text{MgCO}_3}$ ), and supersaturation decreases with increasing temperature between 25 and 80°C. Moreover, at constant  $\log \Omega_{\text{MgCO}_3}$  higher Mg-contents in HMC are favored with increasing temperatures.

Although mostly HMC was formed during precipitation from supersaturated solutions amorphous carbonate co-precipitating occurs. Nearly quantitative dissolution of amorphous carbonate can be achieved by stepwise acid leaching leaving almost pure HMC. This HMC purification process does not change the mineral structure or the oxygen isotopic composition of the precipitated HMC. Based on the purified HMC samples a new oxygen isotope fractionation equation for the HMC - water system was established in this study.

The new equation combines the published calcite-water fractionation equation and a term (this study) considering the isotope fractionation change with respect to the Mg-content in HMC. The new equation is valid at HMC formation temperatures between 25 and 80°C.

The effect of magnesium on the oxygen isotope fractionation of HMC-H<sub>2</sub>O is reduced at elevated temperature. Our fractionation data at 40-80°C temperatures are in good agreement with mechanical statistical calculations. Our experimentally determined oxygen isotope fractionation value at 25°C is larger compared to the theoretically calculated fractionation value, and slightly lower compared to recent laboratory studies. By combining the 25°C-isotope fractionation values a mean  $10^3 \ln \alpha$  HMC-H<sub>2</sub>O value of 29.57 ( $\pm 0.04$ ) can be calculated for a 10 mol % MgCO<sub>3</sub> HMC. The range of variation is still too large to e.g. accurately constrain climatic variations of temperatures from HMC (which is abundant in marine and lacustrine environment). Therefore, further research is needed to precisely define the effect of Mg<sup>2+</sup> on the  $\delta^{18}\text{O}$  values of Mg-calcites at low temperatures.

## References

Addadi L., Raz S. and Weiner S. (2003) Taking Advantage of Disorder: Amorphous Calcium Carbonate and Its Roles in Biomineralization. *Adv. Mater.* **15**, 959-970.

Adler H. H. and Kerr P. F. (1962) Infrared study of aragonite and calcite. *Am. Mineral.* **47**, 700-717.

Aizenberg J., Addadi L., Weiner S. and Lambert G. (1996) Stabilization of amorphous calcium carbonate by specialized macromolecules in biological and synthetic precipitates. *Adv. Mater.* **8**, 222-226.

Aizenberg J., Lambert G., Weiner S. and Addadi L. (2002) Factors Involved in the Formation of Amorphous and Crystalline Calcium Carbonate: A Study of an Ascidian Skeleton. *J. Am. Chem. Soc.* **124**, 32-39.

Aizenberg J., Muller D. A., Grazul J. L. and Hamann D. R. (2003) Direct Fabrication of Large Micropatterned Single Crystals. *Science* **299**, 1205-1208.

Ajikumar P. K., Wong L. G., Subramanyam G., Lakshminarayanan R. and Valiyaveetil S. (2005) Synthesis and Characterization of Monodispersed Spheres of Amorphous Calcium Carbonate and Calcite Spherules. *Cryst. Growth. Des.* **5**, 1129-1134.

Beniash E., Aizenberg J., Addadi L. and Weiner S. (1997) Amorphous calcium carbonate transforms into calcite during sea urchin larval spicule growth. *Proc. Roy. Soc. Lond. B Biol. Sci.* **264**, 461-465.

Berner R.A. (1975) The role of magnesium in the crystal growth of calcite and aragonite from sea water. *Geochim. Cosmochim. Acta* **39**, 489-504.

Berner R. A. (1978) Equilibrium, kinetics, and the precipitation of magnesian calcite from seawater; discussion. *Am J Sci* **278**, 1475-1477.

Bischoff W. D., Bishop F. C. and Mackenzie F. T. (1983) Biogenically produced magnesian calcite; inhomogeneities in chemical and physical properties; comparison with synthetic phases. *Am. Mineral.* **68**, 1183-1188.

Bischoff W. D., Sharma S. K. and Mackenzie F. T. (1985) Carbonate ion disorder in synthetic and biogenic magnesian calcites; a Raman spectral study. *Am. Mineral.* **70**, 581-589.

Bischoff W. D., Mackenzie F. T. and Bishop F. C. (1987) Stabilities of synthetic magnesian calcites in aqueous solution; comparison with biogenic materials. *Geochim. Cosmochim. Acta* **51**, 1413-1423.

Böttcher M. E. (1996)  $^{18}\text{O}/^{16}\text{O}$  and  $^{13}\text{C}/^{12}\text{C}$  Fractionation during the reaction of carbonates with phosphoric acid: effects of cationic substitution and reaction temperature. *Isot. Environ. Health Stud.* **32**, 299-305.

Böttcher M. E., Gehlken P. L. and Steele D. F. (1997) Characterization of inorganic and biogenic magnesian calcites by Fourier Transform infrared spectroscopy. *Solid State Ionics* **101-103**, 1379-1385.

Brecevic L. and Nielsen A. E. (1989) Solubility of amorphous calcium carbonate. *J. Cryst. Growth* **98**, 504-510.

Brecevic L., Nothig-Laslo V., Kralj D. and Popovit S. (1996) Effect of divalent cations on the formation and structure of calcium carbonate polymorphs. *J. Chem. Soc. Faraday Trans.* **92**, 1017-1022.

Budd D. A. and Hiatt E. E. (1993) Mineralogical stabilization of high-magnesium calcite; geochemical evidence for intracrystal recrystallization within Holocene porcellaneous foraminifera. *J. Sediment. Petrol.* **63**, 261-274.

Chacko T. and Deines P. (2008) Theoretical calculation of oxygen isotope fractionation factors in carbonate systems. *Geochim. Cosmochim. Acta* **72**, 3642-3660.

Chen T., Neville A. and Yuan M. (2006) Influence of Mg<sup>2+</sup> on CaCO<sub>3</sub> formation-bulk precipitation and surface deposition. *Chem. Eng. Sci.* **61**, 5318-5327.

Clarkson J. R., Price T. J. and Adams C. J. (1992) Role of metastable phases in the spontaneous precipitation of calcium carbonate. *J. Chem. Soc. Faraday Trans.* **88**, 243-249.

Comas-Bru L. (2007) CaMg-carbonate precipitation experiments: Geochemical, Mineralogical and stable isotopes investigations. MSc. Thesis, Univ. Kiel, Germany.

Coplen T. B., Kendall C. and Hopple J. (1983) Comparison of stable isotope reference samples. *Nature* **302**, 236-238.

Craig H., (1961) Standard for reporting concentrations of deuterium and oxygen-18 in natural waters. *Science* **133**, 1833-1834.

Donners J. J. J. M., Heywood B. R., Meijer E. W., Roeland J. M., Nico N. and Sommerdijk A. J. M. (2002). Control over calcium carbonate phase formation by dendrimer/surfactant templates. *Chem. Eur. J.* **8**, 2561-2567.

Falini G., Gazzano M. and Ripamonti A. (1994) Crystallization of calcium carbonate in presence of magnesium and polyelectrolytes. *J. Cryst. Growth* **137**, 577-584.

Glover E. D. and Sippel R. F. (1967) Synthesis of magnesium calcites. *Geochim. Cosmochim. Acta* **31**, 603-613.

Goldsmith J. R., Graf D.L. and Heard H. C. (1961) Lattice constants of the calcium-magnesium carbonates. *Am. Mineral* **46**, 453-457.

Gueta R., Natan A., Addadi L., Weiner S., Refson K. and Kronik L. (2007) Local atomic order and infrared spectra of biogenic calcite. *Angew. Chem.* **119**, 295-298.

Horita J. and Clayton R. (2007) The studies of oxygen isotope fractionation between calcium carbonates and water at low temperatures; discussion. *Geochim. Cosmochim. Acta* **71**, 3131-3135.

House W. A., Howson M. R. and Pethybridge A. D. (1988) Crystallization kinetics of calcite in the presence of magnesium ions. *Faraday Trans.* **84**, 2723-2734.

Jimenez-Lopez C., Romanek C. S., Huertas F. J., Ohmoto H. and Caballero E. (2004) Oxygen isotope fractionation in synthetic magnesian calcite. *Geochim. Cosmochim. Acta* **68**, 3367-3377.

Kim S. T., Mucci A. and Taylor B.E. (2007) Phosphoric acid fractionation factors for calcite and aragonite between 25 and 75°C: Revisited. *Chem Geol.* **246**, 135-146.

Kim S. T. and O' Neil J. R. (1997) Equilibrium and nonequilibrium oxygen isotope effects in synthetic carbonates. *Geochim. Cosmochim. Acta* **61**, 3461-3475.

Kitamura M. (2001) Crystallization and transformation mechanism of calcium carbonate polymorphs and the effect of magnesium ion. *J. Colloid Interface Sci.* **236**, 318-327.

Königsberger E., Schmidt P. and Gamsjäger H. (1992) Solid-solute phase equilibria in aqueous solution. VI. Solubilities, complex formation, and ion-interaction parameters in the system  $\text{Na}^+ - \text{Mg}^{2+} - \text{ClO}_4^- - \text{CO}_2 - \text{H}_2\text{O}$  at 25°C. *J. Solution Chem.* **21**, 1195-1261.

Kralj D., Kontrec J., Brecevic L., Falini G. and Nöthig-Laslo V. (2004) Effect of inorganic anions on the morphology and structure of magnesium calcite. *Chem. Eur. J.* **10**, 1647-1656.

Levi-Kalisman Y., Raz S., Weiner S., Addadi L. and Sagi I. (2000) X-Ray absorption spectroscopy studies on the structure of a biogenic "amorphous" calcium carbonate phase. *J. Chem. Soc. Dalton. Trans.* 3977-3982.

Levi-Kalisman Y Raz S., Weiner S., Addadi L. and Sagi I. (2002) Structural differences between biogenic amorphous calcium carbonate phases using x-ray absorption spectroscopy. *Adv. Funct. Mater.* **12**, 43-48.

Loste E., Wilson R. M., Seshadri R. and Meldrum F. C. (2003) The role of magnesium in stabilising amorphous calcium carbonate and controlling calcite morphologies. *J. Cryst. Growth* **254**, 206-218.

Mackenzie F. T., Bischoff W. D., Bishop F. C., Loijens M., Schoonmaker J. and Wollast R. (1983) Magnesian calcites; low-temperature occurrence, solubility and solid-solution behavior. *Rev. Mineral. Geochem.* **11**, 97-144.

Meldrum F. C. and Hyde S. T. (2001) Morphological influence of magnesium and organic additives on the precipitation of calcite. *J. Cryst. Growth* **231**, 544-558.

Mickler P. J., Banner J. L., Stern L., Asmerom Y., Edwards R. L. and Ito, E. (2004) Stable isotope variations in modern tropical speleothems; evaluating equilibrium vs. kinetic isotope effects. *Geochim. Cosmochim. Acta* **68**, 4381-4393.

Morse J. W. (1983) The kinetics of calcium carbonate dissolution and precipitation. *Rev. Mineral. Geochem.* **11**, 227-264.

Morse J. W. and Arvidson R. S. (2002) The dissolution kinetics of major sedimentary carbonate minerals. *Earth Sci. Rev.* **58**, 51-84.

Morse J. W., Arvidson R. S. and Lutge A. (2007) Calcium carbonate formation and dissolution. *Chem. Rev.* **107**, 342-381.

Mucci A. and Morse J. W. (1983) The incorporation of Mg<sup>2+</sup> and Sr<sup>2+</sup> into calcite overgrowths; influences of growth rate and solution composition. *Geochim. Cosmochim. Acta* **47**, 217-233.

Ogino T., Suzuki T. and Sawada K. (1987) The formation and transformation mechanism of calcium carbonate in water. *Geochim. Cosmochim. Acta* **51**, 2757-2767.

Parkhurst, D.L., Appelo, C.A.J. (1999) User's guide to PHREEQC (Version 2) - A computer program for speciation, batch-reaction, one-dimensional transport, and inverse geochemical calculations. U.S. Geological Survey Water-Resources Investigations Report 99-4259, Denver, Colorado, 312

Pokrovsky O. S. (1998) Precipitation of calcium and magnesium carbonates from homogeneous supersaturated solutions. *J. Cryst. Growth* **186**, 233-239.

Raz S., Weiner S. and Addadi L. (2000) Formation of high-magnesian calcites via an amorphous precursor phase: Possible biological implications. *Adv. Mater.* **12**, 38-42.

Reddy M. M. and Wang K. K. (1980) Crystallization of calcium carbonate in the presence of metal ions: I. Inhibition by magnesium ion at pH 8.8 and 25°C. *J. Cryst. Growth* **50**, 470-480.

Rushdi, A. I., Pytkowicz, R. M., Suess, E. and Chen, C. T. (1992) The effects of magnesium-to-calcium ratios in artificial seawater, at different ionic products, upon the induction time, and the mineralogy of calcium carbonate; a laboratory study. *Geol Rundsch Z Allg Geol* **81**, 571-578.

Sawada K., Ogino T. and Suzuki T. (1990) The distribution coefficients of  $Mg^{2+}$  ion between  $CaCO_3$  polymorphs and solution and the effects on the formation and transformation of  $CaCO_3$  in water. *J. Cryst. Growth* **106**, 393-399.

Schmidt M., Xeflide S., Botz R. and Mann S. (2005) Oxygen isotope fractionation during synthesis of Ca-Mg carbonate and implications for sedimentary dolomite formation. *Geochim. Cosmochim. Acta* **69**, 4665-4674.

Sharma S. D., Patil D. J. and Gopalan, K. (2002) Temperature dependence of oxygen isotope fractionation of  $CO_2$  from magnesite-phosphoric acid reaction. *Geochim. Cosmochim. Acta* **66**, 589-593.

Tarutani T., Clayton R. N. and Mayeda T. K. (1969) The effect of polymorphism and magnesium substitution on oxygen isotope fractionation between calcium carbonate and water. *Geochim. Cosmochim. Acta* **33**, 987-996.

Wada N., Yamashita K. and Umegaki T. (1995) Effects of divalent cations upon nucleation, growth and transformation of calcium carbonate polymorphs under conditions of double diffusion. *J. Cryst. Growth* **148**, 297-304.

White W. B. (1974) The carbonate minerals. In *The infrared spectra of minerals*, (ed. V. C. Farmer). Mineralogical Society, London pp. 227-284.

Zhang Y. and Dawe R. A. (2000) Influence of Mg<sup>2+</sup> on the kinetics of calcite precipitation and calcite crystal morphology. *Chem. Geol.* **163**, 129-138.

Zheng Y. and Zhou G. (2007) The studies of oxygen isotope fractionation between calcium carbonates and water at low temperatures; reply. *Geochim. Cosmochim. Acta* **71**, 3136-3143.

Zhou G. T. and Zheng Y. F. (2005) Effect of polymorphic transition on oxygen isotope fractionation between aragonite, calcite, and water; a low-temperature experimental study. *Am. Mineral.* **90**, 1121-1130.



## Chapter IV

**Dissolution kinetics of a marine authigenic high-Mg calcite sample: an experimental approach.**

## Abstract

This study investigates the dissolution of authigenic high Mg-calcite (13 mol % MgCO<sub>3</sub>) dissolution in aqueous media at atmospheric pCO<sub>2</sub>. The dissolution reaction order and the kinetic constants were determined using an open system approach according to the empirical rate equation:

$$r = k(1 - \Omega)^n$$

where R is the rate, the constant k and the reaction order n are empirical fitting terms, and 1-Ω describes the degree of disequilibrium with respect to calcite. Dissolution experiments were performed in distilled water and 0.6 M NaCl solution. The reaction order n is determined as 0.7 for distilled water experiments whereas in seawater it is estimated as 4.1.

Using the calculated kinetic order and rate constant as input parameters, the dissolution of CaMg-carbonate was simulated in a numerical model. The obtained results have shown that the model-estimated reactive surface is in good agreement with the geometrical surface of the samples in distilled water experiments, denoting that geometric surface is controlling the dissolution rate. However, the dissolution rate of the carbonate sample in NaCl solutions is much higher and does not correlate with the geometric surface of the samples but rather to the ionic strength of the solution.

## 4.1 Introduction

Carbonate minerals are abundant in earth's surface. They play a very important role in controlling the chemical composition of natural waters and in the global CO<sub>2</sub> cycle. Thus, numerous studies focused on their formation and dissolution mechanisms. The dissolution of calcite and dolomite, the most common carbonate minerals in nature, has received a lot of attention. Several parameters like the influence of 'foreign ions' in solution, the temperature, the CO<sub>2</sub> partial pressure, and other factors affecting the dissolution of these minerals were previously examined (Berner and Wilde, 1972; Berner and Morse, 1974; Sjöberg and Rickard, 1983; Walter and Morse, 1984b, 1985; Herman and White, 1985; Brady and House, 1996; Alkattan et al., 1998; Pokrovsky and Schott, 2001, 2002 ; Morse and Arvidson, 2002; Arvidson et al., 2003; Harstad and Stipp, 2007; Zhang et al., 2007).

Magnesium is the cation that most commonly replacing calcium in calcite crystal lattice. Formation of low- (<5 mol % MgCO<sub>3</sub>) and high- (>5 mol % MgCO<sub>3</sub>) Mg-calcites is of great importance in processes like biomineralization, carbonate diagenesis and control of seawater saturation state (Plummer and Mackenzie, 1974; Bertram et al., 1991; Bischoff, 1998).

Although the dissolution of calcite has been previously well studied, only few dissolution experiments have been performed on biogenic and synthetic Mg-calcites. These experimental investigations provided important information for the dissolution mechanism of the mineral under environmental conditions (Keir, 1980; Walter and Morse, 1984b; Cubillas et al., 2005). However, the knowledge on Mg-calcite precipitation and dissolution kinetics is still limited and recent debates underline that Mg-calcite dissolution cannot be understood simply as a reverse crystal growth reaction (Morse et al., 2007). Moreover, special attention has to be given on Mg-calcite dissolution; hence this multi-component, metastable mineral phase often does not attain necessarily equilibrium during dissolution experiments, as less soluble mineral phases (i.e. dolomite, calcite) can precipitate prior to equilibrium with the initial solid Mg-CC phase (Bertram et al., 1991).

In the present work, we discuss dissolution experiments on a marine authigenic high-Mg calcite sample using an open system approach under atmospheric CO<sub>2</sub> pressure. Additionally, we used a biogenic low-Mg calcite, calcite and dolomite standards for a better comparison of our method with previously published data. We believe that the proposed dissolution kinetics can improve the current diagenetic models simulating dissolution/precipitation processes of authigenic carbonates in cold vent sites using first order kinetics e.g.: Luff and Wallmann, 2003; Luff et al., 2004.

## 4.2 Theoretical background

### 4.2.1 Mechanism of carbonate dissolution

The chemical reactions describing the dissolution of calcium carbonate in an open system are (Morse, 1983):



At the present work the above equation can be reformed, including the presence of magnesium in calcite crystals.

Additionally, the acid-base reactions of the carbonate system, taking place simultaneously and have always to be taken into account are:





where  $CO_2^* \leftrightarrow CO_2^* + H_2CO_3$  .

#### 4.2.2 Dissolution kinetics and constants

The dissolution rate  $r$  of carbonate minerals at neutral to basic pH values has been empirically well established by several authors (Morse, 1978; Walter and Morse, 1984b, 1985) to be defined as:

$$r = k(1 - \Omega)^n \quad (10)$$

where  $k$  is the rate constant,  $n$  refers to the reaction order and equilibrium  $\Omega$  can be defined as:

$$\Omega = \frac{\alpha_{Ca^{2+}} \cdot \alpha_{CO_3^{2-}}}{K} \quad (11)$$

where  $\alpha_i$  is the activity of the  $i$ th aqueous species (or the *Ion Activity Product*) and  $K$  the equilibrium constant for the carbonate mineral phase.

In the case of magnesium incorporation into calcite lattice, it has been previously shown (Plummer and Mackenzie, 1974; Thorstenson and Plummer, 1977; Mucci and Morse, 1984; Walter and Morse, 1985; Bischoff et al., 1987) that, the ionic activity product should be written as:

$$IAP_{Mg-calcite} = \alpha_{Ca^{2+}}^{1-x} \cdot \alpha_{Mg^{2+}}^x \cdot \alpha_{CO_3^{2-}} \quad (12)$$

where  $x$  refers to the percentage of  $MgCO_3$  in the crystal lattice.

Hence the equation (11) will be written as:

$$\Omega = \frac{\alpha_{Ca^{2+}}^{1-x} \cdot \alpha_{Mg^{2+}}^x \cdot \alpha_{CO_3^{2-}}}{K} \quad (13)$$

The calculation of the reaction order and the dissolution rate constant, is possible if equation (10) becomes linear. In its logarithmic form, the order of the

reaction  $n$  and the rate constant  $k$  could then be determined from the slope and the intercept in a  $\log(r)$  versus  $\log(1-\Omega)$  diagram (Morse, 1978; 1983)

### 4.2.3 Equilibrium constants and IAP of dissolution for CaMg-carbonates

The temperature dependent equilibrium constant of calcite ( $10^{-8.48}$  at  $25^\circ\text{C}$ ) in aqueous solution is well established in the literature and was determined using liquid-junction corrected pH measurements in Ca-HCO<sub>3</sub> solutions (Plummer and Busenberg, 1982). The equilibrium constant of dolomite ( $10^{-17.09}$  at  $25^\circ\text{C}$ ), is based on calorimetric measurements (Robie and Hemingway, 1995). The equilibrium constants of the Mg-calcites used in this study, are calculated according to the model proposed and evaluated by Busenberg and Plummer (Plummer and Busenberg, 1987; Busenberg and Plummer, 1989). The equilibrium constant  $K$  is defined as:

$$K_x = \frac{x(1-x)}{RT} [A_o + A_1(2x-1)] + (1-x)\ln[K_c(1-x)] + x\ln(K_D x) \quad (14)$$

where  $x$  is the mole fraction of the end member Ca<sub>0.5</sub>Mg<sub>0.5</sub>CO<sub>3</sub> in the solid-solution,  $R$  is the molar gas constant and  $T$  is the temperature (K). The Guggenheim mixing parameters  $A_o$  and  $A_1$  were evaluated from the authors at  $25^\circ\text{C}$  and take the values 12.6 and 4.7 KJ mol<sup>-1</sup> respectively.

The ionic activity products for the dissolved species can be calculated with PHREEQC (Parkhurst and Appelo, 1999).

## 4.3 Methods

### 4.3.1 Sample preparation and characterization

A marine authigenic high Mg-calcite (HMC) sample and a biogenic low Mg-calcite (LMC) sample (see origin and mineralogy in Table 4.1) were used in the dissolution experiments. Dissolution experiments were also performed with pure samples of naturally occurring calcite and dolomite crystals (Alfa Aesar

GmbH). All samples were grained mechanically and the surface area of the powders (Table 4.1) was determined by BET measurements (Brunauer et al., 1938).

For a dissolution study, the homogeneity of the solid sample is very important, that fore the isotopic composition and the total carbonate and organic carbon content of the authigenic concretion used have been examined in detail. Isotopic composition of the sample was measured with a Finnigan MAT 251 IR-MS spectrometer after the reaction of carbonate powder with 100 % phosphoric acid at 73 °C with precisions  $\pm 0.04\text{‰}$  and  $\pm 0.06\text{‰}$  for  $\delta^{13}\text{C}$  and  $\delta^{18}\text{O}$  respectively. Total carbon was analyzed by combustion of bulk samples at 900 °C (702-LI Ströhlein Instruments). Total inorganic carbon content was measured with a Carbon Coulometer by sample treatment with phosphoric acid (20%). The precision was 2%. Total organic carbon was calculated by subtraction. Photo of the sample and sampling spots for isotopic measurements can be found in Plate 1a. The results for the sub-sample isotopic measurements, mineralogy and total carbonate content can be found in Table 4.2.

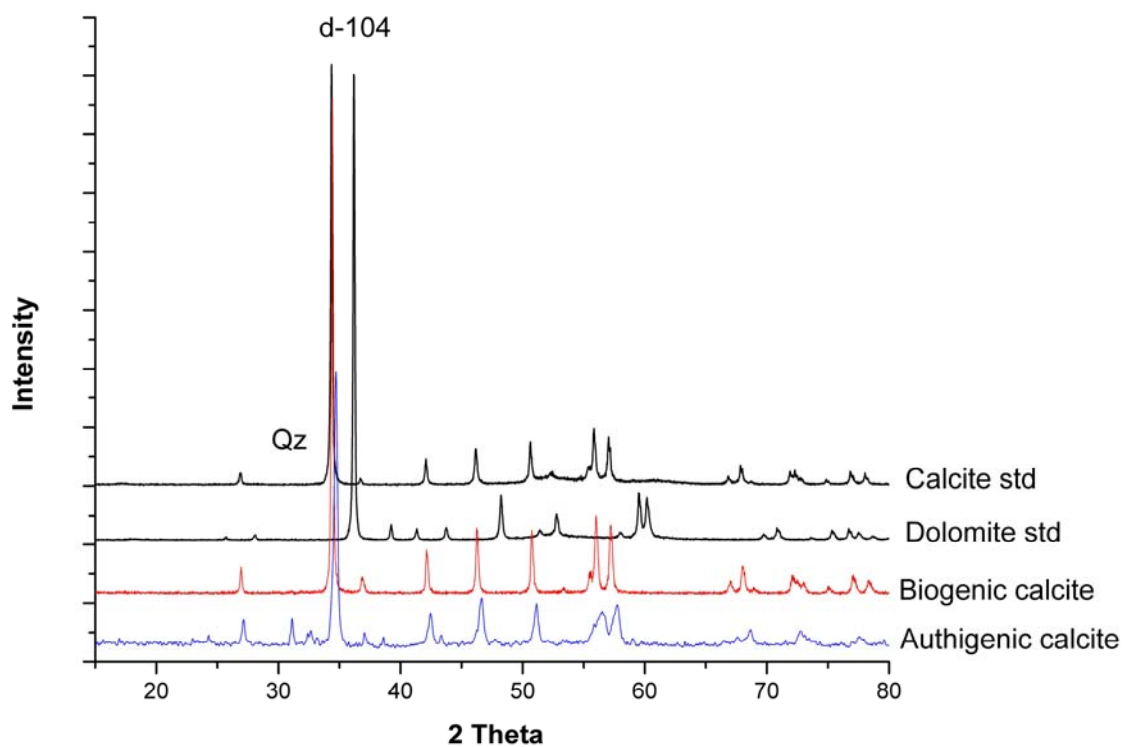


Figure 4.1: X-ray diffraction patterns of the used minerals. The presence of quartz in the marine authigenic calcite is obvious.

Table 4.1: Carbonates used in the dissolution experiments, their composition and specific surface area

Sample	Origin	Mineral phases	Mole % MgCO <sub>3</sub>	Specific surface area (m <sup>2</sup> g <sup>-1</sup> )
Calcite std	Natural mineral occurring	Calcite	>1	3.0
Dolomite std	Natural mineral occurring	Dolomite	50	2.4
Authigenic calcite (marine)	Mound Quetzal, Costa Rica forearc	Mg-calcite, Quartz	13	11.1
Biogenic calcite	<i>Cidaris</i> sp. (spikes)	Mg-calcite	4	3.3

### 4.3.2 X-ray diffraction (XRD measurements)

The mineralogy of the samples was defined using X-ray diffraction (PW 1710/Philips, Co-K $\alpha$ , 0.02° s<sup>-1</sup>) technique. The detection limit for a mineral phase is 2% of the sample mass. The d-104 peak was used to determine the molar percentage of MgCO<sub>3</sub> in the crystal lattice (Goldsmith et al., 1961). The error of this calculation is defined as  $\pm 1\%$  of MgCO<sub>3</sub> in the crystal lattice. The results are presented in Table 4.1 and Fig. 4.1.

### 4.3.3 Experimental set-up

20 mg of each powdered carbonate sample were added into 200 ml of CO<sub>2</sub>-free distilled water and stored in 300 ml beakers. All experiments were conducted at laboratory room temperature (20°C). Sub-samples for elemental composition (1 ml) were collected after 1 and 4 hours and in an interval of 24 hours, up to 360 hours. Parallel the pH of the solutions was monitored by a WTW Multi340i pH-meter ( $\pm 0.08$  pH units,  $\pm 0.3$  °C). The sample beakers were stirred frequently. For “seawater” experiments 35 g NaCl of analytical grade was added per liter of distilled water, and for this work the expression “seawater” will refer to the described composition.

Table 4.2: Mineralogical and geochemical data of subsamples taken from the authigenic concretion used for the present work (Plate 1a).

Subsample	$\delta^{13}\text{C}$	$\delta^{18}\text{O}$	Mineralogy	CaCO <sub>3</sub> %	TOC%
1	-46,90	5,44	HMC13%	74	0.6
2	-47,37	5,44	HMC13%		
3	-46,51	5,35	HMC13%	75	0.3

#### 4.3.4 Ca and Mg analyses (ICP-AES)

The concentrations of  $\text{Ca}^{2+}$  and  $\text{Mg}^{2+}$  in the aqueous sub-samples were determined by Inductively Coupled Plasma Atomic Emission Spectrometry (JY 170 Ultrace), after the addition of 20  $\mu\text{l}$  HCl ( $\sim 12\text{M}$ ) into 1 ml of sample. The standard error of the method was estimated as 0.3% for  $\text{Mg}^{2+}$  and 0.5% for  $\text{Ca}^{2+}$  according to deviations from laboratory standards.

#### 4.3.5 Dissolution rates

For the calculation of carbonate dissolution rates, the increase of  $\text{Ca}^{2+}$  and  $\text{Mg}^{2+}$  concentrations in the aqueous solution were used. The dissolution rates were calculated according to the following equation:

$$r = \frac{C_{\text{Ca+Mg}} \cdot V_{\text{sol}}}{A \cdot m} \quad (15)$$

where  $r$  gives the sum of moles of  $\text{Ca}^{2+}$  and  $\text{Mg}^{2+}$  released per square meter of the mineral surface ( $\text{mol/l/m}^2$ ),  $C_{\text{Ca+Mg}}$  is the sum of the concentrations of  $\text{Ca}^{2+}$  and  $\text{Mg}^{2+}$  in solution (mM) at the certain time-step.  $V_{\text{sol}}$  is the volume of solution (L),  $A$  is the initial surface area ( $\text{m}^2 \text{g}^{-1}$ ) and  $m$  is the mass of the sample powder (mg).

#### 4.3.6 Reactive surface calculation

The reaction order and the kinetic constants calculated from the experimental runs (see section 4.3) were also imported into PHREEQC (v2.15) to calculate the reactive surface area. The model includes calculations of the decrease in the mineral surface (spheres) by progressing dissolution. The results are then compared with the estimated geometric surfaces of the samples. Geometric surface areas ( $S_{\text{gsa}}$ ) in the present study were estimated by assuming that all grains were identical-sized smooth spheres (Walter and Morse, 1984b; Cubillas et al., 2005):

$$S_{\text{gsa}} = \frac{3}{r\rho} \quad (16)$$

where  $r$  represents the sphere radius and  $\rho$  stands for sample density.

## 4.4 Results and discussion

### 4.4.1 pH changes in aqueous solution by CaMg-carbonate dissolution

The pH changes over time in the experimental runs (Tables 4.3 and 4.4), are plotted in Fig. 4.2. A common feature of all the dissolution experiments is the increasing pH from the initial value of 7.0 to a maximum of 10.02. Later the pH values are decreasing rapidly within the first 50 hours and at a smoother rate up to 150 hours. After this time point, the pH value of all the samples remains nearly constant. Thus near-equilibrium conditions are expected.

There are two major processes controlling the pH value of solutions at the first hours of the experiment. These are the dissolution of the carbonate phase and the subsequent diffusion of atmospheric CO<sub>2</sub> in the alkaline aqueous solutions. The rapid increase of the pH value recorded at the first hours of dissolution is a kinetic process well examined in the literature (Berner and Morse, 1974; Plummer and Mackenzie, 1974; Plummer and Wigley, 1976). Initially, the solution is under-saturated with respect to every dissolved inorganic carbon (DIC) species. The addition of the solid carbonate mineral to the solution, results in a rapid increase of the pH value, which is barely resolved by our sampling steps (Fig. 4.2). According to Rickard and Sjöberg, 1983, the dissolution of calcite in neutral to alkaline solutions is independent of pH and controlled by mixed kinetics and the rate constant is dependent on the nature of the calcite reactant. Dissolution is generally accepted to be described by a sequence of three reactions (Eqn. 2, 4 and 5) that occur simultaneously at the calcite surface (Plummer et al., 1978; Reddy et al., 1981; Busenberg and Plummer, 1986; Svensson and Dreybrodt, 1992), and has been observed for other carbonate minerals like aragonite, witherite and magnesite (Chou et al., 1989).

However, the maximum pH value is not only defined by carbonate equilibrium but also by the diffusion of atmospheric CO<sub>2</sub> in the solution, which is lowering the pH according to eq. 6-8. The pH values are constant after ~150

Table 4.3:  $\text{Ca}^{2+}$ ,  $\text{Mg}^{2+}$  concentrations and pH values of dissolution experiments in distilled water.

Time (hours)	Calcite			Dolomite			Biogenic			Authigenic		
	Ca (mM)	Mg (mM)	pH	Ca (mM)	Mg (mM)	pH	Ca (mM)	Mg (mM)	pH	Ca (mM)	Mg (mM)	pH
1	0,27	-	9,79	0,14	0,133	9,49	0,19	0,01	9,91	0,21	0,027	9,75
4	0,16	-	9,95	0,07	0,062	9,66	0,15	0,009	10,02	0,14	0,016	9,95
24	0,15	-	9,9	0,05	0,044	9,67	0,15	0,009	9,94	0,14	0,017	9,95
48	0,16	-	9,02	0,11	0,112	8,47	0,18	0,011	8,9	0,21	0,019	9,03
72	0,44	-	8,78	0,21	0,174	8,38	0,23	0,013	8,8	0,21	0,021	8,76
96	0,54	-	8,69	0,17	0,163	8,26	0,23	0,013	8,65	0,29	0,023	8,71
120	0,57	-	8,74	0,22	0,218	8,28	0,27	0,015	8,74	0,31	0,034	8,67
144	0,58	-	8,59	0,2	0,186	8,21	0,33	0,016	8,39	0,38	0,043	8,48
168	0,6	-	8,43	0,22	0,206	8,25	0,32	0,016	8,47	0,4	0,045	8,43
192	0,63	-	8,37	0,25	0,251	8,15	0,33	0,017	8,21	0,42	0,052	8,36
216	0,65	-	8,37	0,29	0,268	8,2	0,35	0,018	8,45	0,44	0,053	8,33
240	0,58	-	8,34	0,31	0,276	8,25	0,37	0,019	8,25	0,44	0,053	8,31
264	0,68	-	8,29	0,32	0,285	8,17	0,38	0,019	8,31	0,45	0,055	8,3
288	0,69	-	8,31	0,34	0,297	8,1	0,39	0,019	8,35	0,45	0,055	8,27
312	0,69	-	8,1	0,33	0,288	8	0,41	0,02	8,25	0,44	0,055	8,27
336	0,68	-	8,21	0,34	0,3	8,06	0,42	0,021	8,2	0,46	0,055	8,21
360	0,7	-	7,97	0,34	0,316	7,85	0,43	0,021	8,2	0,47	0,058	8,14

Table 4.4:  $\text{Ca}^{2+}$ ,  $\text{Mg}^{2+}$  concentrations and pH values of dissolution experiments in seawater

Time (hours)	Calcite			Dolomite			Biogenic			Authigenic		
	Ca (mM)	Mg (mM)	pH	Ca (mM)	Mg (mM)	pH	Ca (mM)	Mg (mM)	pH	Ca (mM)	Mg (mM)	pH
1	0,51	-	9,67	0,11	0,111	9,22	0,35	0,017	9,53	0,29	0,04	9,57
4	0,61	-	9,63	0,2	0,189	9,17	0,3	0,015	9,54	0,34	0,045	9,58
24	0,78	-	9,27	0,29	0,276	8,75	0,39	0,019	9,23	0,5	0,067	9,22
48	0,79	-	9,04	0,3	0,321	8,52	0,49	0,023	9,01	0,51	0,068	9,03
72	0,82	-	8,82	0,34	0,33	8,31	0,55	0,026	8,86	0,57	0,077	8,9
96	0,75	-	8,75	0,36	0,344	8,26	0,64	0,029	8,73	0,59	0,078	8,74
120	0,83	-	8,65	0,35	0,335	8,28	0,68	0,03	8,7	0,63	0,084	8,7
144	0,74	-	8,56	0,35	0,338	8,25	0,7	0,031	8,63	0,64	0,086	8,6
168	0,85	-	8,55	0,36	0,354	8,23	0,73	0,032	8,59	0,64	0,086	8,64
192	0,8	-	8,52	0,37	0,359	8,15	0,75	0,034	8,48	0,66	0,086	8,55
216	0,86	-	8,46	0,35	0,371	8,13	0,77	0,034	8,47	0,69	0,088	8,42
240	0,83	-	8,58	0,38	0,384	8,22	0,79	0,034	8,54	0,67	0,087	8,44
264	0,82	-	8,53	0,39	0,387	8,25	0,82	0,036	8,56	0,67	0,088	8,42
288	0,85	-	8,47	0,39	0,392	8,28	0,81	0,036	8,51	0,68	0,088	8,41
312	0,85	-	8,5	0,4	0,397	8,28	0,84	0,037	8,54	0,67	0,089	8,45
336	0,84	-	8,48	0,4	0,41	8,24	0,82	0,036	8,58	0,68	0,089	8,45
360	0,84	-	8,42	0,41	0,404	8,16	0,84	0,037	8,48	0,73	0,09	8,38

hours in all the experiments. From this time point, the pH in solution (pH~8.25-8.75), is defined by the equilibrium of the carbonate-water system and the solubility of atmospheric CO<sub>2</sub>.

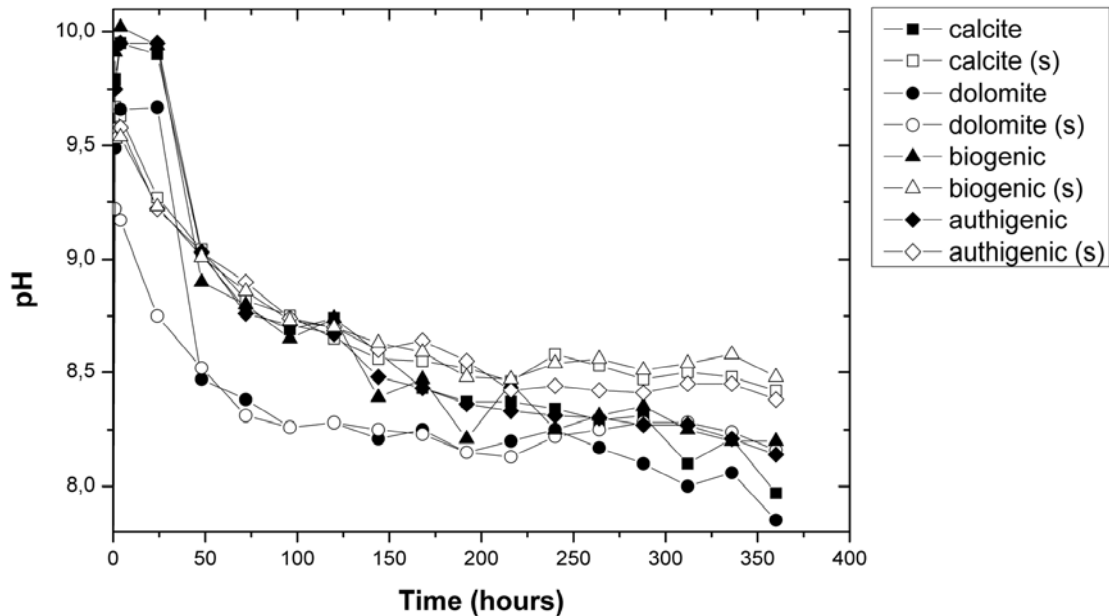
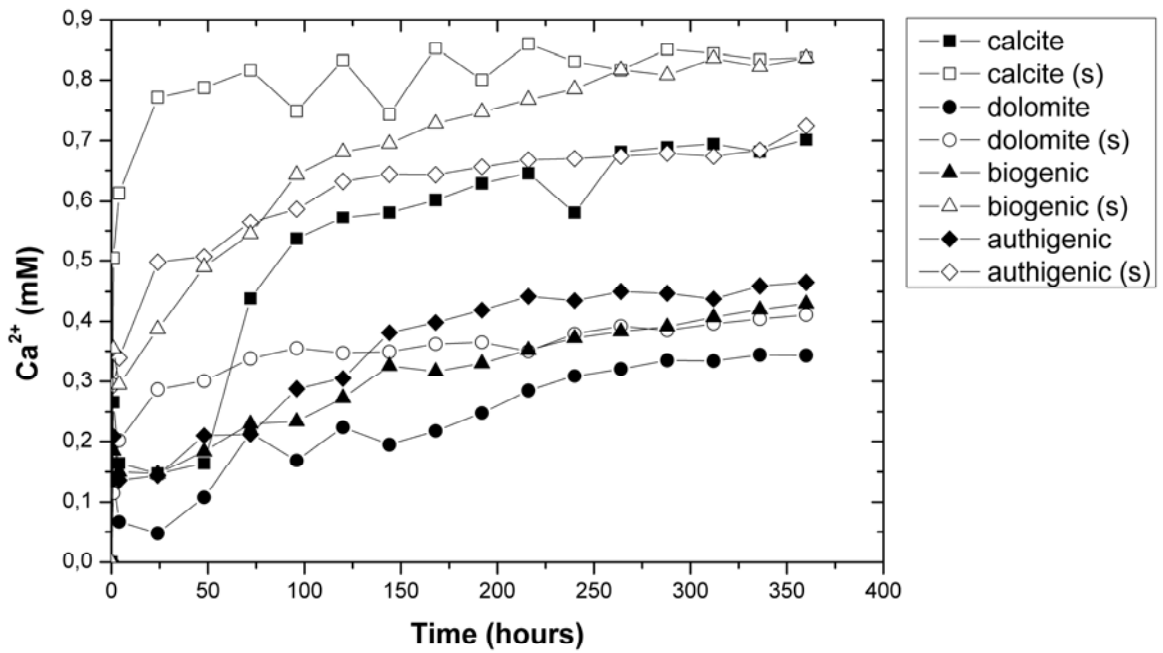


Figure 4.2: pH value over time for the performed dissolution experiments. The “S” samples denote seawater matrix.

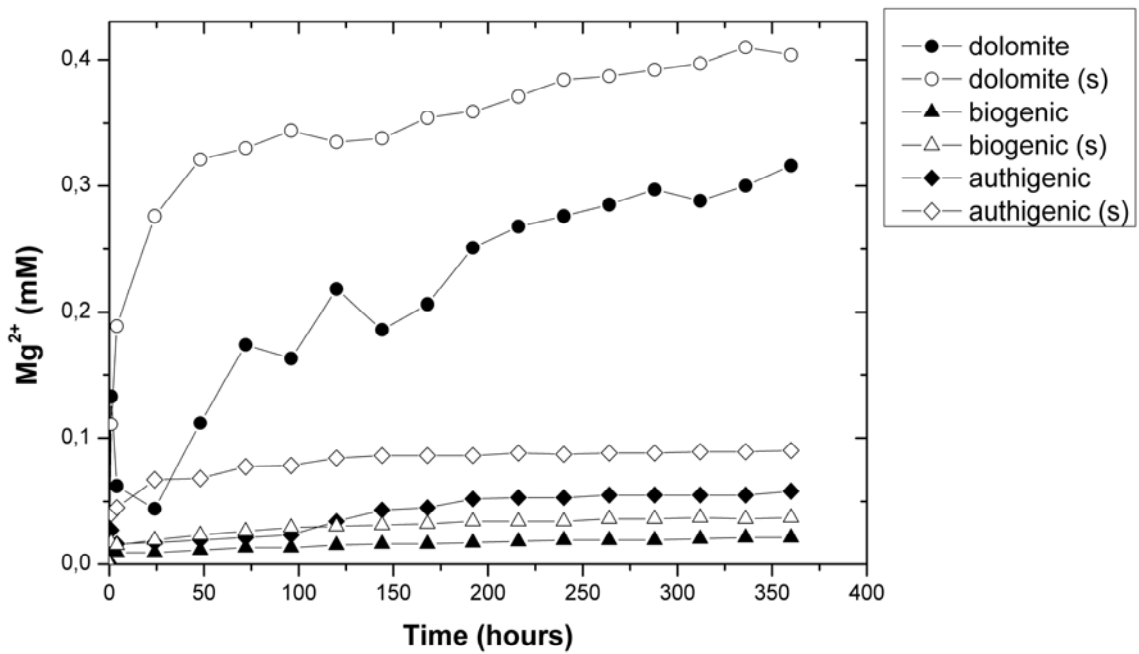
#### 4.4.2 Ca, Mg-release from CaMg-carbonates and solubility calculations

The Ca<sup>2+</sup> concentrations in solution are increasing over time (Fig. 4.3a). The first 100 hours the concentrations increase at a much higher rate, than the later steps to the end of the experiment. In Fig. 4.3a it can be observed that the final Ca<sup>2+</sup> concentration is always higher in seawater solutions than in NaCl solution experiments.

Mg<sup>2+</sup> follows the same pattern as Ca<sup>2+</sup> concentrations over time (Fig. 4.3b). During the first 100 hours, a rapid release of magnesium from the solid phase to solution is observed, followed by a smoother increase of the Mg-concentration to the end of the experiment. The Mg/(Ca+Mg)-ratio in the solutions (Fig. 4.4) generally reflect the Mg-content of the mineral (Table 4.1). Thus congruent dissolution can be assumed. However, there are deviations from the expected Mg/(Ca+Mg) ratios observed for dolomite and the authigenic high-Mg



a



b

Figure 4.3:  $\text{Ca}^{2+}$  (a) and  $\text{Mg}^{2+}$  (b) concentrations (mM) over time. "S" denotes seawater matrix.

calcite sample (Fig. 4.4). Congruent dissolution of dolomite with relatively constant  $Mg^{2+}/Ca^{2+}$  ratios is achieved faster at NaCl solution than in distilled water.  $Ca^{2+}$  is preferentially released during the first steps of dolomite dissolution according to (Busenberg and Plummer, 1982; Pokrovsky and Schott, 2001).

The increase of calcium and magnesium concentrations in solutions, is dependent on the saturation state  $\Omega$ , of the respected carbonate mineral (Morse and Arvidson, 2002). Using Minteq database and PHREEQC in combination with Mg-calcite equilibrium constants from the literature (Busenberg and Plummer, 1989), the theoretical concentrations of  $Ca^{2+}$  and  $Mg^{2+}$  and the pH of the solution in thermodynamic equilibrium can be estimated.

Furthermore, the experimental stoichiometric solubility of the dissolved minerals in the used solvents can be defined by extrapolation of the  $Ca^{2+}$  and  $Mg^{2+}$  concentrations to infinite time on an inverse time plot of  $\log$  [element] vs.  $Time^{-0.5}$  (Fig. 4.5) (Plummer and Mackenzie, 1974; Walter and Morse, 1984a; Bischoff et al., 1987). The calculated parameters are summarized in Table 5. The sums of the concentrations of  $Ca^{2+}$  and  $Mg^{2+}$  and the pH values determined with our experiments and the respected theoretically calculated data using PHREEQC program are presented in Table 4.6.

Measured pH values are in good agreement with their theoretical counterparts, with maximum differences ( $\sim 0.2$  units) to be observed in dissolution of dolomite for both NaCl solution and distilled water experiments (Table 4.6). The extrapolated concentrations in saturation equilibrium are also in good agreement with the calculated from PHREEQC, in all NaCl solution experiments.

Table 4.5: Basic parameters of the equation  $y=ax+b$  where  $y$  is the  $\log$  [Ca or Mg] in mM and  $x$  the  $time^{-0.5}$  in hours.

Element	Distilled water				Seawater		
	Sample	a	b	R <sup>2</sup>	a	b	R <sup>2</sup>
Ca	Calcite	-2.43	-0.02	0.9769	-1.03	-0.02	0.9449
	Dolomite	-7.22	-0.07	0.9488	-1.43	-0.33	0.705
	Biogenic	-5.23	-0.09	0.9720	-2.43	0.05	0.9827
	Marine authigenic	-4.36	-0.08	0.9137	-1.22	-0.10	0.9195
Mg	Calcite	-	-	-	-	-	-
	Dolomite	-6.23	-0.17	0.9456	-2.41	-0.26	0.9707
	Biogenic	-4.13	-1.46	0.9755	-2.29	-1.31	0.9722
	Marine authigenic	-5.14	-0.95	0.8629	-0.96	-0.99	0.8245

However, the experimentally derived equilibrium concentrations in distilled water are about 15% higher for calcite and dolomite standards and about 60% higher for the biogenic and authigenic Mg-calcite samples than the calculated data (Table 4.6). For the solubility calculation in PHREEQC, samples were forced to equilibrate with water in atmospheric CO<sub>2</sub> pressure. Thus, precipitation of less soluble phase (i.e. calcite) cannot be excluded. Indeed, in the forced dissolution of the Mg-calcite samples in PHREEQC, calcite is saturated, resulting in underestimation of dissolved Ca<sup>2+</sup> concentrations. Furthermore, it has to be considered that close to equilibrium carbonate dissolution is progressing extremely slowly over time (Berner, 1976), thus the potential error of misestimation due to extrapolation is increased.

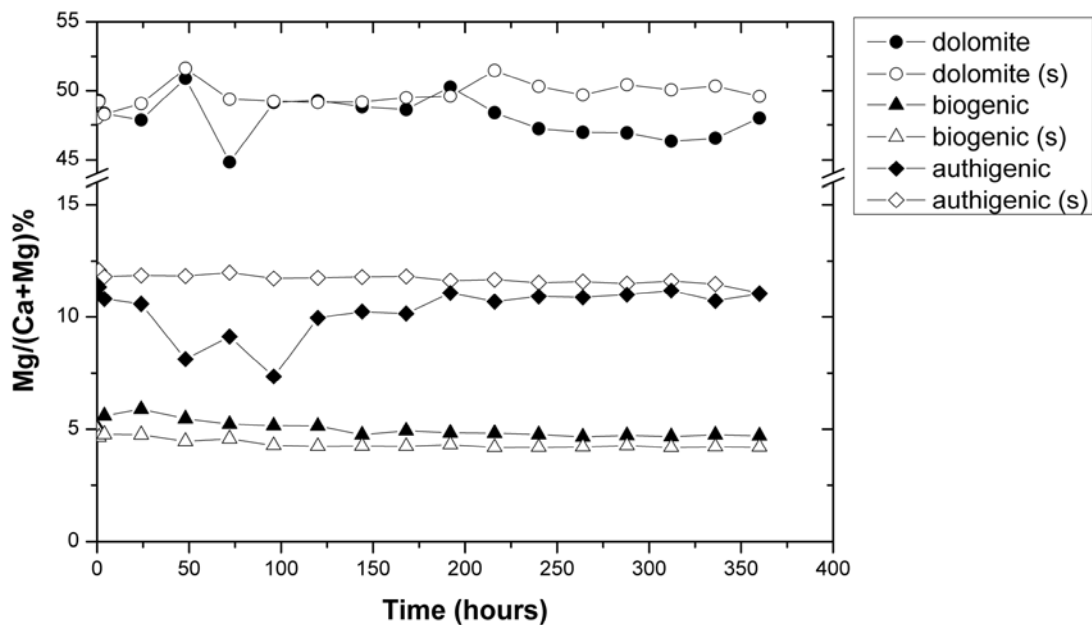


Figure 4: Relative Mg % in the solutions over time. “S” denotes seawater matrix.

Comparison of the equilibrium concentrations (sum of Ca+Mg), shows that for all the (Mg)-calcite samples used, the solubility is slightly higher in NaCl solutions compared to distilled water experiments. The solubility of dolomite is slightly lower in NaCl solutions experiments (Table 4.6). However, this might be only an artifact of the lower correlation during the dissolution of sample (see cor. coefficients Table 4.5). Largest differences between experimentally derived NaCl solution and distilled water solubility data is observed for calcite. Here the solubility increases in NaCl solution about a factor of almost 2. This effect is due

Table 8: Calculated dissolution rates and IAP of the experiments in distilled water

Time (hours)	Calcite		Dolomite		Biogenic calcite		Authigenic calcite	
	Rate	IAP	Rate	IAP	Rate	IAP	Rate	IAP
1	9,01E-04	5,02E-10	1,14E-03	3,67E-20	5,93E-04	3,53E-10	2,83E-04	5,45E-10
4	5,57E-04	1,97E-10	5,42E-04	1,17E-20	4,83E-04	3,31E-10	1,83E-04	3,58E-10
24	4,99E-04	1,58E-10	3,83E-04	6,08E-21	4,76E-04	8,24E-10	1,93E-04	4,11E-10
48	5,57E-04	1,96E-10	9,29E-04	5,02E-20	5,92E-04	6,45E-10	2,75E-04	5,70E-10
72	1,48E-03	1,30E-09	1,63E-03	2,40E-19	7,40E-04	9,71E-10	2,80E-04	6,75E-10
96	1,82E-03	1,91E-09	1,40E-03	1,09E-19	7,53E-04	8,08E-10	3,73E-04	1,29E-09
120	1,93E-03	2,15E-09	1,86E-03	2,65E-19	8,76E-04	1,28E-09	4,07E-04	1,36E-09
144	1,96E-03	2,21E-09	1,60E-03	2,01E-19	1,05E-03	1,58E-09	5,10E-04	1,99E-09
168	2,03E-03	2,36E-09	1,78E-03	2,45E-19	1,02E-03	1,54E-09	5,32E-04	1,83E-09
192	2,12E-03	2,57E-09	2,09E-03	3,31E-19	1,06E-03	1,60E-09	5,66E-04	2,29E-09
216	2,18E-03	2,70E-09	2,32E-03	5,39E-19	1,13E-03	1,79E-09	5,96E-04	2,48E-09
240	1,96E-03	2,21E-09	2,46E-03	5,15E-19	1,19E-03	1,97E-09	5,86E-04	2,45E-09
264	2,30E-03	2,98E-09	2,55E-03	4,70E-19	1,22E-03	2,11E-09	6,07E-04	2,53E-09
288	2,33E-03	3,05E-09	2,66E-03	5,07E-19	1,25E-03	2,25E-09	6,04E-04	2,61E-09
312	2,34E-03	3,09E-09	2,61E-03	5,75E-19	1,30E-03	2,43E-09	5,93E-04	2,75E-09
336	2,30E-03	2,99E-09	2,71E-03	7,08E-19	1,35E-03	2,30E-09	6,17E-04	2,67E-09
360	2,37E-03	3,15E-09	2,77E-03	7,40E-19	1,38E-03	2,35E-09	6,29E-04	2,71E-09

Table 9: Calculated dissolution rates and IAP of the experiments in seawater

Time (hours)	Calcite		Dolomite		Authigenic calcite		Biogenic calcite	
	Rate	IAP	Rate	IAP	Rate	IAP	Rate	IAP
1	1,72E-03	8,79E-10	9,50E-04	4,13E-21	4,02E-04	3,11E-10	1,13E-03	4,12E-10
4	2,09E-03	1,11E-09	1,64E-03	1,43E-20	4,63E-04	3,93E-10	9,44E-04	4,61E-10
24	2,62E-03	1,34E-09	2,37E-03	3,40E-20	6,80E-04	7,09E-10	1,24E-03	7,54E-10
48	2,68E-03	1,48E-09	2,61E-03	4,15E-20	6,91E-04	8,81E-10	1,56E-03	9,51E-10
72	2,77E-03	1,42E-09	2,81E-03	5,45E-20	7,72E-04	1,01E-09	1,74E-03	9,52E-10
96	2,55E-03	1,82E-09	2,94E-03	6,74E-20	7,99E-04	1,14E-09	2,05E-03	1,24E-09
120	2,83E-03	2,14E-09	2,87E-03	7,19E-20	8,62E-04	1,16E-09	2,17E-03	1,36E-09
144	2,53E-03	2,07E-09	2,88E-03	8,13E-20	8,78E-04	1,29E-09	2,21E-03	1,61E-09
168	2,90E-03	2,37E-09	3,01E-03	9,79E-20	8,77E-04	1,25E-09	2,32E-03	1,83E-09
192	2,72E-03	2,44E-09	3,04E-03	1,56E-19	8,92E-04	1,44E-09	2,39E-03	1,88E-09
216	2,92E-03	2,57E-09	3,03E-03	1,31E-19	9,10E-04	1,44E-09	2,45E-03	1,98E-09
240	2,82E-03	2,54E-09	3,21E-03	1,60E-19	9,11E-04	1,47E-09	2,50E-03	2,12E-09
264	2,77E-03	2,55E-09	3,28E-03	1,81E-19	9,16E-04	1,48E-09	2,60E-03	2,36E-09
288	2,89E-03	2,48E-09	3,27E-03	1,80E-19	9,22E-04	1,42E-09	2,57E-03	2,29E-09
312	2,87E-03	2,52E-09	3,33E-03	1,87E-19	9,17E-04	1,41E-09	2,66E-03	2,42E-09
336	2,84E-03	2,43E-09	3,42E-03	2,14E-19	9,29E-04	1,43E-09	2,62E-03	2,38E-09
360	2,85E-03	2,56E-09	3,42E-03	2,14E-19	9,80E-04	1,58E-09	2,66E-03	2,47E-09

to a decrease of the ion activity coefficients of the calcium and carbonate ions in solutions with increasing ionic strength (Mucci, 1983).

Table 4.6: Estimated concentration in mM of the sum of  $\text{Ca}^{2+}$  and  $\text{Mg}^{2+}$  at stoichiometric saturation.

	Distilled water				Seawater			
	Ca+Mg (mM)	pH	Ca+Mg (mM)*	pH*	Ca+Mg (mM)	pH	Ca+Mg (mM)*	pH*
<b>Calcite std</b>	0.57	8.26	0.49	8.28	0.96	8.5	1.00	8.33
<b>Dolomite std</b>	1.53	8.11	1.32	8.36	1.10	8.22	1.32	8.43
<b>Marine authigenic calcite</b>	0.91	8.3	0.57	8.34	1.18	8.48	1.00	8.33
<b>Biogenic calcite</b>	0.83	8.3	0.52	8.30	0.93	8.54	1.00	8.33

\* estimated using PHREEQC

#### 4.4.3 Dissolution rate, rate constant, and reaction order determination for CaMg-carbonate dissolution

Calculated dissolution rates for dissolution experiments with distilled water and NaCl solutions respectively, are summarized in Tables 4.8 and 4.9.. For the marine authigenic carbonate sample, corrections on the total mass of carbonate content applied from the estimation of the  $\text{CaCO}_3$  wt. % content in the sample (75%) as other mineral phases (i.e. quartz) were present. The reaction rates and constants can be found in Table 4.7. The ionic activity products of the dissolved carbonate species as they were obtained from PHREEQC software at the different time steps of the experimental process are summarized in Tables 4.8 and 4.9. Dolomite dissolution kinetics cannot be calculated by the empirical method described in paragraph 4.2.2. That fore the following discussion on reaction orders is intentionally excluding this mineral phase.

Table 4.7: Calculated rate constants and orders of reaction. For the calculation, only data after 150 hours were taken into account.

Sample	Distilled water		Seawater	
	logk	n	logk	n
Calcite std	-4.7	0.3	-2.7	3.7
Authigenic calcite (marine)	-5.2	0.7	-4.4	4.1
Biogenic calcite	-5.1	0.6	-4.6	0.9

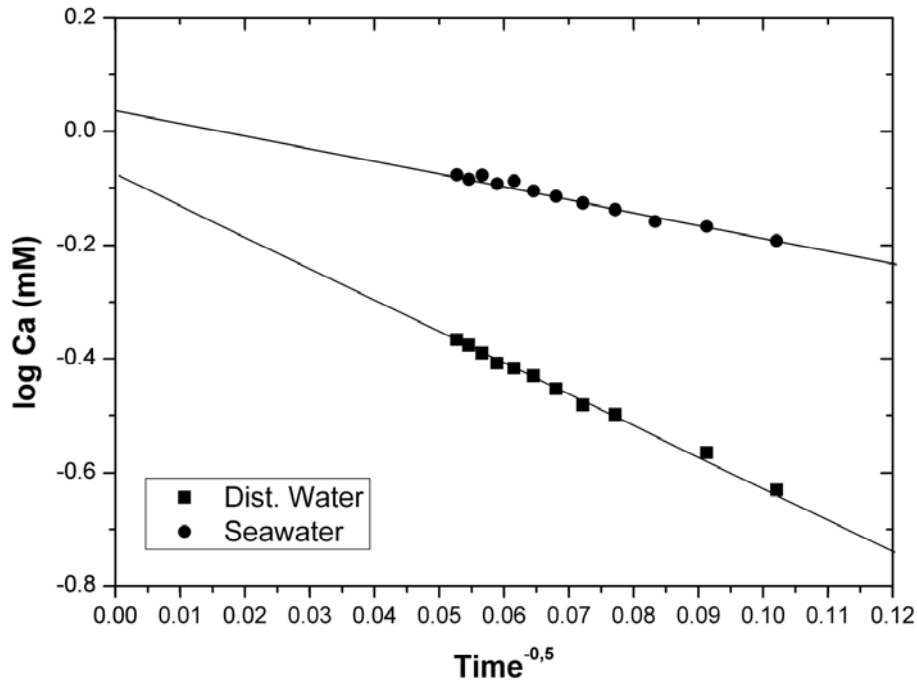


Figure 4.5: Example of a reciprocal time plot used to extrapolate  $\log [\text{Ca}^{2+}]$  for the dissolution of the biogenic Mg-calcite at distilled and seawater experiments.

Pokrovsky et al. (2005) presented that calcite dissolution rates ( $r$ ) are independent of ionic strengths in solution with 0.01 to 0.1M NaCl. However, in our experiment in NaCl solution, the calculated dissolution rates are about 1.1 to 1.9 orders of magnitude higher compared to the distilled water experiment (Tables 4.7 and 4.8). In the presence of NaCl, the dissolution of calcite and dolomite is retarded as a result of lower water activity (Zuddas and Mucci, 1998). However, presence of Na and Cl in solutions is possible to activate “inactive” sites, resulting to higher measured dissolution rates in NaCl solution.

The reaction orders ( $n$ ) as they are calculated for (Mg)-calcite dissolution from eqn. (10) are ranging between 0.3 and 4.1 (Table 4.7). The respected linear regression analyses are plotted in Figs. 4.6 a-d. Comparison of NaCl solution and distilled water dissolution experiments (Figs. 4.6 a-d) shows higher reaction orders when NaCl solution is used as the solvent, and come in good agreement with the experimental results of Gledhill and Morse (2006). Dissolution experiments have also been performed with synthetic and biogenic calcium carbonate, at saturation states close to equilibrium with  $\Omega=0.5-0.9$  (Keir, 1980; Walter and Morse, 1984a; Walter and Morse, 1985; Svensson and Dreybrodt, 1992). Keir (1980) reports  $n=4$  for synthetic calcites in artificial seawater,

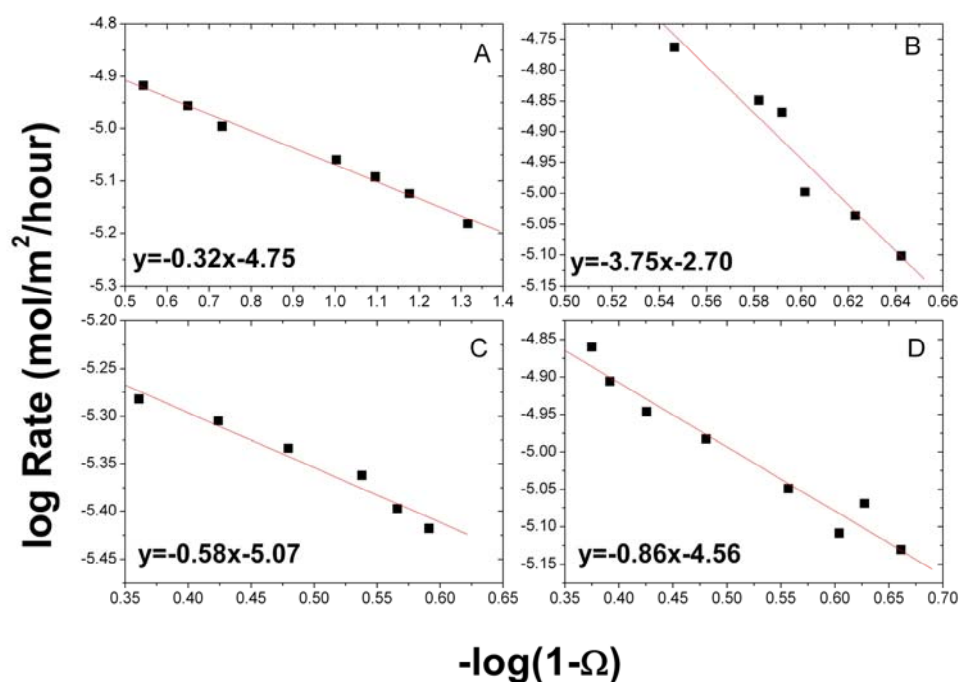


Figure 4.6: Surface area normalized dissolution rate in distilled (a,c) and sea water (b,d) as a function of fluid saturation state for calcite (a,b) and biogenic Mg-calcite (c-d). The line represents the least square fit of the experimental results, where  $y = \log \text{Rate}$  and  $x = -\log(1-\Omega)$ .

whereas, Walter and Morse (1985) observed a value of  $n=3$ . Svensson and Dreybrodt (1992) report  $n$ -values, which range between 3 and 4. Interestingly, the difference in the reaction order between the standard calcite and the biogenic Mg-calcite is in NaCl solution much higher than the one observed in distilled water. The difference most probably reflects the difference between the geometric surface of the biogenic sample and the standard calcite (Table 4.10).

Although the total (BET) surface area of the authigenic calcite is almost four times larger compared to this of standard calcite, the differences in the dissolution rate do not reflect it. In contrast, the relative rate (eqn. 10) of standard calcite in distilled water is three times higher than the authigenic sample and double compared to the biogenic sample after one hour of dissolution (Tables 4.8 and 4.9). The fact that biogenic samples do not have their total area available for dissolution, has been previously reported (Walter and Morse, 1985). Biogenic  $\text{CaCO}_3$  consists of a matrix of organic matter and crystals. Sample preparation, including grinding and cleaning, leads to the formation of micropores at the near surface. However, it has been argued that such micropores

will contribute negligibly to the overall dissolution of the mineral (Jeschke and Dreybrodt, 2002). The formation of this micropore network originally filled with organic material may also be enhanced by the drying of the ground shells, which results in dehydration of the organic material. Such dehydration would decrease the volume of this organic material further opening the micropore network. As such, measured BET surface areas for biogenic carbonates may be significantly larger than the surface area actually in contact with the reactive solution during the experiments.

Furthermore, the dissolution rates of biogenic carbonates are independent of grain size (Keir, 1980; Walter and Morse, 1984b). Our results obtained from the dissolution experiment with the authigenic sample seem to follow the same pattern, showing no dependence of the dissolution rate to the grain size reflecting that dissolution does not occur homogeneously at its total (BET) surface. Authigenic carbonates can grow in layers, including distinct crystal faces, having irregular surfaces, and complex internal microstructures (e.g. Plate 4.1b), which are known to dissolve in different rates (Park et al., 1996; Liang and Baer, 1997; Lea et al., 2001).

#### **4.4.4 Reactive surface determination of (Mg)-calcites**

The calculated kinetic orders and rate constants (Table 4.7) were used to calculate the reactive surface of the dissolved mineral using PHREEQC 2.15. The theoretical increase of i.e.  $\text{Ca}^{2+}$  in distilled water is fitted against the measured data (Fig. 4.7).

For distilled water, the calculated values of the reactive surfaces are significantly lower compared to the specific surface area (BET measured) of the sample (Tables 4.1 and 4.10). Earlier Cubillas et al. (2005) have shown that in dissolution experiments with biogenic calcium carbonate the dissolution rates of biogenic calcite are comparable to dissolution rates of inorganic calcite if they are normalized to their geometric surface area, which rather reflects the reacting surface. In our experiments with the biogenic Mg(4%)-calcite and the authigenic Mg(13%)-calcite it is indicated that the same assumption is valid. In order to simulate the dissolution kinetics of our samples with PHREEQC much lower reactive surface used (Table 4.10). When the specific surface (BET measured)

used for the simulations, equilibrium achieved faster than the experiments indicated. This observation shows that in the samples not the total of the surface was available for reaction, but only a rather small part of it. Small differences between the reactive and the geometric surface presented in Table 4.10 are probably caused by in-homogeneity in the grain size of the samples.

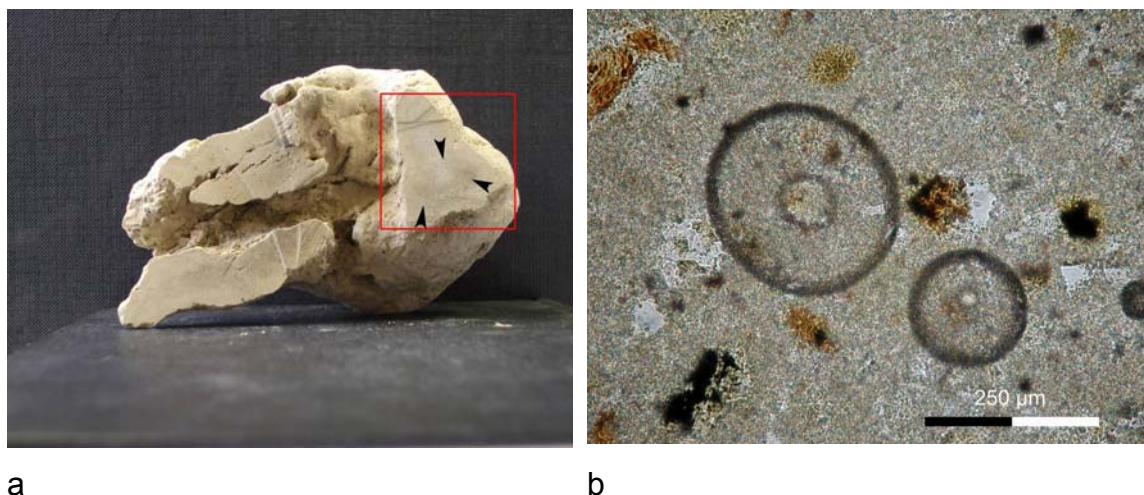


Plate 4.1: a) Photograph of the authigenic carbonate concretion used in the experiments. The sampling location is indicated (rectangular). The arrows refer to subsample locations for isotopic measurements (Table 1). b) Thin-section photo micrographs.

The reactive surfaces of (Mg)-calcites samples calculated for NaCl solution experiments are much lower than the respected geometrical surfaces (Table 4.10). However, the calculated reactive surface of standard calcite and the authigenic Mg-calcite sample are comparable possibly indicating that the dissolution of calcite in sodium chloride solution ( $\sim 0.6\text{M}$ ) is rather controlled by the ionic strength of the solution than by the surface of the dissolved mineral.

Table 4.10: Geometric and reactive surface of the samples as they were calculated according to eqn. (16) and estimated by PHREEQC respectively.

Sample	Geometric surface ( $\text{m}^2\text{g}^{-1}$ )	Reactive surface (dist. water; $\text{m}^2\text{g}^{-1}$ )	Reactive surface (seawater; $\text{m}^2\text{g}^{-1}$ )
Calcite std	0.22	-	0.00005
Marine authigenic calcite	0.22	0.3	0.00006
Biogenic calcite	0.0022*	0.001	0.000005

\* Biogenic calcite sample had significant larger grains.

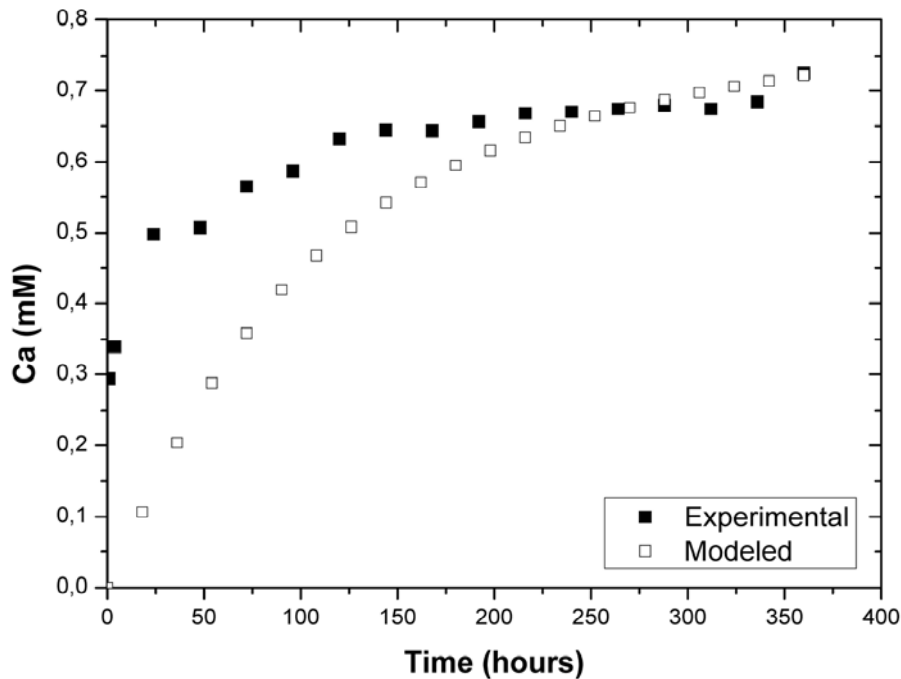


Figure 4.7: Calcium concentration over time in distilled water experiments as it was measured in the experimental runs (closed rectangulars) and modeled, importing the calculated dissolution kinetic constant and reaction order in PHREEQC .

## 4.5 Geochemical applications and conclusions

Our results presented here demonstrate that under seawater conditions ( $T=20^{\circ}\text{C}$ ,  $S\sim 35\%$ ,  $\text{pH}\sim 8.3$ ) the dissolution of authigenic high Mg-calcite can be described by a reaction order value of  $n=4.1$ , which is comparable to data known from literature for biogenic and synthetic calcites.

It is obvious that dissolution is not controlled by the specific (BET) surface area, but that only a few reactive sites (reactive surface) control the dissolution process.

It is assumed that the obtained results on authigenic Mg-calcite dissolution in 0.6M sodium chloride solution can reflect the natural dissolution processes in seawater. However, NaCl solutions are not identical to seawater in a chemical point of view.

In the present work, the effect of pressure or the presence of e.g. organic compounds (important for natural samples) on the Ca,Mg-carbonate dissolution was not investigated. These parameters are important for dissolution (and pre-

precipitation) processes of authigenic Mg-calcite in e.g. marine cold seep areas. However, our kinetic data may improve existing reaction models describing carbonate diagenesis at seafloor conditions.

## References

Alkattan M., Oelkers E., Dandurand J. L. and Schott J. (1998) An experimental study of calcite and limestone dissolution rates as a function of pH from -1 to 3 and temperature from 25 to 80 °C. *Chem Geol* **151**, 199-214.

Arvidson R. S., Ertan I. E., Amonette J. E. and Luetttge A. (2003) Variation in calcite dissolution rates; a fundamental problem? *Geochim Cosmochim Acta* **67**, 1623-1634.

Berner R. A. (1976) The solubility of calcite and aragonite in seawater at atmospheric pressure and 34.5 ‰ salinity. *Am J Sci* **276**, 713-730.

Berner R. A. and Morse J. W. (1974) Dissolution kinetics of calcium carbonate in sea water; IV, Theory of calcite dissolution. *Am J Sci* **274**, 108-134.

Berner R. A. and Wilde P. (1972) Dissolution kinetics of calcium carbonate in sea water; I, Saturation state parameters for kinetic calculations. *Am J Sci* **272**, 826-839.

Bertram M. A., Mackenzie F. T., Bishop F. C. and Bischoff W. D. (1991) Influence of temperature on the stability of magnesian calcite. *Am Mineral* **76**, 1889-1896.

Bischoff W. D. (1998) Dissolution enthalpies of magnesian calcites, Geochemistry of low temperature processes. *Aquat Geochem* **4**, 321-336.

Bischoff W. D., Mackenzie F. T. and Bishop F. C. (1987) Stabilities of synthetic magnesian calcites in aqueous solution; comparison with biogenic materials. *Geochim Cosmochim Acta* **51**, 1413-1423.

Brady P. V. and House W. A. (1996) Surface-controlled dissolution and growth of minerals, In: Physics and chemistry of mineral surfaces. CRC Press, Boca Raton, FL, United States.

Brunauer S., Emmett P. H. and Teller E. (1938) Adsorption of Gasses in Multimolecular layers. *J Am Chem Soc* **60**, 309-319.

Busenberg E. and Plummer L. N. (1982) The kinetics of dissolution of dolomite in CO<sub>2</sub>-H<sub>2</sub>O systems at 1.5 to 65 °C and 0 to 1 atm pCO<sub>2</sub>. *Am J Sci* **282**, 45-78.

Busenberg E. and Plummer L. N. (1986) A Comparative Study of the Dissolution and Crystallization Kinetics of Calcite and Aragonite In: Mumpton, F. A. (Ed.), *Studies in Diagenesis*. U.S. Geological Survey.

Busenberg E. and Plummer L. N. (1989) Thermodynamics of magnesian calcite solid-solutions at 25 °C and 1 atm total pressure. *Geochim Cosmochim Acta* **53**, 1189-1208.

Chou L., Garrels R. M. and Wollast R. (1989) Comparative study of the kinetics and mechanisms of dissolution of carbonate minerals, *Chem Geol* **78**, 269-282.

Cubillas P., Koehler S., Prieto M., Chairat C. and Oelkers E. H. (2005) Experimental determination of the dissolution rates of calcite, aragonite, and bivalves. *Chem Geol* **216**, 59-77.

Gledhill D. K. and Morse J. W. (2006) Calcite solubility in Na-Ca-Mg-Cl brines. *Chem Geol* **233**, 249-256.

Goldsmith J. R., Graf D. L. and Heard H. C. (1961) Lattice constants of the calcium-magnesium carbonates. *Am Mineral* **46**, 453-457.

Harstad A. O. and Stipp S. L. S. (2007) Calcite dissolution: Effects of trace cations naturally present in Iceland spar calcites. *Geochim Cosmochim Acta* **71**, 56-70.

Herman J. S. and White W. B. (1985) Dissolution kinetics of dolomite: Effects of lithology and fluid flow velocity. *Geochim Cosmochim Acta* **49**, 2017-2026.

Jeschke A. A. and Dreybrodt W. (2002) Dissolution rates of minerals and their relation to surface morphology. *Geochim Cosmochim Acta* **66**, 3055-3062.

Keir R. S. (1980) The dissolution kinetics of biogenic calcium carbonates in seawater. *Geochim Cosmochim Acta* **44**, 241-252.

Lea A. S., Amonette J. E., Baer D. R., Liang Y. and Colton N. G. (2001) Microscopic effects of carbonate, manganese, and strontium ions on calcite dissolution. *Geochim Cosmochim Acta* **65**, 369-379.

Liang Y. and Baer D. R. (1997) Anisotropic dissolution at the CaCO<sub>3</sub> (1014)--water interface. *Surf Sci* **373**, 275-287.

Luff R. and Wallmann K. (2003) Fluid flow, methane fluxes, carbonate precipitation and bio-geochemical turnover in gas hydrate-bearing sediments at Hydrate Ridge, Cascadia Margin: numerical modeling and mass balances. *Geochim Cosmochim Acta* **67**, 3403-3421.

Luff R., Wallmann K. and Aloisi G. (2004) Numerical modeling of carbonate crust formation at cold vent sites; significance for fluid and methane budgets and chemosynthetic biological communities. *Earth Planet Sci Lett* **221**, 337-353.

Morse, J. W. (1978) Dissolution kinetics of calcium carbonate in sea water; VI, The near-equilibrium dissolution kinetics of calcium carbonate-rich deep sea sediments. *Am J Sci* **278**, 344-353.

Morse, J. W. (1983) The kinetics of calcium carbonate dissolution and precipitation. *Rev Mineral Geochem* **11**, 227-264.

Morse J. W. and Arvidson R. S. (2002) The dissolution kinetics of major sedimentary carbonate minerals. *Earth Sci. Rev.* **58**, 51-84.

Morse J. W., Arvidson R. S. and Luttge A. (2007) Calcium carbonate formation and dissolution. *Chem. Rev.* **107**, 342-381.

Mucci A. (1983) The solubility of calcite and aragonite in seawater at various salinities, temperatures, and one atmosphere total pressure. *Am J Sci* **283**, 780-799.

Mucci A. and Morse J. W. (1984) The solubility of calcite in seawater solutions of various magnesium concentration,  $I_t = 0.697$  m at 25 °C and one atmosphere total pressure. *Geochim Cosmochim Acta* **48**, 815-822.

Park N.-S., Kim M.-W. Langford S. C. and Dickinson J. T. (1996) Tribological Enhancement of CaCO<sub>3</sub> Dissolution during Scanning Force Microscopy. *Langmuir* **12**, 4599-4604.

Parkhurst D. L. and Appelo C. A. J. (1999) User's Guide to PHREEQC (Version 2) - A Computer Program for Speciation, Batch- Reaction, One-Dimensional Transport, and Inverse Geochemical Calculations: U.S. Geological Survey Water-Resources Investigations Report 99-4259, 310 pp.

Plummer L. N. and Busenberg E. (1982) The solubilities of calcite, aragonite and vaterite in CO<sub>2</sub>-H<sub>2</sub>O solutions between 0 and 90 °C, and an evaluation of the aqueous model for the system CaCO<sub>3</sub> -CO<sub>2</sub>-H<sub>2</sub>O. *Geochim Cosmochim Acta* **46**, 1011-1040.

Plummer L. N. and Busenberg E. (1987) Thermodynamics of aragonite-strontianite solid solutions: Results from stoichiometric solubility at 25 and 76°C. *Geochim Cosmochim Acta* **51**, 1393-1411.

Plummer L. N. and Mackenzie F. T. (1974) Predicting mineral solubility from rate data; application to the dissolution of magnesian calcites. *Am J Sci* **274**, 61-83.

Plummer L. N. and Wigley T. M. L. (1976) The dissolution of calcite in CO<sub>2</sub>-saturated solutions at 25°C and 1 atmosphere total pressure. *Geochim Cosmochim Acta* **40**, 191-202.

Plummer L. N., Wigley T. M. L. and Parkhurst D. L. (1978) The kinetics of calcite dissolution in CO<sub>2</sub>-water systems at 5 to 60 °C and 0.0 to 1.0 atm CO<sub>2</sub>. *Am J Sci* **278**, 179-216.

Pokrovsky O. S., Golubev S. V. and Schott J. (2005) Dissolution kinetics of calcite, dolomite and magnesite at 25 °C and 0 to 50 atm pCO<sub>2</sub>, *Chem Geol.* **217**, 239-255.

Pokrovsky O. S. and Schott J. (2001) Kinetics and Mechanism of Dolomite Dissolution in Neutral to Alkaline Solutions Revisited. *Am J Sci* **301**, 597-626.

Pokrovsky O. S. and Schott J. (2002) Surface Chemistry and Dissolution Kinetics of Divalent Metal Carbonates. *Environ. Sci. Technol.* **36**, 426-432.

Reddy M. M., Plummer L. N. and Busenberg E. (1981) Crystal growth of calcite from calcium bicarbonate solutions at constant  $P_{CO_2}$  and 25 degrees C; a test of a calcite dissolution model. *Geochim Cosmochim Acta* **45**, 1281-1289.

Rickard D. and Sjöberg E. L. (1983) Mixed kinetic control of calcite dissolution rates. *Am J Sci* **283**, 815-830.

Robie R. A. and Hemingway B. S. (1995) Thermodynamic properties of minerals and related substances at 298.15 K and 1 bar ( $10^5$  pascals) pressure and at higher temperatures USGS Bulletin. USGS.

Sjöberg E. L. and Rickard D. (1983) The influence of experimental design on the rate of calcite dissolution. *Geochim Cosmochim Acta* **47**, 2281-2285.

Svensson U. and Dreybrodt W. (1992) Dissolution kinetics of natural calcite minerals in CO<sub>2</sub>-water systems approaching calcite equilibrium. *Chem Geol* **100**, 129-145.

Thorstenson D. C. and Plummer L. N. (1977) Equilibrium criteria for two-component solids reacting with fixed composition in an aqueous phase; example, the magnesian calcites. *Am J Sci* **277**, 1203-1223.

Walter L. M. and Morse J. W. (1984a) Magnesian calcite stabilities; a reevaluation. *Geochim Cosmochim Acta* **48**, 1059-1069.

Walter L. M. and Morse J. W. (1984b) Reactive surface area of skeletal carbonates during dissolution; effect of grain size. *J Sediment Petrol* **54**, 1081-1090.

Walter L. M. and Morse J. W. (1985) The dissolution kinetics of shallow marine carbonates in seawater; a laboratory study. *Geochim Cosmochim Acta* **49**, 1503-1513.

Zhang R., Hu S., Zhang X. and Yu, W. (2007) Dissolution Kinetics of Dolomite in Water at Elevated Temperatures. *Aquat Geochem* **13**, 309-338.

Zuddas P. and Mucci, A. (1998) Kinetics of Calcite Precipitation from Seawater: II. The Influence of the Ionic Strength. *Geochim Cosmochim Acta* **62**, 757-766.



## Appendix

Table 1a: Geochemical parameters of pore water samples and carbonate- and organic carbon content of sediments from mound 11.

Core	Depth (cm)	Alkalinity (mM)	H <sub>2</sub> S (μM)	NH <sub>4</sub> (μM)	PO <sub>4</sub> (μM)	Cl (mM)	SO <sub>4</sub> (mM)	B (mM)	Ca (mM)	K (mM)	Li (μM)	Mg (mM)	Na (mM)	Sr (μM)	C <sub>org</sub> wt %	CaCO <sub>3</sub> wt %	CH <sub>4</sub> (mM)	CH <sub>4</sub> Depth (cm)
M54-	100	35	2,71	2	32,5	5,92	563,8	29,1	0,44	10,3	10,7	24,5	478,6	87,8	1,83	3,76	0	92
	85	2,83	18,5	32,5	5,57	554,3	29	0,45	10,3	10,8	25,7	52	475,4	87,8	1,45	1,76	0	192
	135	2,81	28,01	35,21	5,22	555,2	28,5	0,45	10,2	10,7	26,5	52,2	476,5	87,8	1,22	17,09	0,001	292
	185	3,02	45,51	39,27	5,22	555,7	28,8	0,44	10,2	10,7	24,6	52,5	482,7	87,6	1,25	3,07		
	235	3,18	117	36,56	5,22	555,2	28,6	0,44	10,1	10,7	25,4	52,1	476,3	87,4	1,29	2,3		
	280	3,59	137	54,16	4,87	546,4	27,7	0,42	10	10,5	24,5	52,3	478,9	87	1,23	2,44		
M54-	102	25	2,34	0	14,24	4,82	553,3	29,5	0,47	10,4	10,8	24,8	479,3	88,2	1,37	17	0,0003	34
	85	2,54	0	22,01	4,48	548,4	29,1	0,46	10,3	10,8	23,7	52,3	477,8	88,3	1,41	20,97	0,0013	100
	105	2,75	8,5	24,6	4,13	547,9	28,4	0,44	10,3	10,7	24	52,5	481,2	87,9	1,49	14,71	0,0012	141
	145	2,81	20,5	28,48	3,79	546,4	28,3	0,42	10,3	10,5	25,7	52,5	484	88	1,3	19,99	0,0029	231
	185	3,71	165,5	41,43	3,44	543,9	26,6	0,41	9,79	10,4	23,5	52,3	475,3	86,9	1,27	15,57		
	225	5,64	480,6	63,44	3,44	543,5	22,7	0,38	8,62	10,2	25,6	51,3	469	83,7	1,26	17,77		
M54-	143	25	2,87	53,01		557,8		0,38	10,2	10,3	39,7	51,7	463,2	86,6				
	50	2,89	42,98			559,8		0,31	9,98	11	34,4	51,2	473,1	86,3				
	103	4,68	89,54			548,3		0,37	9,27	10,2	29,5	49,6	458,4	83				
	125	15,95		115,3		490,4		0,57	4,34	9,07	26,2	37,7	403	59,8				
	152	2,1		457,6		260,6		1,03	6,22	6,54	26,4	12,3	217	29,1				
M54-	155	5	2,35	1,5	0	5,33	549,1	27,9	0,44	10,4	10,2	22,2	478,7	88,9	1,27	24,21	0,06	0
	25	2,44	2	0	4,57	554,1	27,9	0,45	10,4	10,3	23,1	53,1	478,9	88,6	1,13	16,96	0,02	82
	45	2,74	4,75	4,98	3,81	553,6	27,2	0,43	10,4	10,3	24	52,6	477,2	88,5	1,15	23,8	2,91	100
	65	3,08	77,52	13,5	4,19	556,2	27,5	0,44	10,3	10,2	20,9	52,7	475,1	88	1,11	22,88	2,91	120
	85	9,93	3521	131,5	11,4	541,6	19,8	0,49	8,77	9,92	22,4	48,9	457,6	81,6	0,87	37,47	2,46	140
	105	17,5	5326	547,3	15,6	464,7	1,08	0,75	5,75	8,3	22,4	34,1	388,8	57,8	1,14	16,3	1,89	160
	125	12,09	1760	1011	6,09	418,5	0,69	0,79	6,3	7,59	15,6	27,7	348,9	47,1	1,19	9,37	6,05	174
	145	10,4	1080	1318	4,95	389,4	0,51	0,82	6,29	6,91	14,6	25,6	328,5	42,2	1,12	9,84		
	165	14,88	4236	1102	14,1	401,9	1,18	0,89	6,25	6,78	15,6	30,4	345,2	45,4	0,9	17,85		

Table 1b: Geochemical parameters of pore water samples and carbonate- and organic carbon content of sediments from mound 12.

Core	Depth (cm)	Alkali nity (mM)	H <sub>2</sub> S (μM)	NH <sub>4</sub> (μM)	PO <sub>4</sub> (μM)	Cl (mM)	SO <sub>4</sub> (mM)	B (mM)	Ca (mM)	K (mM)	Li (μM)	Mg (mM)	Na (mM)	Sr (μM)	C <sub>org</sub> wt %	CaCO <sub>3</sub> wt %	CH <sub>4</sub> (mM)	CH <sub>4</sub> (mM)	Depth (cm)
SO173-110/1	5	2,95	0	31,62	11,8	555,1	29	0,46	10,1	11,2	27,2	53,2	478,8	89,4	1,22	26,57	0,05		34
	17	3,91	213,9	25,57	7,48	555,1	28	0,44	9,9	11,3	28	53,2	474,7	88,2	1,35	3,13	9,59		120
	30	10,89	3509	19,51	8,91	557,1	21,4	0,45	8,56	11,2	24,3	52,4	477,4	85,1	1,33	3,35			
	45	31,33	13410	16,15	16,4	554,2	2,88	0,43	4,82	10,8	20,1	50,6	472,8	72,1	1,14	6,9			
	65	35,96	15916	33,64	33,1	555,7	0,05	0,39	3,85	11	18,1	51,6	471,5	65,2	1,4	3,05			
	85	37,18	16292	39,7	35,6	552,3	0,25	0,39	3,81	11,2	19,8	51,5	477,3	62,8	1,32	6,49			
	105	36,79	14078	35,66	39,2	551,9	0,28	0,36	3,67	11	15,6	49,3	475	58,7	1,52	3,68			
	120	29,95	6183	31,62	50,9	552,8	0,32	0,29	3,54	11,5	19,3	49,4	478,8	55,3	1,43	3,11			
SO173-135/1	40	2,65	0	34,71		559,9	29,4	0,48	9,94	11,4	24,1	51,3	475,6	88,3					
	80	2,65	0	25,66		561,9	29,4	0,48	9,97	11,2	29,8	51,2	471	88,3					
	105	2,68	0	33,21		563,1	29,5	0,47	9,99	11,4	27,1	50,8	477,3	88,3					
	140	2,65	0	31,7		559,1	29,2	0,47	9,91	11,5	31,6	53,2	480,5	88,7					
	180	3,11	0	33,21		563,3	28,8	0,44	9,77	11,6	30,8	50,9	479,7	87,7					
	205	3,89	14,62	49,81		565,3	28,1	0,42	9,57	11,7	26,5	51	485,2	87,4					
	250	5,02	169,2	67,92		561,4	27,1	0,44	9,5	11,4	28,7	51,5	478,1	87,5					
	280	6,93	296,6	116,2		564,8	24,8	0,42	9,02	11,6	23,4	50,4	479	86					
	315	12,32	881,4	140,4		561,4	16,1	0,39	6,52	11,8	23,8	49,5	475,5	78,6					
	340	21,21	17232	172,1		565,1	4,67	0,4	4,01	11,4	18,8	48,5	472,3	67,8					
	365	24,75	15268	243		557,3	0,56	0,36	3,53	11,2	19	46,8	463,9	63,2					
	415	28,52	19717	398,4		558,9	0,43	0,41	4,22	11,2	14,3	46,6	468,6	68,8					
	440	25,23	1880	519,2		559,3	0,6	0,4	3,61	11,3	14	45,7	471,6	64,8					
	465	27,71	1157	861,8		532,6	0,49	0,44	2,49	10,5	11,7	43,6	452,2	58					
	515	27,63	2218	721,4		522,9	0,5	0,45	2,66	10,5	13,6	44,2	449,9	58,1					
	540	25,76	355,1	748,6		517,3	0,28	0,4	2,33	10,4	13,3	40,8	441,2	53,7					
565	25,68	2477	492		522,6	1,28	0,39	3,45	10,5	11,1	43,4	448,8	61,2						
M54-84	20	2,53		26,95	6,54	540,2	28,5	0,44	10,2	10,6	26,5	53,1	474,9	10,6	1,71	3,35	0,0003		84
	70	2,86		28,36	5,85	545,1	28,3	0,41	10,2	10,6	24,8	52,7	476,4	10,6	1,37	7,22	0,0003		192
	120	2,78		26,24	4,48	539,7	28,4	0,43	10,3	10,8	22,2	52,8	473,2	10,8	1,4	5,84	0,0004		282
	170	2,9		30,49	4,82	548	28,2	0,43	10,2	10,8	23,7	52,9	474,2	10,8	1,45	1,75			
	220	2,86		28,36	4,48	547,5	27,7	0,4	10,2	10,6	23,8	53,5	483	10,6	1,16	21,15			

Table 1b: continued

Core	Depth (cm)	Alkali nity	H <sub>2</sub> S (µM)	NH <sub>4</sub> (µM)	PO <sub>4</sub> Cl (µM)	SO <sub>4</sub> (mM)	B	Ca	K	Li	Mg (mM)	Na (mM)	Sr (µM)	Corrg wt %	CaCO <sub>3</sub> wt %	CH <sub>4</sub> (mM)	CH <sub>4</sub> (mM)	CH <sub>4</sub> Depth (cm)
M54-84	270	2,92		34,75	3,79	551	28,2	0,38	9,98	10,7	25,2	52,6	474,2	10,7	1,47	8,84		
M54-91	90	2,97	0	26,41	5,95	543,6	29	0,45	10,1	10,7	24,9	52,1	472,7	88,2	1,91	3,42	0,001	151
	120	2,83	0	35,89	6,3	546,6	28,8	0,45	10,1	10,8	25,7	51,9	472,8	88,2	1,78	1,07	0,001	251
	170	2,71	0	36,56	5,6	544,1	28,9	0,42	10	10,8	24,4	51,2	472,4	87,8	1,6	6,07	0,001	343
	220	2,87	0	38,6	5,95	558,8	28,9	0,39	10,2	11	27,6	52,5	480,8	89,2	1,03	3,58		
	270	3,24	6	44,01	5,6	547,6	28,6	0,41	10,1	10,9	24,8	52,2	475,6	88,8	1,42	3,58		
	320	3,24	18,85	46	5,6	546,1	28	0,41	10,2	10,5	23,6	52,6	474,2	88,6	1,35	3,09		
M54-92	20	2,52	0	21,67	7,35	544,1	30,2	0,44	10,2	10,2	28,6	51,5	450,7	88,6	2,03	3,76	0	78
	70	2,69	0	23,7	7	548,5	30,2	0,43	10,3	10,3	27,6	51,6	455,3	88,6	1,68	3,85	0	178
	115	2,75	0	20,31	5,25	548	30,2	0,42	10,2	10,4	28,2	51,2	453	88,4	1,58	3,05	0,002	268
	160	2,71	13	19,64	4,9	546,6	30,2	0,43	10,3	10,2	26,7	51,8	458,6	88,9	1,39	2,3		
	205	2,89	20,5	18,28	4,9	547,6	29,7	0,41	10,2	10,4	28,6	51,7	458,5	88,7	1,33	2,63		
	250	3,73	260,6	20,99	4,55	550	28,4	0,4	9,91	10,2	26,8	51,8	454,2	88	1,22	2,44		
M54-94	20	2,67	0	29,74	7,71	554,4	29	0,4	10	11,2	28,2	52,9	485,5	88,9	2,08	1,98		
	50	2,69	0	29,74	6,66	553,9	29,5	0,44	8,67	9,8	28,7	53,1	498,4	76,3	1,63	5,9		
	80	2,56	0	28,06	7,71	553,4	29	0,48	9,26	10,1	23,5	52,9	492,3	81,6	1,55	7,62		
	110	2,6	0	17,18	5,96	553	27,8	0,47	9,56	10,4	24,1	52,7	490,3	83,8	1,49	9,23		
	140	2,69	0	21,81	6,31	553,4	29,1	0,47	9,8	10,7	23,2	52,3	487,5	85,9	1,31	10,65		
	170	2,69	3,5	22,47	5,61	553,9	28,7	0,44	10,1	10,8	25,9	53,5	483	88,4	1,41	9,27		
	200	2,71	4	27,1	5,26	553,9	28,9	0,49	9,62	10,7	25,6	52,7	485,3	85,4	1,48	6,03		
	230	2,79	14	33,71	5,26	554,4	28,9	0,49	9,61	10,5	23,6	52,3	490,5	84,9	1,37	9,82		
	260	3,2	74,52	40,32	5,61	556,9	28,4	0,48	9,78	10,8	24,8	51,6	479,9	86,2	1,38	5,15		
	290	3,22	48,01	47,59	5,61	555,4	27,6	0,46	9,75	11,5	31,1	52,3	481,9	87,7	1,48	13,32		
	320	3,77	43,01	79,31	6,66	554,9	27,2	0,51	8,72	10,5	20,4	51,4	490,8	79,7	1,55	6,44		
	350	4,76	134	97,15	7,36	554,4	25,9	0,46	9,11	10,9	26	50,8	481,5	84,8	1,53	4,85		
M54-97/2	10	2,54	0,5	17,59	5,79	553	28,4	0,43	10,5	10,5	24,3	52,8	471	88,4	2,76	2,9	0,01	0
	45	2,67	0	21,65	5,45	549	28,4	0,43	10,4	10,5	23,8	53	475	88,4	2,5	2,45	0	90
	80	2,73	0	33,82	5,45	549,5	28,3	0,42	10,3	10,5	23,7	52,8	470,6	88,5	2,22	2,82		190
	115	2,75	1	28,41	5,11	549	28	0,41	10,3	10,6	23,6	53,2	472,8	87,8	1,37	3,08		290
	150	6,69	1118	33,82	7,09	549,5	23	0,42	9,1	10,2	24,7	50,9	460,9	83,9	1,24	6,46		390
	185	24,45	7052	182,6	19,5	509,8	0,33	0,4	3,81	9,37	17,7	42,2	426,9	62,9	1,3	6,5		
	220	19,32	1010	311,2	14,5	474	0,34	0,36	3,01	9,2	16,5	36,7	408,7	53,5	1,32	3,83		
	255	18,87	65,02	470,1	17,4	441,1	0,09	0,37	2,5	9,09	13,4	31,4	381	46,3	1,22	3,77		

Table 1b: continued

Core	Depth (cm)	Alkali (mM)	H2S (µM)	NH4 (µM)	PO4 (µM)	Cl (mM)	SO4 (mM)	B (mM)	Ca (mM)	K (mM)	Li (µM)	Mg (mM)	Na (mM)	Sr (µM)	Corg wt %	CaCO3 wt %	CH4 (mM)	CH4 Depth (cm)
M54-97/2	285	18,75	63,01	693,4	22,8	414,1	0,09	0,43	2,08	8,76	12,1	28,4	370,2	41,3	1,27	8,44		
	315	19,22	167	710,3	31	393	0,1	0,46	1,81	8,34	10,5	25,5	349,9	37,7	1,3	7,62		
	345	19,16	79,52	784,7	33,4	381,7	0,13	0,48	1,65	8,17	12,2	23,7	338,6	35	1,4	5		
	370	19,69	277,6	848,9	43,6	360,6	0,12	0,56	1,44	7,81	11,3	21,2	323,6	31,8	1,2	11,46		
M54-100	35	2,71	2	32,5	5,92	553,8	29,1	0,44	10,3	10,7	24,5	52,1	478,6	87,8	1,83	3,76	0	92
	85	2,83	18,5	32,5	5,57	554,3	29	0,45	10,3	10,8	25,7	52	475,4	87,8	1,45	1,76	0	192
	135	2,81	28,01	35,21	5,22	555,2	28,5	0,45	10,2	10,7	26,5	52,2	476,5	87,8	1,22	17,09	0,001	292
	185	3,02	45,51	39,27	5,22	555,7	28,8	0,44	10,2	10,7	24,6	52,5	482,7	87,6	1,25	3,07		
	235	3,18	117	36,56	5,22	555,2	28,6	0,44	10,1	10,7	25,4	52,1	476,3	87,4	1,29	2,3		
	280	3,59	137	54,16	4,87	546,4	27,7	0,42	10	10,5	24,5	52,3	478,9	87	1,23	2,44		
M54-102	25	2,34	0	14,24	4,82	553,3	29,5	0,47	10,4	10,8	24,8	52,5	479,3	88,2	1,37	17	0,0003	34
	65	2,54	0	22,01	4,48	548,4	29,1	0,46	10,3	10,8	23,7	52,3	477,8	88,3	1,41	20,97	0,0013	100
	105	2,75	8,5	24,6	4,13	547,9	28,4	0,44	10,3	10,7	24	52,5	481,2	87,9	1,49	14,71	0,0012	141
	145	2,81	20,5	28,48	3,79	546,4	28,3	0,42	10,3	10,5	25,7	52,5	484	88	1,3	19,99	0,0029	231
	185	3,71	165,5	41,43	3,44	543,9	26,6	0,41	9,79	10,4	23,5	52,3	475,3	86,9	1,27	15,57		
	225	5,64	480,6	63,44	3,44	543,5	22,7	0,38	8,62	10,2	25,6	51,3	469	83,7	1,26	17,77		
M54-164	10	2,62	3,25	13,75	4,84	558,7	28,7	0,42	10,3	10,6	23,6	52,9	472,1	88,5	2,38	4,6	0,01	0
	35	2,77	3,5	20,62	6,13	557,2	28,8	0,43	10,3	10,3	24,9	52,7	463,4	88,1	2,29	1,15	0	48
	60	2,85	3,5	13,75	4,84	553,1	28,7	0,43	10,2	10,7	25,6	52,9	474	88,2	2,22	6,7	0	108
	85	2,87	29,51	12,03	3,87	557,2	29,4	0,43	10,3	10,6	26,8	52,9	471,1	88,5	2,1	5,82	12,64	208
	110	3,26	137,3	18,9	2,91	558,7	28,7	0,36	9,92	10,7	25,7	52,5	472,9	87,5	1,9	6,01	2,43	298
	135	5,65	742,7	27,49	3,23	558,2	28	0,38	9,36	10,3	22	52,9	466,7	86,3	1,65	7,2		
	160	14,98	3671	85,9	9,44	561,2	25,6	0,35	5,55	10,4	25,2	50,2	464,1	77,1	0,73	21,84		
	185	29,33	10878	40,54	17,8	560,7	13,3	0,39	3,62	10,4	22,5	49,3	460,4	70,6	1,14	5,52		
	210	30,09	10003	53,6	22,3	561,2	1,09	0,38	3,58	10,5	22,1	49,8	466,2	70	1,27	4,1		
	235	28,96	8027	85,9	25,7	562,2	0,93	0,35	3,49	10,5	16,5	49,3	461,7	68,7	1,27	2,72		
260	27,26	8177	90,71	26,8	561,2	1,62	0,35	3,23	10,3	14,2	49,3	465,7	66,6	1,26	4,24			
285	26,85	6027	34,36	28,7	560,2	1,62	0,31	2,96	10,4	15,4	49,4	467,8	64,5	1,43	3,32			

Table 1b:continued

Core	Depth (cm)	Alkali nity	H <sub>2</sub> S	NH <sub>4</sub> (µM)	PO <sub>4</sub> (µM)	Cl	SO <sub>4</sub> (mM)	B	Ca	K	Li	Mg	Na	Sr	Corg wt %	CaCO <sub>3</sub> wt %	CH <sub>4</sub>	CH <sub>4</sub> Depth (cm)
M66-																		
197	20	3,27	0	25,7	9,88	559,5	28,8	0,46	10	11,7	26,4	51,4	476	90,4	1,81	0,37	0	3
	37	3,24	0	20,8	8,69	560	28,8	0,47	9,89	11,9	27,1	51,6	473	89,3	1,42	-0,01	0	47
	60	3,05	0	21,42	8,18	556,5	28,6	0,49	9,83	11,9	26,4	50,6	473	89,3	1,29	0,04	0	147
	80	3,01	0	21,42	7,52	552,9	28,4	0,48	9,82	12,2	27,2	51	481	89,7	1,03	2,26	0,02	197
	105	3,09	0	24,66	7,84	557	28,5	0,47	9,96	12,3	26,9	50,9	478	90	1,68	1,34	0,01	248
	130	3,16	0	23,96	7,24	552,4	28,6	0,49	9,91	12,1	26,5	51,9	476	89,7	1,42	8,34	6,79	348
	150	3,09	0	26,14	6,76	560,5	28,4	0,5	9,96	11,9	26,6	51	477	89,6	1,49	2,18		
	170	3,46	0	35,5	6,37	560,5	28,2	0,51	10,1	11,8	26,3	51,2	479	89,8	1,47	2,11		
	190	3,53	4,18	35,78	6,21	547,9	27,9	0,51	10	11,8	26,4	51,2	478	89,8	1,35	7,66		
	210	3,98	28,2	48,2	7,33	554,4	27,3	0,51	9,88	11,6	26,2	50,7	474	89,1	1,35	4,89		
	230	5,06	199,4	77,96	7,24	550,4	25,5	0,51	9,41	11,7	26	51,2	472	87,3	1,25	5,5		
	260	10,19	2191	153,8	12,7	550,4	19,7	0,59	8,42	11,1	24,1	48,5	461	83	1,49	2,19		
	290	18,53	6243	213	23,3	549,4	9,04	0,68	6,37	11	22,8	44,9	447	75	1,39	6,25		
	320	25,22	8553	271,4	36,6	510,4	0,93	0,83	5,15	10,4	20,1	41,3	424	67,5	1,3	1,65		
	345	15,96	160,4	814,8	26,2	467,3	0,21	0,84	4,73	10,5	16,3	35,1	399	57	1,28	4,67		
	350	16	740,9	498	28,9	466,3	0,88	0,91	4,89	10,1	15,9	34,6	392	56,5	1,06	4,17		
M66-																		
213	100	13	2311	51,28	10,7	473,6	6,67	0,66	4,56	10,1	21,2	38,3	401	60,1	1,2	16,39	3,4	164
	120	15,98	2752	237	21,2	419,6	1,19	1,13	3,77	9,6	18,3	29,4	357	48,7	1,29	10,29	2,11	204
	140	13,91	2845	277	24,6	382	2,07	1,47	4,18	8,9	16,7	24,3	329	44	1,19	15,57	0,97	225
	170	9,52	72,92	829,8	20,1	310,3	0,17	1,69	3,64	7,8	12,2	15	258	29,3	1,64	5,36	1,44	247
	190	9,26	143	1638	21,5	282,3	0,26	1,82	3,65	7,4	11,7	14,2	244	27,8	1,56	6,22	1,83	247
	210	8,83	29,07	1719	20,8	268,1	0,24	1,77	3,51	7,3	11,4	13,2	234	25,8	1,11	34,99		
	225	8,39	20,65	1721	20,6	262	0,18	1,77	3,51	7,3	11,5	12,6	231	25,2	1,42	6,29		
	240	8,39	18,33	1768	21,5	247,7	0,09	1,72	3,52	6,9	10,8	11,3	217	23,2	1,31	4,53		